Springer Theses
Recognizing Outstanding Ph.D. Research

Dong-Sheng Ding

Broad Bandwidth and High Dimensional Quantum Memory Based on Atomic Ensembles

Springer

Springer Theses

Recognizing Outstanding Ph.D. Research

Aims and Scope

The series "Springer Theses" brings together a selection of the very best Ph.D. theses from around the world and across the physical sciences. Nominated and endorsed by two recognized specialists, each published volume has been selected for its scientific excellence and the high impact of its contents for the pertinent field of research. For greater accessibility to non-specialists, the published versions include an extended introduction, as well as a foreword by the student's supervisor explaining the special relevance of the work for the field. As a whole, the series will provide a valuable resource both for newcomers to the research fields described, and for other scientists seeking detailed background information on special questions. Finally, it provides an accredited documentation of the valuable contributions made by today's younger generation of scientists.

Theses are accepted into the series by invited nomination only and must fulfill all of the following criteria

- They must be written in good English.
- The topic should fall within the confines of Chemistry, Physics, Earth Sciences, Engineering and related interdisciplinary fields such as Materials, Nanoscience, Chemical Engineering, Complex Systems and Biophysics.
- The work reported in the thesis must represent a significant scientific advance.
- If the thesis includes previously published material, permission to reproduce this must be gained from the respective copyright holder.
- They must have been examined and passed during the 12 months prior to nomination.
- Each thesis should include a foreword by the supervisor outlining the significance of its content.
- The theses should have a clearly defined structure including an introduction accessible to scientists not expert in that particular field.

More information about this series at http://www.springer.com/series/8790

Dong-Sheng Ding

Broad Bandwidth and High Dimensional Quantum Memory Based on Atomic Ensembles

Doctoral Thesis accepted by
University of Science and Technology of China, Hefei, China

Springer

Author
Dr. Dong-Sheng Ding
Optics and Optical Engineering
University of Science and Technology of China
Hefei, Anhui
China

Supervisor
Prof. Bao-Sen Shi
Key Laboratory of Quantum Information
University of Science and Technology of China
Hefei, Anhui
China

ISSN 2190-5053 ISSN 2190-5061 (electronic)
Springer Theses
ISBN 978-981-10-7475-2 ISBN 978-981-10-7476-9 (eBook)
https://doi.org/10.1007/978-981-10-7476-9

Library of Congress Control Number: 2017960203

Printed on acid-free paper

This Springer imprint is published by Springer Nature
The registered company is Springer Nature Singapore Pte Ltd.
The registered company address is: 152 Beach Road, #21-01/04 Gateway East, Singapore 189721, Singapore

To my parents and wife,
and my teachers.

Supervisor's Foreword

Arbitrary electromagnetic fields have linear momentum, spin angular momentum and orbital angular momentum (OAM), and other characteristic features such as pulse width or bandwidth etc. Light carrying OAM has broad applications in microparticle manipulation, high-precision optical metrology, and potential high-capacity optical communications. In the field of quantum information, a photon encoded with information in its OAM degree of freedom enables quantum networks to carry much more information and increase their channel capacity greatly compared with those of current technology because of the inherent infinite Hilbert spaces. Quantum memories are indispensable to construct quantum networks of communication and computation, in which the distant nodes can be made to demonstrate information processing in time synchronization. Storing OAM states has attracted significant attention recently, and many important advances in this direction have been achieved during the past years. This thesis reports some excellent works in five parts of the quantum memory with high-speed and high-bandwidth properties, and the authors demonstrate quantum memories using OAM states, including OAM qubits and qutrits at true single-photon level, OAM states entangled in a two-dimensional and a high-dimensional space, and polarization and OAM entangled state with Raman memory scheme. All achievements described here are very helpful to study high-speed quantum information processing and quantum information encoded in high-dimensional space.

Hefei, China
August 2017

Prof. Bao-Sen Shi

Preface

Since last century, quantum mechanics and information science had produced a cross-subject: quantum information science. In this field, quantum communications can realize absolute security information exchange; it is becoming the next generation of focus in various national security communication systems and has very likely incalculable impacts on human society economic development. In classical communication, information can be transmitted in long distance by using a repeater of direct amplification. In quantum communications, based on quantum entanglement swapping and quantum storage for realizing quantum repeaters, the information could be transmitted in long distance. Thus, quantum memory as a key quantum logic device to realize the storage and release of information, which is one of the key techniques of quantum computation and quantum networks, affects the practical feasibility of quantum communication. In enhancement of storage capacity, quantum memory based on OAM space can significantly improve the capacity of quantum networks and is very promising to high-capacity quantum networks. For high-speed property, Raman quantum memory has the advantages of broadband, which is the key of high-speed quantum networks. This thesis is mainly on the goal of achieving high-capacity, high-speed quantum memory and focuses on experimental research of storing orbital angular momentum, Raman quantum memory, etc. The works in this paper are very promising in high-speed and high-capacity quantum networks in future.

The main content of this thesis includes:

1. Quantum storage of single photon's image. We prepare two cold atomic ensembles via magnetic optical trapping technology, which act as our experimental medium. We prepare the heralded single-photon source through spontaneous Raman scattering in one atomic ensemble and encode the single photon with a spatial structure via a spiral phase plate. Via electromagnetically induced transparency storage scheme, we realize quantum storage of single photon carrying orbital angular momentum and its superposition state. At last, the experimental results show that the property of recovery single photon is

remained, and obtain that its'spatial coherence is maintained in the storage process.

2. Quantum memory of a high-dimensional state of single photon. Based on the realization of quantum storing single photon carrying orbital angular momentum and encoding the input and projecting output state with spatial modulators and a single-mode fiber, we implement the encode, storage, and measurement of high-dimensional state of true single photon in the storage process. In order to perform the storage of qutrit state, we use nine spatial modes to construct the quantum tomography. The results show that our storage is better for qutrit state. Most importantly, we perform the quantum memory of two special qutrit states of true single photon, which gives the quantum state is retained in our memory well.
3. Quantum storage of two-dimensional OAM entanglement. We prepare two-dimensional orbital angular momentum entanglement between a single photon and atomic spin excitation state through spontaneous Raman scattering in one of the two cold atomic ensembles. Via Raman memory scheme, we input this photon into another atomic cloud for storage, and then, we establish the orbital angular momentum entanglement between these two atomic ensembles. In order to check the nature of quantum entanglement, we transfer the atomic spin collective excitation-entangled state into photonic state. Through performing quantum tomography, calculating the fidelity of storage, checking the inequality of CHSH, and verifying the interference of two photons, we obtain that the entanglement of orbital angular momentum is highly retained in the storage process.
4. Experimental realization of high-dimensional entanglement storage. Through spontaneous Raman scattering in one atomic ensemble, we prepare orbital angular momentum high-dimensional entanglement between a photon and an atomic spin collective excitation state. Through Raman storage of the photon, high-dimensional entanglement could be established between these two atomic ensembles. In our experiment, we verify the dimension number of entanglement before and after storage by using an entanglement witness. Via the measurement of 11-dimensional orbital angular momentum (quanta –5 -> 5) modes, the results show that 8-dimensional entanglement is stored in our memory, and there is a 7-dimensional entanglement retrieved.
5. Raman quantum memory of photonic polarized entanglement. We realize two storage processes: (1) Raman quantum memory of single-photon hybrid-entangled state between path and polarization and (2) Raman quantum memory of polarization entanglement. In the first process, we prepare the heralded single photon via spontaneous Raman scattering, encode the single photon into hybrid entanglement with a Sagnac interferometer, and realize storage and retrieval processes. In the second process, via an active locking interferometer, we prepare the photonic polarization and atomic ensemble entanglement and store it with the Sagnac interferometer. At last, through quantum tomography, we calculate the fidelity before and after storage to characterize the properties of entanglement.

The main innovations of thesis are:

1. We for the first time realize quantum memory of orbital angular momentum carried by single photon and its superposition state in the world. The results show that the single photon encoded by a spiral phase plate can be stored in our system and retrieved again, and its spatial coherence is maintained in this process. Our experiment creates a new project in quantum memory and brings a new challenge in quantum information field.
2. We realize quantum memory of high-dimensional state of single photon; in our system, the dimension is three. By using our quantum memory device, the qutrit state of single photon can be stored and retrieved with high fidelity. At same time, we explore the situation of the higher dimensional state of single photon and obtain that the different efficiency for different number of orbital angular momentum must be considered in storing higher dimensional state.
3. We achieve the orbital angular momentum entanglement storage based on two atomic ensembles. Through spontaneous Raman scattering process, we first establish the orbital angular momentum-entangled state and establish the entanglement between two atomic ensembles by performing Raman storage. The results give that the primary quantum network node based on orbital angular momentum two-dimensional subspace is established for the first time, which is very promising for realizing high-dimensional quantum network in future.
4. We firstly realize high-dimensional entanglement storage based on two atomic ensembles. We prepare the high-dimensional entanglement in orbital angular momentum space through spontaneous Raman scattering process and establish the high-dimensional entanglement between two atomic ensembles via Raman storage scheme for the first time. We successfully realize a quantum memory of eight-dimensional entangled state, and the retrieved number of entanglement dimension is seven. We firstly give the feasibility of high-dimensional quantum networks.
5. We realize Raman quantum memory of polarization entanglement in cold atoms for the first time. We realize storing single photon's hybrid entanglement of polarization and path, and also demonstrate quantum memory of two-photonic polarization entanglement. The quantum storage of photonic polarization entanglement is very promising in realization of high-speed quantum networks based on fiber.

Hefei, China
August 2017

Dr. Dong-Sheng Ding

Acknowledgements

At the end of my research career in University of Science and Technology of China, I would like to summarize my five-year research works by publishing this doctoral Thesis. To this occasion, I owe my sincerest gratitude to all teachers and friends we met during my Ph.D.

I offer the sincerest gratitude to the leader of laboratory, Prof. Guang-Can Guo, and he is the earliest scientific researcher in the field of quantum information science in china. His profound knowledge, positive attitude, and passion for scientific research have deeply influenced me. His report every time deeply touched me. Since the beginning of doing scientific research, he had taught us a model of a successful scientific research career, and he provides young researchers a good academic atmosphere and excellent research environment, thus resulting in many achievements in our laboratory. His advice to my research career makes me having not taken a lot of detours on my road, so that I have owned my definition of scientific research. In addition, as an elite teacher especially in quantum information, he is good at teaching according to one's aptitude, explaining the profound course in a simple way, and encourages creativity and innovation. I enjoy the great benefit of his instructions.

I also owe my sincerest gratitude and highest respect to Prof. Bao-Sen Shi, my supervisor. I cannot use words to express my gratitude for Prof. Shi, because he touched me too much. During my Ph.D. study, he guided me to study quantum information, quantum optics, and nonlinear optics, and he also taught me the basic concepts and methods for engaging in scientific research. Prof. Shi has endless passion on scientific research as well as serious and responsible attitude to his graduate students, which influence me deeply. I could still remember that the first time I meet with him, he taught me that: if you wanna do some research, do not be idle. Prof. Shi as a leader in managing our group, go alone to plan our group, make the purchase of laboratory equipment, but also to guide us every day to do experiments. Every experiment is made through discussions with him, and he taught me how to write an article in a scientific journal, how to deal with the recorded data, and how to answer the comments raised by the reviewers; his active thinking, the strict scientific attitude, and the perseverance spirit make my scientific research smooth. We sincerely wish him get more achievements in the scientific research. I wish him and his family health, happy life. and happiness!

The gratitude should be given to many teachers in Key Laboratory of Quantum Information, including Prof. Chuanfeng Li, Prof. Guoping Guo, Prof. Zhengfu Han, Prof. Xubo Zou, Prof. Zhengwei Zhou, Prof. Yongjian Han, Prof. Wei Yi, Prof. Yunfeng Huang, Prof. Yongsheng Zhang, Prof. Fangwen Sun, Prof. Wei Chen, Ms. Huai Ye, Mr. Tao Wang, Mr. Kaimin Duan, Ms. Li Wu. I would also like to express my appreciation to my colleagues Jinshi Xu, Chunhua Dong, Haiou Li, Gang Cao, Shuang Wang, Shengli Zhang, Song Yang, Jinming Cui, Zhiyuan Zhou for their help in study, work and life during my five-year doctoral career. I also thank Mr. Jinghui Wu and Yang Liu for teaching me how to trap and operate cold atoms. Key Laboratory of Quantum Information is just like a big family. Every time when I got lost, confused or frustrated, their humor and wise always cheer me up. I would like to give them all my support and wish them happy forever!

Finally, I would like to be grateful to my parents, my wife, and my children, and it was also them who supported me and made me happy when I was bothered about the work. They are always my greatest spiritual power and the source of happiness.

Contents

About the Author

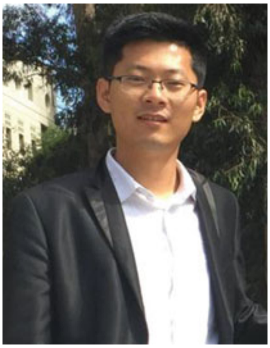

Dong-Sheng Ding received his B.Sc. in Physics from Anhui Normal University, China, in 2006. He obtained his Ph.D. in Optics from the Department of Optics and Optical Engineering of the University of Science and Technology, China, in 2015. His major research project in the Prof. Bao-Sen Shi group is quantum memory based on cold atomic ensemble. Now, he is a Professor in University of Science and Technology, China. His main interests are interactions between the light and atoms, including quantum memory, atomic nonlinearity, Rydberg atoms, and many-body physics.

Acronyms

AFC	An atomic frequency comb is an atomic energy level whose spectrum consists of a series of discrete, equally spaced frequency lines. Frequency combs can be generated by a number of mechanisms, including periodic modulation (in amplitude and/or phase) of a continuous wave laser and stabilization of the pulse train generated by a mode-locked laser
AFG	An arbitrary function generator (AFG) is a piece of electronic test equipment used to generate electrical waveforms. These waveforms can be either repetitive or single-shot (once only) in which case some kind of triggering source is required (internal or external). The resulting waveforms can be injected into a device under test and analyzed as they progress through it, confirming the proper operation of the device or pinpointing a fault in it
AOM	An acousto-optic modulator (AOM), also called a Bragg cell, uses the acousto-optic effect to diffract and shift the frequency of light using sound waves (usually at radio frequency). They are used in lasers for Q-switching, telecommunications for signal modulation, and in spectroscopy for frequency control
CCD	A charge-coupled device (CCD) is a device for the movement of electrical charge, usually from within the device to an area where the charge can be manipulated, for example, conversion into a digital value. This is achieved by "shifting" the signals between stages within the device one at a time. CCDs move charge between capacitive bins in the device, with the shift allowing for the transfer of charge between bins
CHSH	In physics, CHSH stands for John Clauser, Michael Horne, Abner Shimony, and Richard Holt, who described it in a much-cited paper published in 1969 (Clauser et al., 1969). The CHSH inequality can be used in the proof of Bell's theorem, which states that certain consequences of entanglement in quantum mechanics cannot be reproduced by local hidden variable theories

CRIB Controlled reversible inhomogeneous broadening is a scheme of quantum memory, in which optical pumping is used to burn an absorptive hole in the original broad spectrum, and an external magnetic or electric field is added for broadening, so that the broadened absorption spectrum width is controllable

DLCZ Duan–Lukin–Cirac–Zoller is a quantum information protocol, always called as DLCZ protocol or scheme, that is, a scheme that allows the implementation of robust quantum communication over long lossy channels by using laser manipulation of atomic ensembles, beam splitters, and single-photon detectors with moderate efficiencies

DOF In many scientific fields, the degrees of freedom of a system are the number of parameters of the system that may vary independently

ECDL External-cavity diode laser (ECDL) is a compact, efficient laser, which contains external cavities use either a diffraction grating as one end reflector or a piezo-actuator providing fine wavelength tuning

EIT Electromagnetically induced transparency is a coherent optical nonlinearity which renders a medium transparent window over a narrow spectral range within an absorption line. Extreme dispersion is also created within this transparency "window" which leads to "slow light," described below. It is in essence a quantum interference effect that permits the propagation of light through an otherwise opaque atomic medium

FC Fiber-optic collimator, which contains a lens that is either accurately positioned with respect to the fiber or is adjustable. To achieve the best injection efficiency into single-mode fiber, the direction, position, size, and divergence of the beam must all be optimized. With good beams, 70–90% coupling efficiency can be achieved

FORTPT Far off-resonant two-photon transition is a scheme of coupling between light and atoms, the single-photon detuning between light and atoms is far from the resonance transition, but the two-photon detuning is near resonant with atomic levels

FP In optics, a Fabry–Pérot interferometer (FPI) or etalon is typically made of a transparent plate with two reflecting surfaces, or two parallel highly reflecting mirrors. Its transmission spectrum as a function of wavelength exhibits peaks of large transmission corresponding to resonances of the etalon

FWM Four-wave mixing is an intermodulation phenomenon in nonlinear optics, whereby interactions between three wavelengths produce another extra wavelengths in the signal. It is similar to the third-order intercept point in electrical systems. Four-wave mixing can be compared to the intermodulation distortion in standard electrical systems

HBT Hanbury-Brown and Twiss are always used to describe any of a variety of correlation and anti-correlation effects in the intensities received by two detectors from a beam of particles. HBT effects can generally be attributed to the dual wave-particle duality nature of the beam, and the results of a given experiment depend on whether the beam is composed of fermions or bosons. Devices which use the effect are commonly called intensity interferometers and were originally used in astronomy, although they are also heavily used in the field of quantum optics

HWP Half-wave plate shifts the polarization direction of linearly polarized light

LG Laguerre—Gaussian mode are the beam profiles which are circularly symmetric (or lasers with cavities that are cylindrically symmetric) are often best solved using the Laguerre-Gaussian modal decomposition. These functions are written in cylindrical coordinates using generalized Laguerre polynomials. Each transverse mode is again labeled using two integers, in this case the radial index $p \geq 0$ and the azimuthal index which can be positive or negative (or zero)

MOT A magneto-optical trap (MOT) is an apparatus that uses laser cooling with magneto-optical trapping in order to produce samples of cold, trapped, neutral atoms at temperatures as low as several microkelvins, two or three times the recoil limit. By combining the small momentum of a single photon with a velocity and spatially dependent absorption cross section and a large number of absorption-spontaneous emission cycles, atoms with initial velocities of hundreds of meters per second can be slowed to tens of centimeters per second

OAM The orbital angular momentum of light is the component of angular momentum of a light beam that is dependent on the field spatial distribution and not on the polarization. It can be further split into an internal and an external OAM. The internal OAM is an origin-independent angular momentum of a light beam that can be associated with a helical or twisted wavefront. The external OAM is the origin-dependent angular momentum that can be obtained as cross-product of the light beam position (center of the beam) and its total linear momentum

OD Optical depth is the natural logarithm of the ratio of incident to transmitted radiant power through a material, and spectral optical depth or spectral optical thickness is the natural logarithm of the ratio of incident to transmitted spectral radiant power through a material. Optical depth is dimensionless and in particular is not a length, though it is a monotonically increasing function of path length and approaches zero as the path length approaches zero

PBS Beam-splitting polarizers split the incident beam into two beams of differing linear polarization. For an ideal polarizing beamsplitter, these would be fully polarized, with orthogonal polarizations. For many common beam-splitting polarizers, however, only one of the two output beams is fully polarized. The other contains a mixture of polarization states

PMT Photomultiplier tubes (photomultipliers or PMTs), members of the class of vacuum tubes, and more specifically vacuum phototubes are extremely sensitive detectors of light in the ultraviolet, visible, and near-infrared ranges of the electromagnetic spectrum. These detectors multiply the current produced by incident light by as much as 100 million times (i.e., 160 dB), in multiple dynode stages, enabling, for example, individual photons to be detected when the incident flux of light is low

QWP Quarter-wave plate shifts the polarization direction of circularly polarized light

SFWM Spontaneous four-wave mixing is a nonlinear process, whereby interactions between only two pump fields spontaneously produce another two signal fields. This process is always used to generate single-photon source

SMF In fiber-optic communication, a single-mode optical fiber (SMF) is an optical fiber designed to carry light only directly down the fiber—the transverse mode

Chapter 1
Introduction

Abstract Quantum information science is the study of the information processing that may be accomplished by quantum mechanical systems by using all the quantum properties of a physical information carrier. Quantum information science has two main goals: one is the realization of a universal quantum computer, which can help us perform tasks as a classical computer does. The other goal is to realize quantum communication and quantum cryptography networks. Quantum communication can be used to transfer quantum states between remote users, and by quantum cryptography, two legal users can communicate with each other in a secure way. China launched the first-ever quantum communication satellite into space in 2016, and achieved several important advances such as successfully creating and sending entangled photons from space to earth-based ground stations [61]. Quantum memories are indispensable to realize both goals of Quantum information science. In quantum memory, a quantum state such as a single photon, entanglement, or squeezed state of a quantum information carrier is recorded faithfully and recalled on demand. Before introducing the main experimental results on quantum memory, we introduce a brief description of background on quantum information, and quantum memory. Some important parameters of quantum memory, including fidelity, efficiency, bandwidth and capacity etc. are introduced.

1.1 Introduction to Quantum Information

Since the 1980s, quantum mechanics and information science spurred on the interdisciplinary field of quantum information science. It exploits a very important physical principle in quantum mechanics: quantum superposition and non-cloning. In classical information theory, the bit is the fundamental unit. From a physical perspective, a bit is one or other of two identifiable states of a system, e.g., a voltage between capacitor plates in a digital computer can represent information bits, the presence of charge represents 1, and the absence of charge represents 0. The quantum information unit is called qubit, and it is generally a superposition of two ground states, $|\psi\rangle = c_1 |0\rangle + c_2 |1\rangle$, $|c_1|^2 + |c_2|^2 = 1$, and the classical bit can be regarded as a special case of qubit ($c_1 = 0$ or $c_2 = 0$). The most important property by which

D.-S. Ding, *Broad Bandwidth and High Dimensional Quantum Memory Based on Atomic Ensembles*, Springer Theses, https://doi.org/10.1007/978-981-10-7476-9_1

the qubit differs from the classical bit is its coherent superposition. The core goal of quantum information science is to build a quantum computer and quantum network. It promises absolute security and practical long-range quantum communication. A quantum computer is based on the principle of parallel quantum algorithm allowing much faster decoding of complex encryption compared with existing classical computer. In quantum communication, quantum non-cloning theorem would enable us to achieve absolute secure quantum communication in a one-time pad encryption mode [6]. Its absolute security would ensure that user information is not detected. The idea is gradually changing human life and technological outlook with a wide range of prospects in defense and military applications as well as civilian applications. Quantum communication technology represents a strategic direction in future developments of communication technology, and thus has become the focus around the world since its inception.

Quantum communication uses quantum entanglement to connect different quantum nodes to transmit information, including quantum key distribution and quantum teleportation. However, the long-distance distribution of entanglement is affected by decoherence and losses in the fiber or free space. For the most mature and practical quantum key distribution currently available, losses and noise in the transmission channel are inevitable creating exponential decay in signal intensity with increasing transmission distance that seriously compromises quantum state transmission over long distances. A typical example is an optical fiber with losses of 0.2 dB/km used to transmit a single photon over 1000-km distance at 10-GHz photon-repetition rate. The probability of reaching the destination is only 10^{-10} Hz, which means that it takes 300 years to transmit a single photon. With free-space communication systems, communications are confined to stations in line of sight and restricted by weather conditions. These factors can be overcome to a certain extent by establishing satellite and ground stations. However, if the measurement process in key distribution needs to be performed at a satellite, the key distribution process requires third-party participation, which undoubtedly increases the risk of key disclosure and reduces the security of key distribution. To overcome the loss of channel transmission and to eliminate the need for third-party disclosure, users need to use other quantum technologies. Briegel et al. proposed the concept of a quantum repeater to solve this problem [7].

In a quantum repeater, a channel between the two communicating parties is divided into several sub-channels, and the length of each sub-channel is smaller than the characteristic length for losses in the channel. During the communication, a maximum entanglement state can be established between the ends of each sub-channel, and then entanglement switching between adjacent channels can be used to expand communication distances, and thus a maximum entanglement is established between the two parties. Therefore, quantum-repeater technology in principle can be used to achieve long-distance quantum communication. Importantly, quantum memory is required for real-time synchronization in this process to establish entanglement switching between adjacent channels and bring about a polynomial dependence between transmission loss and distance. Entanglement purification achieves long-distance entanglement. Quantum memory is an indispensable device in quantum information processing. Without quantum memory, losses from exponential decay with distance eventually will cause a break-down in communication.

1.2 Brief Introduction to Quantum Memory

Broadly speaking, quantum memory is a system that stores and retrieves quantum states as needed. If a quantum state is prepared or manipulated by photons in the visible or near-infrared band, the quantum memory is commonly referred to as optical quantum memory. Optical quantum memory must be able to store a non-classical light field, such as a single photon, a single-bit quantum state, entanglement or a continuous-variable squeezed state. In this book, we focus on optical quantum memory [43]. The largest field of application for light quantum storage is the network of quantum repeaters. Repeaters are very useful devices in other important areas, e.g., linear optics, single photon sources, and photon detection. To achieve quantum computations based on probabilistic quantum logic gates also requires quantum memory to achieve real-time synchronization [39]. In quantum metrology [26], optical quantum memory establishes an entanglement between two atoms to provide a precise measurement of their states. In addition, quantum memory prepares deterministic single-photon sources.

1.2.1 The Parameter of Quantum Memory

Indices of quantum memory are fidelity, efficiency, lifetime, capacity, bandwidth, and wavelength of storage. Of course, different physical systems have specific requirements.

Storage fidelity: fidelity refers to the degree of overlap between the quantum state before storage and the recovered quantum state. For quantum memory, it is the most important index, as it directly determines whether memory is classical or quantum. The fidelity is always greater for memory that is quantum than classical. In an experiment, the fidelity of quantum memory is estimated by quantum tomography: the density matrix of the quantum state to be stored and recovered is calculated after a measurement on a specific basis vector, and the fidelity of the storage procedure can then be calculated.

Storage efficiency: storage efficiency refers to the probability of recovering a stored single photon, or the ratio of light-field intensities before and after storage. Because it is difficult to obtain single-photon storage efficiency directly from the single process, in a quantum-storage experiment, single-photon detection technology is generally used to accumulate counting statistics of single photons before storage and recovered single photons after storage, and finally calculate the ratio to obtain the storage efficiency.

Storage time: storage time refers to the time difference between recovered photons and input photons. Its limits depend on the lifetime of a memory. In long-distance quantum communication, the storage time is needed to be greater than the time required to achieve a repeater through entanglement swapping [55]. The length of the storage time determines the segmentation distance in a repeater, which is critical to achieving long-distance quantum communication. In actual quantum communication, multi-mode storage can be used to reduce the storage time required in a repeater [9, 16, 17].

Storage capacity: storage capacity refers to the capability for memory to store quantum information and reflects the ability to store uncertain states. If a single photon encoded on a high-dimensional space can be stored in memory, as a result, this memory has the ability to store high-dimensional information as compared with quantum memory that stores two-dimensional information and has a high storage capacity [15, 18, 47]. The high-dimensional information can be encoded in the orbital angular momentum (OAM) degrees of freedom of a photon, and in theory this can be infinite. At present, this field is a research hot-spot.

Storage mode: storage mode refers to different optical modes of stored single photons in space, time, and frequency. It uses space and time compatibility of memory to achieve mutually independent operations for the degrees of freedom in space [16] and the degree of freedom in time [13].

Storage bandwidth: storage bandwidth corresponds to the frequency bandwidth (reflecting the time width of a pulse) [52] and the spatial bandwidth of a mode (corresponding to the number of modes) of memory. Currently, for enhancing bandwidth, the most promising storage scheme is the Raman storage scheme. Its bandwidth can reach THz levels [23, 49], and experiments in regard to storing real single photons have been reported [22]. Presently, the highest reported spiral bandwidth of storage space modes is 15, in which the 7-dimensional modes are of quantum category [14].

Storage wavelength: wavelength refers to the working wavelength band of memory. The typical storage medium is atomic vapor, which operates in the visible band. For example, Rb-atom storage wavelength is in the 780-nm and 795-nm band [10] whereas for the Cs atom the wavelength is in the 852-nm band [52]; the wavelength of the rare-earth-doped crystal Nd:Y2SiO5 is in the 883-nm band [24], and for Pr:Y2SiO5 is in the 795-nm band [12]. These media support states used in quantum memory devices that operate in the optical band. If applied to fibers operating in the telecommunications band, we must achieve frequency conversions between visible and infrared bands. The latest advances have demonstrated a single-photon quantum memory in erbium-doped fiber using infrared photons [54]. This experimental result shows that future quantum memory can be compatible with existing optical fiber communication systems.

1.2.2 Storage Media and Quantum Storage Schemes

The realization of quantum memory is inseparable from the storage medium. Different storage systems work in different storage schemes. The most common storage systems include gaseous atomic ensembles, solid-state-doped crystals, single atom and single-ion systems, and optical micro-resonator systems. There are some other storage systems such as nitrogen-vacancy color centers in diamond, hydrogen atoms, and hybrid systems with molecules. In these storage media, those using gaseous atoms employ storage schemes such as electromagnetically induced transparency (EIT) [10, 28, 63], Raman [19, 20, 22, 23, 40, 44, 48, 49, 52, 53], gradient echo [8, 32], and the non-resonant Faraday effect [35, 36]. The solid-state systems generally employ frequency-based controlled reversible inhomogeneous broadening (CRIB) [2, 3, 41, 45], atomic frequency combs (AFC) [1], and photon-echo schemes [8, 32], where the photon and gradient echo schemes are basically similar in principle, with both using atomic re-phasing to achieve photon re-radiation. However, single-atom and single-ion storage media mainly use resonance absorption and the EIT effect for storage. The optical micro-resonator exploits the mutual coupling of the light field and phonon field in the micro-cavity to realize optical storage, and the basic principle is to use the EIT effect to generate a physical response in the dark state. For storage systems like diamond and hydrogen, the storage scheme currently reported is based on Raman storage [22, 23, 49] far away from resonance.

The storage schemes of these different systems have their own features, but the heart of each scheme is a simple transfer of a photon state onto an atomic ground state with a long lifetime for the purpose of storing the light field. For the atomic ensemble, the two-level atom jumps from a ground state $|\mathrm{g}\rangle$ to an excited state $|\mathrm{e}\rangle$ by absorbing a single photon. Using photon-echo technology, this process can be used to store a photon. However, the storage time of this process depends on the lifetime of the excited state $|\mathrm{e}\rangle$ of the atom. If we want to extend the lifetime, we can transfer the atomic state from an excited state $|\mathrm{e}\rangle$ to a metastable state $|\mathrm{s}\rangle$ using a control light field.

With a single photon interacting with the atomic ensemble, the atomic state of the collective excitation can be expressed as

$$|\mathrm{s}\rangle = \frac{1}{\sqrt{N}} \sum_{i}^{N} c_i \left| g_1 g_2 \cdot \cdot s_i \cdot \cdot g_N \right\rangle , \tag{1.1}$$

where the $c_i\,(i = 1, .., N)$ are complex amplitudes, which determine the propagation of the light field in the atomic ensemble and the position of the atoms. This state corresponds to a spin-like wave (we now called as spin-wave) of the collective excitation. As long as a pulsed control light is used to transfer the atomic state of the spin collective excitation into a photon state, we can perform single-photon recovery process at any time. Different storage schemes have different performances of this process, and some schemes like the AFC process only need two levels.

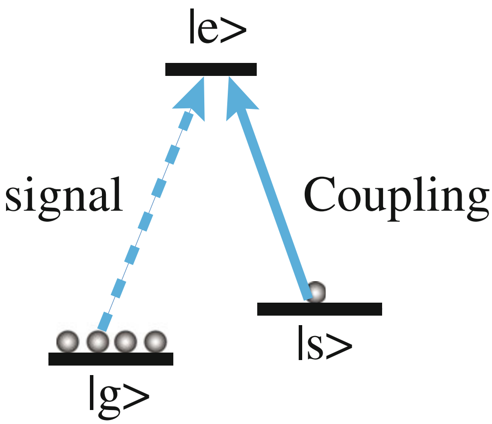

Fig. 1.1 Three-level atom comprising ground state |g⟩, metastable state |s⟩, and excited state |e⟩. Signal denotes the signal field; Coupling denotes the control field. This atomic configuration is the standard atomic Λ energy diagram

For single-atom or single-ion storage systems, a strong interaction between photon and medium can be achieved by placing a medium in a high-precision cavity to demonstrate single-photon storage. It is assumed that the ground state of the single atom in the cavity is |g⟩ and the single-photon input into the cavity is reflected many times. The interaction over the time period is then a direct-product of the interaction of ground states of single atom. Thus, the ground state for N interacting single atoms in the cavity can be written as $|\mathrm{g}\rangle = |g_1 g_2 \cdot \cdot g_N\rangle$. This expression fully expresses the concept of an atomic ensemble.

Here the storage schemes are specifically described:

EIT: the EIT-based storage scheme, illustrated in Fig. 1.1, begins with the absence of the control field and the medium directly absorbing the signal field; when the control light field is turned on, the dispersion characteristics of the medium are changed and the signal field is no longer absorbed by the atom. The group velocity of the signal field is slowed down and the pulse of the signal field is greatly compressed in the medium, determined by the compression ratio c/v_g, where c is the speed of light in the vacuum and v_g is the group velocity for the signal field. When the control light field is turned off adiabatically, the group velocity of the signal field falls to zero, and the partially compressed signal field is transferred to the internal state of atomic ensemble. After a certain period of time, the signal field is directly read out from the internal atomic state when the control light field is turned on again.

Photon-echo: in a two-level medium with inhomogeneous broadening, atoms absorb single photons and transform into excited atomic states. By adding a pump π-pulse at time t, the atomic state undergoes a reverse process. The atomic state can undergo re-phasing and directly radiate photons at time t. In this process, the added π-pulse generates noise from the amplified spontaneous emission, and in general, it is difficult to store single photons for a long time periods for this scheme. Hence CRIB technology is explored to enable low-noise quantum memory (Fig. 1.2).

CRIB: general inhomogeneous broadening reduces the fidelity in the storing process and produces decoherence in the stored atoms. In an inhomogeneous broadened

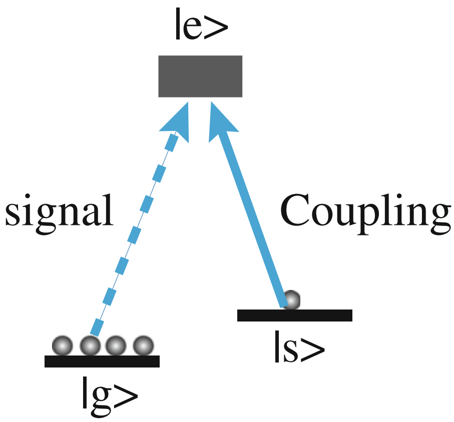

Fig. 1.2 Three-level CRIB atom with ground state $|g\rangle$, metastable state $|s\rangle$ and the excited state $|e\rangle$ which is broadened with large absorption linewidth. Signal denotes the signal field; Coupling denotes the control field

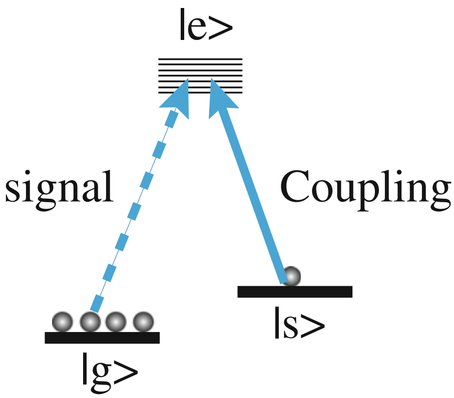

Fig. 1.3 Three-level AFC atom comprising a ground state $|g\rangle$, metastable state $|s\rangle$, and excited state $|e\rangle$. Signal denotes the signal field. Coupling represents the control field. Here, the signal field is modulated-into-comb, thus is composed to standard AFC atomic configuration accompany with control field

medium, optical pumping is used to burn an absorptive hole in the original broad spectrum, and then a magnetic or electric field is added for broadening, so that the broadened absorption spectrum width is higher than the spectral width of the actual signal light. The excited state $|e\rangle$ is artificially broadened (Fig. 1.2). After the signal light is absorbed by the atoms, re-phasing of the excited state is performed at time $t = \tau$ so that the excited state $|e\rangle$ re-radiates the signal photon at time $t = 2\tau$ and thereby effectuates storage and retrieval of photons.

AFC: the atomic frequency comb storage scheme uses the photon-echo principle, which is similar to the CRIB storage scheme but implements re-phasing spontaneously as the comb-like frequency structure of the excited state ensures that a photon radiates naturally at time $2\pi/\Delta$, where Δ is the frequency spacing for the comb. The energy levels are shown in Fig. 1.3.

Raman: The Raman storage scheme is based on a two-photon Raman transition in an atomic medium. The atomic detuning for the control light field is far beyond the natural line width of the excited state, in the presence of the control light field. The media can be excited by a virtual level (see Fig. 1.4); when a signal field is sent under

Fig. 1.4 Three-level Raman atom with a ground state $|g\rangle$, metastable state $|s\rangle$, and excited state $|e\rangle$. Signal denotes the signal field; Coupling is the control field. There is large detuning Δ for both signal and coupling fields

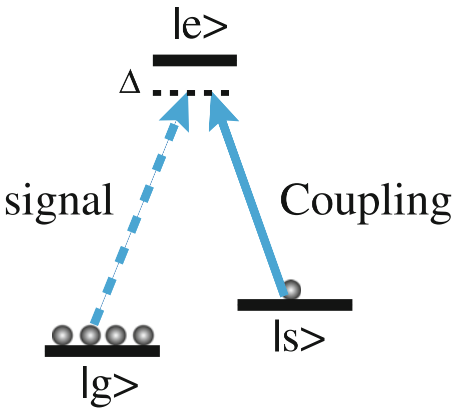

the double-photon resonance conditions, it can be directly absorbed by the metastable state $|s\rangle$ through a virtual level and stored. To retrieve the signal photon, we need to turn on the control light field again to establish a virtual level and transform the atomic state directly into a photonic state. Moreover, the Raman-excited virtual-level bandwidth is broadened by increasing the effective optical thickness of the atoms, and also generally by increasing the control-light-field power. Hence we can use this Raman storage scheme to store ultra-short pulses to accelerate memory access and enhance speeds.

The storage schemes associated with AFC, CRIB, and gradient echo are based on atomic re-phasing, with photon-echo intensities. The non-resonant Faraday storage scheme uses the Raman transition mechanism to realize optical storage. These storage schemes convert a photon state into an atomic internal state and then use the control light field to convert the single photons that we need. The Raman storage scheme is the focus of this book and is described in detail in Chap. 6. All storage schemes tend only to be implementable in a specific storage system, but some storage systems can be implemented in multiple storage scenarios. For example, the atomic ensemble can be simultaneously implemented in the EIT and Raman storage schemes.

An ideal storage medium should have the following two features:

1. High optical density to provide strong interactions between the optical signal and the storage medium to obtain higher storage efficiency;
2. Long coherence times so that quantum states can be retained for long times.

With a large number of atoms in an atomic ensemble, a high optical density is expected. Atomic ensemble includes cold atomic ensemble such as those composed of alkali-metal elements, thermal atomic ensembles, and crystal materials mixed with rare earth elements. The cold atomic ensemble is obtained by laser cooling and trapping technology, which had mature methods in control and use of the EIT [25] and Duan–Lukin–Cirac–Zoller (DLCZ) schemes [21] to demonstrate a quantum memory. At low temperatures, the atoms have low speeds. Decoherence caused by collisions between atoms and atomic diffusion are both weak. A cold atom-based quantum memory has advantages such as high efficiency, high fidelity, and long storage times. Their limitations include small storage bandwidth and weak multi-mode storage capacity in the time domain. The thermal atomic ensemble is simple and easy to realize but, because atoms move at high speed, it has large non-uniform broadening and strong decoherence that is caused by the atomic motion and collisions. In addition, despite using the EIT and DLCZ schemes for storage, the thermal atomic system can use far-detuning to achieve Raman storage [52], and the gradient echo technique for storage [32]. As crystal materials doped with rare-earth elements have long coherence times and large inhomogeneous broadening features, they can achieve long storage times and multi-mode storage operation [2], but nonetheless have small optical thickness because low-temperature equipment is needed. The main storage schemes in crystal materials are CRIB [45] and atomic frequency combs [1]. Although the EIT method is also used for storage, it is relatively difficult to store single photons because to distinguish the frequency difference between ground state and metastable state is difficult. The storage of single photon can also be demonstrated by single atom system. To improve the interaction between photon and atom, atoms are usually placed in a cavity, as described above, so that the probability of collision between photon and atom is increased through resonance [38]. Recall that a single atom has a small collision cross section. The nitrogen-vacancy color center in diamond also achieves optical storage [22], with one major advantage in that it operates at room temperature conditions. Different storage media and different storage methods have their own advantages and disadvantages. A single index is relatively easy to satisfy in a given application, but satisfying a comprehensive range of indices is difficult. In practice, what medium and scheme to use can be determined more readily based on specific applications and requirements.

1.3 Introduction to High-Dimensional State Storage

As mentioned earlier, multi-mode and high-capacity storages are important indices of quantum memory. Theoretical studies show that multi-mode storage in the time domain greatly improves the efficiency of the entanglement distribution in the quantum-repeater process [1] whereas multi-mode storage in the spatial domain greatly reduces the requirements for memory storage time. Hence multi-mode storage has attracted wide attention from domestic and foreign researchers and significant progress has been made in recent years [16, 17, 27, 29, 31, 34, 46, 50, 56]. In this book, Chaps. 2–5 introduce in detail spatial multi-mode storage. In recent years, the main reason why spatial multi-mode storage is highly regarded is its special spatial multi-mode structure. The light field with OAM offers exciting prospects in quantum information applications, because the OAM states of the beam achieve high-dimensional coding that substantially increases the amount of information carried by photons, the speed of information transmitted and processed, and the capacity of quantum networks.

1.3.1 Introduction to OAM Light

The OAM state of the photon is generated in a helical phase front of the electromagnetic wave. The most common mode for OAM-carrying light is the Laguerre–Gaussian (LG) mode. In 1992, Allen et al. observed that photons in different LG modes carry different OAMs [4]. The wavefront of this light is a helical front (see Fig. 1.5) and hence is also called an optical vortex. Around the center of the singularity, the phase increases and the intensity of the light beam also has a special spatial distribution. The electric field distribution for the light in the LG mode normalized using the cylindrical coordinate system is

$$\begin{gathered} LG_p^l(r,\varphi,x) = \sqrt{\frac{2p!}{\pi(|l|+p)!}}\frac{1}{w(x)}\left(\frac{\sqrt{2}r}{w(x)}\right)^{|l|} L_p^{|l|}\left(\frac{2r^2}{w(x)^2}\right)\cdot \\ \exp\left(-\frac{r^2}{w(x)^2}\right)\exp\left(ik\frac{r^2}{2R(x)}\right)\exp\left(-i\left[2p+|l|+1\right]\varsigma\left(x\right)\right)\exp\left(-il\alpha\right) \end{gathered} \tag{1.2}$$

where $L_p^{|l|}$ is the Laguerre polynomial, l the winding number of light, and $(p+1)$ the number of nodes in radial direction; the sign of l represents the direction of winding or chirality. Different OAM states correspond to different spatial distributions of light intensity (Fig. 1.5); the entire set of states forms a complex Hilbert space of infinite dimension. If the photon is encoded in OAM space, and d is the number of orthogonal basis vectors in the Hilbert space, the amount of information that is carried by a single photon can be increased from one bit to qudit. The amount of information carried can greatly increase the rate of information transmitted at a given communication rate: in 2012, Ref [60] reported that a THz-bit information transfer rate was successfully achieved by encoding light pulses in OAM space. It received great attentions within the academic community. Recently, the information transfer rate has increased to 100-THz bits using this same coding method [33]. In quantum communication, we can construct networks with high-dimensional quantum repeaters streaming enormous amounts of information once the storage of high-dimensional encoded photonic states and the quantum swapping operation are achieved. In addition, such encoding technology brings many other applications, such as quantum key transmission [5] and achieving quantum information protocols different from two-dimensional coding, such as quantum holographic teleportation [57], quantum image-dense coding [62], and holographic quantum computing [58]. In the fundamental research of quantum mechanics, the difference between quantum prediction based on high-dimensional coding states and classical predictions is also more direct and clear. Quantum predictions have greater immunity to noise [37]. Moreover, in the EPR paradox test, the efficiency requirements of detectors are lower [59]. Therefore, research on fundamental problems of quantum information and quantum mechanics based on high-dimensional coding has seen significant activity in these fields.

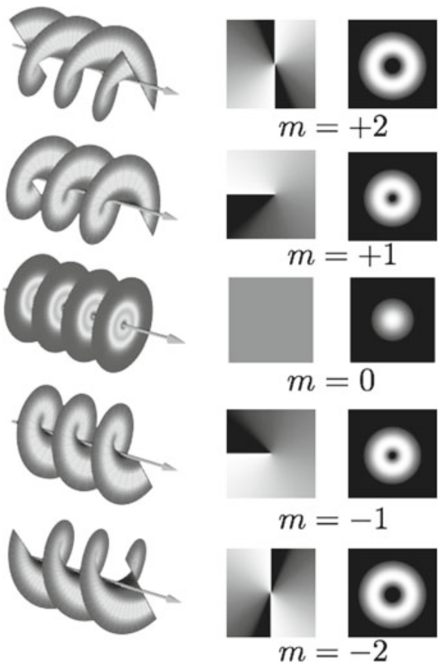

Fig. 1.5 Wavefronts of OAM light are helical structures (left and middle columns), and its light intensity is uniformly distributed radially around its center like an optical vortex (the right column). The vortex light can carry any non-zero m order OAM light. OAM states at different orders are orthogonal. (The above figure is taken from Wikipedia)

1.3.2 Images Storage Progresses

The study of spatial multi-modes begins with how to store image information. The Davidson Group in Israel [51] achieved optical signal storage using a spatial structure and carried OAM information in Rb atomic vapor employing the EIT effect. In 2007, they studied image blurring caused by decoherence resulting from thermal motion of the atoms. Subsequently, the Tabosa Group at University of Cidade, Brazil, used the EIT effect to store signals carrying two different OAM values in a cold atomic ensemble of cesium [46], and they also observed Larmor precession produced by the magnetic field applied in the storage process. In 2008, the Howell Group of University of Rochester [50] used the EIT effect and four-wave mixing to achieve the storage of optical signals with five-peak structures in a thermal Rb atomic ensemble, and demonstrated how to eliminate the impact of diffusion caused by atomic thermal motion on the quality of the stored image. In the same year, the Davidson Group [56] used the EIT effect to achieve the storage of optical signals carrying a digital structure in Rb vapor, and similarly studied how to eliminate the impact of diffusion on image quality by storing optical signals carrying a three-peak structure. The methods given by them show that a π-phase difference between adjacent peaks can improve image quality.

Our group began to focus on image storage problems in 2012, performing research work in this area, and achieved light-pulse storage with a special spatial structure in a cold atomic ensemble using the EIT effect and four-wave mixing [16, 17, 34]. The Laurat Group in France also used cold atomic ensemble to conduct an experimental study on storage of signals with OAM light [42]. They used the EIT effect to achieve storage and reading of light signals carrying OAM in the cold atomic system. The Lam Group of Australian National University used gradient echo technology to achieve storage of light pulses with image information in a thermal atomic ensemble [31]. In a solid-state storage system, image signal storage has been reported; the Halfmann Group in Germany used a Pr3+:Y2SiO5 crystal cooled to 4 K to achieve storage of optical signals carrying digital structure using the EIT effect [29], and in 2013 increased the storage time to one minute [30]. From 2012, researchers began to focus on the storage of optical images with multiple images. NIST researchers used gradient echo technology to achieve the storage of two light pulse sequences carrying two different spatial images in a thermal atomic ensemble [27]. With the capability to read stored information in different orders, they successfully simulated micro-film storage, piquing academic and media attention. Our group also performed storage experimental studies on storing several spatial images, achieved the storage of two beams with space information by multiplexing the angular and frequency degrees of freedom in an atomic ensemble based on the EIT effect. This demonstrated that there was no crosstalk in the images [16, 17]. In 2013, NIST researchers used spatial multiplexing and the gradient echo techniques to store multiple images in a thermal atomic ensemble and realized independent storage and read control of each image [11].

1.4 Summary

In recent years, although many international groups have achieved storage of optical pulses with OAM or special space structures in different physical systems [11, 16, 17, 27, 29–31, 34, 42, 46, 50, 51, 56], all light pulses that were used in the experiments before 2013 were strong light or attenuated coherent light. There has been no report on storing real single photons with space information in any physical system. Storing high-dimensional states of single photons or two-photon entangled state in any physical system has not been undertaken. Achieving quantum storage of quantum and entangled images is actively pursued in the quantum information field. Based on atomic ensembles, the quantum storage of single-photon images and the storage of single-photon high-dimensional quantum states were realized. OAM quantum memory from 2D to high-D entanglements was established in this book. Our experimental results show that high-dimensional quantum memory has been fully achieved in an atomic ensemble-based storage system, which paves the way for future high-dimensional quantum communication networks.

How to use existing technologies to improve communication rates in quantum networks in the future is also a goal we are pursuing. Therefore, in Chaps. 4–6 of this book, the Raman storage scheme has been adopted to illustrate single-photon storage with the purpose to show how to maximize storage speed in single-photon memory devices. We first use the Raman storage scheme to establish storage of two-photon polarization entanglement, and quantum storage of hybrid entanglement between states of single-photon polarization and which-path states. The experimental results provide a foundation for the future high-speed quantum networks.

References

1. Afzelius, Mikael, Christoph Simon, Hugues De Riedmatten, and Nicolas Gisin. 2009. Multimode quantum memory based on atomic frequency combs. *Physical Review A* 79 (5): 052329.
2. Afzelius, Mikael, Thierry Chaneliere, Rufus L. Cone, Stefan Kröll, Sergey A. Moiseev, Matthew Sellars, et al. 2010. Photon-echo quantum memory in solid state systems. *Laser & Photonics Reviews* 4 (2): 244–267.
3. Alexander, A.L., J.J. Longdell, M.J. Sellars, and N.B. Manson. 2006. Photon echoes produced by switching electric fields. *Physical Review Letters* 96 (4): 043602.
4. Allen, Les, Marco W Beijersbergen, RJC Spreeuw, and JP Woerdman. 1992. Orbital angular momentum of light and the transformation of laguerre-gaussian laser modes. *Physical Review A* 45 (11):8185.
5. Bechmann-Pasquinucci, H., and Wolfgang Tittel. 2000. Quantum cryptography using larger alphabets. *Physical Review A* 61 (6): 062308.
6. Bennett, Charles H., and Gilles Brassard. 1984. *Quantum cryptography: public key distribution and con tos5*.
7. Briegel, H.-J., Wolfgang Dür, Juan I Cirac, and Peter Zoller. 1998. Quantum repeaters: the role of imperfect local operations in quantum communication. *Physical Review Letters* 81 (26): 5932.
8. Buchler, B.C., Mahdi Hosseini, Gabriel Hétet, BM Sparkes, and Ping Koy Lam. 2010. Precision spectral manipulation of optical pulses using a coherent photon echo memory. *Optics Letters* 35 (7): 1091–1093.
9. Bussières, Félix, Nicolas Sangouard, Mikael Afzelius, Hugues de Riedmatten, Christoph Simon, and Wolfgang Tittel. 2013. Prospective applications of optical quantum memories. *Journal of Modern Optics* 60 (18): 1519–1537.
10. Chanelière, T., D.N. Matsukevich, S.D. Jenkins, S.Y. Lan, T.A. Kennedy, and A. Kuzmich. 2005. Storage and retrieval of single photons transmitted between remote quantum memories. *Nature* 438 (7069): 833.
11. Clark, Jeremy B, Quentin Glorieux, and Paul D Lett. 2013. Spatially addressable readout and erasure of an image in a gradient echo memory. *New Journal of Physics* 15 (3): 035005.
12. Clausen, C., I. Usmani, F. Bussières, N. Sangouard, M. Afzelius, H. de Riedmatten, and N. Gisin. 2011. Quantum storage of photonic entanglement in a crystal. *Nature* 469 (7331): 508–511.
13. De Riedmatten, Hugues, Mikael Afzelius, Matthias U Staudt, Christoph Simon, and Nicolas Gisin. 2008. A solid-state light-matter interface at the single-photon level. *Nature* 456 (7223): 773–777.
14. Ding, Dong-sheng, Wei Zhang, Shuai Shi, Zhi-yuan Zhou, Yan Li, Bao-sen Shi, and Guang-can Guo. 2016. High-dimensional entanglement between distant atomic-ensemble memories. *Light: Science and Applications*, 5(10): e16157.
15. Ding, Dong-Sheng, Zhi-Yuan Zhou, Bao-Sen Shi, and Guang-Can Guo. 2013. Single-photon-level quantum image memory based on cold atomic ensembles. *Nature Communications* 4.
16. Ding, Dong-Sheng, Wu Jing-Hui, Zhi-Yuan Zhou, Yang Liu, Bao-Sen Shi, Xu-Bo Zou, and Guang-Can Guo. 2013. Multimode image memory based on a cold atomic ensemble. *Physical Review A* 87 (1): 013835.

17. Ding, Dong-Sheng, Wu Jing-Hui, Zhi-Yuan Zhou, Bao-Sen Shi, Xu-Bo Zou, and Guang-Can Guo. 2013. Multiple image storage and frequency conversion in a cold atomic ensemble. *Physical Review A* 87 (5): 053830.
18. Ding, Dong-Sheng, Wei Zhang, Zhi-Yuan Zhou, Shuai Shi, Jian-song Pan, Guo-Yong Xiang, Xi-Shi Wang, Yun-Kun Jiang, Bao-Sen Shi, and Guang-Can Guo. 2014. Toward high-dimensional-state quantum memory in a cold atomic ensemble. *Physical Review A* 90 (4): 042301.
19. Ding, Dong-Sheng, Wei Zhang, Zhi-Yuan Zhou, Shuai Shi, Bao-Sen Shi, and Guang-Can Guo. 2015. Raman quantum memory of photonic polarized entanglement. *Nature Photonics* 9 (5): 332–338.
20. Ding, Dong-Sheng, Wei Zhang, Zhi-Yuan Zhou, Shuai Shi, Guo-Yong Xiang, Xi-Shi Wang, Yun-Kun Jiang, Bao-Sen Shi, and Guang-Can Guo. 2015. Quantum storage of orbital angular momentum entanglement in an atomic ensemble. *Physical Review Letters* 114 (5): 050502.
21. Duan, L.M., M.D. Lukin, J.I. Cirac, and P. Zoller. 2001. Long-distance quantum communication with atomic ensembles and linear optics. *Nature* 414 (6862): 413.
22. Duncan, G., England, Kent AG Fisher, Jean-Philippe W MacLean, Philip J Bustard, Rune Lausten, Kevin J Resch, and Benjamin J Sussman. 2015. Storage and retrieval of thz-bandwidth single photons using a room-temperature diamond quantum memory. *Physical Review Letters* 114 (5): 053602.
23. England, D.G., P.J. Bustard, J. Nunn, R. Lausten, and B.J. Sussman. 2013. From photons to phonons and back: a thz optical memory in diamond. *Physical Review Letters* 111 (24): 243601.
24. Erhan, Saglamyurek, Neil Sinclair, Jeongwan Jin, Joshua A Slater, Daniel Oblak, Félix Bussières, Mathew George, Raimund Ricken, Wolfgang Sohler, and Wolfgang Tittel. 2011. Broadband waveguide quantum memory for entangled photons. *Nature* 469 (7331): 512–515.
25. Fleischhauer, Michael, and Mikhail D Lukin. 2000. Dark-state polaritons in electromagnetically induced transparency. *Physical Review Letters* 84 (22): 5094.
26. Giovannetti, Vittorio, Seth Lloyd, and Lorenzo Maccone. 2011. Advances in quantum metrology. *Nature Photonics* 5 (4): 222–229.
27. Glorieux, Quentin, Jeremy B Clark, Alberto M Marino, Zhifan Zhou, and Paul D Lett. 2012. Temporally multiplexed storage of images in a gradient echo memory. *Optics Express* 20 (11): 12350–12358.
28. Harris, Stephen E., and J.E. Field, and A Imamoğlu. 1990. Nonlinear optical processes using electromagnetically induced transparency. *Physical Review Letters* 64 (10): 1107.
29. Heinze, G., A. Rudolf, F. Beil, and T. Halfmann. 2010. Storage of images in atomic coherences in a rare-earth-ion-doped solid. *Physical Review A* 81 (1): 011401.
30. Heinze, Georg, Christian Hubrich, and Thomas Halfmann. 2013. Stopped light and image storage by electromagnetically induced transparency up to the regime of one minute. *Physical Review Letters* 111 (3): 033601.
31. Higginbottom, Daniel B., Ben M Sparkes, Milos Rancic, Olivier Pinel, Mahdi Hosseini, Ping Koy Lam, and Ben C Buchler. 2012. Spatial-mode storage in a gradient-echo memory. *Physical Review A* 86 (2): 023801.
32. Hosseini, Mahdi, Ben M Sparkes, Geoff Campbell, Ping K Lam, and Ben C Buchler. 2011. High efficiency coherent optical memory with warm rubidium vapour. *Nature Communications* 2: 174.
33. Huang, Hao, Guodong Xie, Yan Yan, Nisar Ahmed, Yongxiong Ren, Yang Yue, Dvora Rogawski, Moshe J. Willner, Baris I. Erkmen, Kevin M. Birnbaum, et al. 2014. 100 tbit/s free-space data link enabled by three-dimensional multiplexing of orbital angular momentum, polarization, and wavelength. *Optics Letters* 39 (2): 197–200.
34. Jinghui, Wu, Yang Liu, Dong-Sheng Ding, Zhi-Yuan Zhou, Bao-Sen Shi, and Guang-Can Guo. 2013. Light storage based on four-wave mixing and electromagnetically induced transparency in cold atoms. *Physical Review A* 87 (1): 013845.
35. Julsgaard, B., A. Kozhekin, and E.S. Polzik. 2001. Experimental long-lived entanglement of two macroscopic objects. *Nature* 413 (6854): 400–403.

36. Julsgaard, B., J. Sherson, J.I. Cirac, J. Fiuràsek, and E.S. Polzik. 2004. Experimental demonstration of quantum memory for light. *Nature* 432 (7016): 482–486.
37. Kaszlikowski, Dagomir, Piotr Gnaciński, Marek Żukowski, Wieslaw Miklaszewski, and Anton Zeilinger. 2000. Violations of local realism by two entangled n-dimensional systems are stronger than for two qubits. *Physical Review Letters* 85 (21): 4418.
38. Kimble, H.J. 2008. The quantum internet. *Nature* 453: 19.
39. Knill, E., R. Laflamme, and Milburn G.J. A scheme for efficient quantum computation with linear optics. *Nature* 409 (8): 46–53.
40. Kozhekin, A.E., Klaus Mølmer, and E Polzik. 2000. Quantum memory for light. *Physical Review A* 62 (3): 033809.
41. Kraus, Barbara, W Tittel, N Gisin, Mattias Nilsson, Stefan Kröll, and JI Cirac.2006. Quantum memory for nonstationary light fields based on controlled reversible inhomogeneous broadening. *Physical Review A* 73 (2): 020302.
42. Lucile, Veissier, Adrien Nicolas, Lambert Giner, and Dominik Maxein, A.S. Sheremet, Elisabeth Giacobino, and Julien Laurat. 2013. Reversible optical memory for twisted photons. *Optics Letters* 38 (5): 712–714.
43. Lukin, M.D. 2003. Colloquium: Trapping and manipulating photon states in atomic ensembles. *Reviews of Modern Physics* 75 (2): 457.
44. Michelberger, P.S., T.F.M. Champion, M.R. Sprague, K.T. Kaczmarek, M. Barbieri, X.M. Jin, D.G. England, W.S. Kolthammer, D.J. Saunders, J. Nunn, et al. 2015. Interfacing ghz-bandwidth heralded single photons with a warm vapour raman memory. *New Journal of Physics* 17 (4): 043006.
45. Moiseev, S.A., and Stefan Kröll. 2001. Complete reconstruction of the quantum state of a single-photon wave packet absorbed by a doppler-broadened transition. *Physical Review Letters* 87 (17): 173601.
46. Moretti, D., D. Felinto, and J.W.R. Tabosa. 2009. Collapses and revivals of stored orbital angular momentum of light in a cold-atom ensemble. *Physical Review A* 79 (2): 023825.
47. Nicolas, A., L. Veissier, L. Giner, E. Giacobino, D. Maxein, and J. Laurat. 2014. A quantum memory for orbital angular momentum photonic qubits. *Nature Photonics* 8 (3): 234–238.
48. Nunn, J., I.A. Walmsley, M.G. Raymer, K. Surmacz, F.C. Waldermann, Z. Wang, and D. Jaksch. 2007. Mapping broadband single-photon wave packets into an atomic memory. *Physical Review A* 75 (1): 011401.
49. Philip J, Bustarrd, Rune Lausten, Duncan G England, and Benjamin J Sussman. 2013. Toward quantum processing in molecules: A thz-bandwidth coherent memory for light. *Physical Review Letters* 111 (8): 083901.
50. Praveen, K., Vudyasetu, Ryan M Camacho, and John C Howell. 2008. Storage and retrieval of multimode transverse images in hot atomic rubidium vapor. *Physical Review Letters* 100 (12): 123903.
51. Pugatch, Rami, Moshe Shuker, Ofer Firstenberg, Amiram Ron, and Nir Davidson. 2007. Topological stability of stored optical vortices. *Physical Review Letters* 98 (20): 203601.
52. Reim, K.F., J. Nunn, V.O. Lorenz, B.J. Sussman, K.C. Lee, N.K. Langford, D. Jaksch, and I.A. Walmsley. 2010. Towards high-speed optical quantum memories. *Nature Photonics* 4 (4): 218–221.
53. Reim, K.F., P. Michelberger, K.C. Lee, J. Nunn, N.K. Langford, and I.A. Walmsley. 2011. Single-photon-level quantum memory at room temperature. *Physical Review Letters* 107 (5): 053603.
54. Saglamyurek, Erhan, and Jeongwan Jin, Varun B Verma, Matthew D Shaw, Francesco Marsili, Sae Woo Nam, Daniel Oblak, and Wolfgang Tittel. 2015. Quantum storage of entangled telecom-wavelength photons in an erbium-doped optical fibre. *Nature Photonics* 9 (2): 83–87.
55. Sangouard, Nicolas, Christoph Simon, Hugues De Riedmatten, and Nicolas Gisin. 2011. Quantum repeaters based on atomic ensembles and linear optics. *Reviews of Modern Physics* 83 (1): 33.
56. Shuker, M., O. Firstenberg, R. Pugatch, A. Ron, and N. Davidson. 2008. Storing images in warm atomic vapor. *Physical Review Letters* 100 (22): 223601.

57. Sokolov, I.V., M.I. Kolobov, A. Gatti, and L.A. Lugiato. 2001. Quantum holographic teleportation. *Optics Communications* 193 (1): 175–180.
58. Tordrup, Karl, Antonio Negretti, and Klaus Mølmer. 2008. Holographic quantum computing. *Physical Review Letters* 101 (4): 040501.
59. Vértesi, Tamás, Stefano Pironio, and Nicolas Brunner. 2010. Closing the detection loophole in bell experiments using qudits. *Physical Review Letters* 104 (6): 060401.
60. Wang, Jian, Jeng-Yuan Yang, Irfan M. Fazal, Nisar Ahmed, Yan Yan, Hao Huang, Yongxiong Ren, Yang Yue, Samuel Dolinar, Moshe Tur, et al. 2012. Terabit free-space data transmission employing orbital angular momentum multiplexing. *Nature Photonics* 6 (7): 488–496.
61. Yin, Juan, Yuan Cao, Yu-Huai Li, Sheng-Kai Liao, Liang Zhang, Ji-Gang Ren, Wen-Qi Cai, Wei-Yue Liu, Bo Li, Hui Dai, et al. 2017. Satellite-based entanglement distribution over 1200 kilometers. *Science* 356 (6343): 1140–1144.
62. Yu Golubeva, T., Yu M Golubev, IV Sokolov, and MI Kolobov. 2006. Quantum parallel dense coding of optical images. *Journal of Modern Optics* 53 (5–6): 699–711.
63. Zhongxiao, Xu, Wu Yuelong, Long Tian, Lirong Chen, Zhiying Zhang, Zhihui Yan, Shujing Li, Hai Wang, Changde Xie, and Kunchi Peng. 2013. Long lifetime and high-fidelity quantum memory of photonic polarization qubit by lifting zeeman degeneracy. *Physical Review Letters* 111 (24): 240503.

Chapter 2
Quantum Memory of Photonic Image and Its' Superposition

Abstract As a critical component device in quantum communications, quantum memory would enable the distribution of quantum information in long-distance node [6]. Single photons are the most perfect candidate of quantum information carriers, thus playing an essential role in quantum information science. Encoding photons with spatial shape through high-dimensional states significantly increases the information carrying capability and network efficiency, because high-dimensional state can implement many protocols, such as high-dimensional quantum communication, that two-dimension cannot [19]. In this chapter, I describe how we demonstrate storing photons carrying images in spatial and frequency multiplexing, and explore the effects in these memory configurations. Then, I introduced the first experimental realization of a true single photon carrying OAM stored via EIT in a cold atomic ensemble. The experiment shows that the non-classical correlated properties between trigger photon and retrieved photon are still retained. The structured profile between input and retrieved photons are strongly similar, giving a high memory fidelity. Most important, the single-photon's spatial coherence during storage exhibits in good-preservation. The resulting data shows that the cold atoms quantum memory has a ability to store spatial structure at the single-photon-level, which opens the possibility for high-dimensional quantum memories.

2.1 Research Motivations on Storing OAM State

As stated in Chap. 1, light carrying OAM exhibit a helical structured phase in wavefront, which is strongly different from Gaussian beam. Due to this special property, laser with OAM has many exciting applications, including optical communications [14, 16], trapping of particles [21, 22], in which the angular momentum of light can be transferred from photon to microscopic particle, and astrophysics [1, 5]. In quantum information and quantum optics, photons encoded with information in its OAM degrees of freedom (DOF) [29, 33], enable networks to carry significantly more information and considerably increase their capacity. Moreover, these higher-dimensional states enable more efficient quantum-information processing, while two-dimensional

D.-S. Ding, *Broad Bandwidth and High Dimensional Quantum Memory Based on Atomic Ensembles*, Springer Theses, https://doi.org/10.1007/978-981-10-7476-9_2

state cannot. Establishing a quantum network involves building the coherent interaction [27] between light and matter.

There are already some experiments based on such light-matter interfaces, for example, establishing OAM entanglement of a photon and collective atomic spin excitation [8, 26] and storing light in matter [2, 12, 17, 23–25, 38, 41, 43]. Recently, light carrying OAM or a spatial structure has been stored via EIT in an atomic ensemble [12, 38, 41, 43], in a cryogenically cooled doped crystal [23], via gradient echo technique in an atomic ensemble [17, 24, 25], and using AFC techniques in solids doped with rare-earth-metal ions [2]. At beginning, people were to explore the image dynamics evolution in the storage process such as [36, 38, 41], for a problem how to eliminate the diffusion effect for an arbitrary image.

However, these important works reported before 2013 involve bright sources. Our group and Laurat's group focus on storing such light at near single-photon levels [11, 40] in that time, but still the input field is a strongly attenuated laser (weak coherent field), not a true single photon. In quantum information science, the reversible transfer of a quantum state between a true single photon and matter is essential, as it is a crucial resource in operating quantum repeaters, it has the potential to overcome distance limitations of quantum communication schemes within transmission losses. Ref. [20] shows theoretically that the transverse as well as longitudinal DOF constitute a valuable resource for multimode quantum memories with excellent capacities, in which they claims that forward quantum memories possess excellent scaling with the physical parameters: quadratic scaling with the Fresnel number and even cubic with the optical depth of the atomic ensemble. This predicted scaling is better than the previous work. Thus, how to store photon's OAM and explore the ability of high-dimensional state in experiment is significant and interesting.

In this chapter, we mainly introduce how we realize a quantum memory of true single photons carrying spatial modes. I will elaborate the main results, including trying to demonstrate multi-mode quantum memories by using a fast camera (ICCD), encoding photons with OAM degree of freedom and storing them. In first section, we introduce multi-mode quantum memory by using spatial and frequency degrees of freedom. Then, I introduce the technique of generating true single photons and how to verify whether or not they are quantum. In the third section, I describe how we perform quantum storing heralded single photon encoded in OAM spiral phase. In last section, the most important coherent property of superposition of OAM state is verified to be maintained well before and after storage.

2.1.1 Image Storage with Coherent Field

Try to establish heralded entanglement between two remote quantum memory includes two elementary processes, one is sending photons from two remote quantum memories to meet each other; another is the Bell state measurement once the photons met. The time needed to implement these two processes is dependent on the probability of photons met and the Bell state measurement succeeded. If the memory can work on in multimode configuration as proposed by [39], that means it can simultaneously store N photons, thus actually can make the system into multiplexing procedure. This thereby increase the probability for entanglement creation per round-trip time by a factor of N, in other words, the time to build entanglement between adjacent nodes can be decreased by N-fold.

If considering the multimode as a high-dimensional state, a quantum memory which could store spatial multimodes or images is very useful because it could dramatically increase the channel bit rate. Additionally, quantum memories that are able to store multiple optical modes offer advantages over single-mode memories in terms of speed and robustness, leading to higher efficiencies in quantum communication and computation experiments [37, 39]. A promising way of storing multiple optical modes is to store the different optical modes in different atomic collective spin excitation states, which could, for example, be realized by a Λ three atomic level configuration. For quantum memory as collective spin excitation states of atomic ensemble, different photonic multimode state, such as optical path in K-vector space, the frequency mode or polarization space and others' DOF, can be stored as different modes of atomic collective spin excitation states that evolves different fashioned behavior. Finally, this collective spin excitation modes can be readout without cross-talk.

In this section, we have a try to demonstrate multimode in K-vector space and frequency space, by using a tripod configuration of atoms. There has been some related progress along this direction [30, 42], the collective spin excitation state can be coherently evolved and manipulated in polarization DOF. However, in our motivations, the different images under different K-vector and frequency spaces can be coherently stored and retrieved, showing no cross-talk in such related complex quantum memory system. The development of multimode quantum image memories should be an important step towards the realization of multimode quantum networks, and is helpful to high-dimensional quantum networks.

2.1.1.1 Spatial and Frequency Multiplexing Modes Quantum Memory

2.1.1.2 Experimental Details for Time Sequence and Detection

Figure 2.1a shows the schematic experimental setup. A double-tripod atomic configuration time sequence shown in Fig. 2.1b, c are used to perform the image storage experiment under K-vector space and frequency space. A cigar-shaped atomic cloud of Rubidium 85 atoms, trapped in a two-dimensional magneto-optical trap (MOT), was used as our memory medium. The size of cloud was about $30 \times 2 \times 2\,\mathrm{mm}^3$ estimated by atomic fluorescence imaging. The total atom number was measured as 9.1×10^8 by detecting the absorption line as mentioned in [44]. The probe fields (probe 1 and 2) and the write (W) or read (R) beam from an external-cavity diode laser (ECDL, DL100, Toptica) had the same wavelength of 795 nm.

The probe fields were imprinted a real image through a standard resolution chart (USAF target). There are two types of optical element with negative and positive

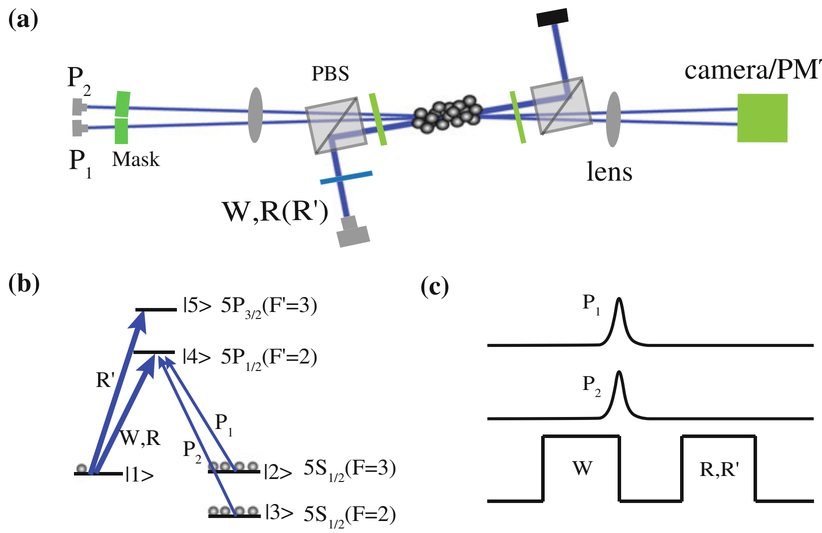

Fig. 2.1 **a** Experimental setup for multimode quantum memory. Energy levels $|1\rangle$, $|2\rangle$ denote atomic metastable state, $|3\rangle$ represents the atomic ground state, $|4\rangle$ and $|5\rangle$ are the atomic excited states respectively. For demonstrating multi-mode quantum memory in spatial domain, probe 1 and probe 2 fields are in same frequency, both coupling atomic transition $|2\rangle \rightarrow |4\rangle$. For performing multi-mode in frequency domain, one of probe fields P2 is switched to be resonant with atomic transition $|3\rangle \rightarrow |4\rangle$. All fields are modulated by series of acoustic-optical modulators (AOM) to generate proper pulses. **b** Experimental energy diagram including double tripod energy levels. **c** Timing sequence. Probe fields are modulated by acoustic-optical modulators to form a Gaussian pulse sequence. The W field writes the probe fields into the atomic collective spin excitation states and the R, R fields read them out

transmissions given by Fig. 2.2. Actually, we used the positive plate shown in Fig. 2.2b to create high-resolution images for each probe beam.

The other read R' beam from another ECDL has the wavelength of 780 nm, which is used for implementing delayed FWM mixing process. Probe 1 ($P1$) and Probe 2 ($P2$) couple the atomic transitions of $5S_{1/2}(F = 3, m_F = -3) \rightarrow 5P_{1/2}(F = 2, m_F = -2)$ resonantly, in which Probe 2 can be switched to resonant transition $5S_{1/2}(F = 2) \rightarrow 5P_{1/2}(F = 2)$ for multimode quantum memories in frequency space. W or R fields are resonant with the transitions of $5S_{1/2}(F = 3, m_F = -1) \rightarrow 5P_{1/2}(F = 2, m_F = -2)$ respectively. The R' field couples the atomic transition of $5S_{1/2}(F = 3) \rightarrow 5P_{3/2}(F = 3)$ for reading the spinwaves out. There are four EIT processes, including $|1\rangle$, $|2\rangle$ and $|4\rangle$ for multimode memory under same frequency, $|1\rangle$, $|3\rangle$ and $|4\rangle$ for multimode memory with 3 GHz frequency difference, and $|1\rangle$, $|2\rangle$ or$|3\rangle$ and $|5\rangle$ are corresponding to the situations with multimode quantum memory with a frequency conversion process. P1 and P2 have the same linear polarizations and copropagate with a small angle of 0.1°. The angle between P1 and the read beam is about 2.5°; their polarizations are orthogonal. The W, R, and R' beams have

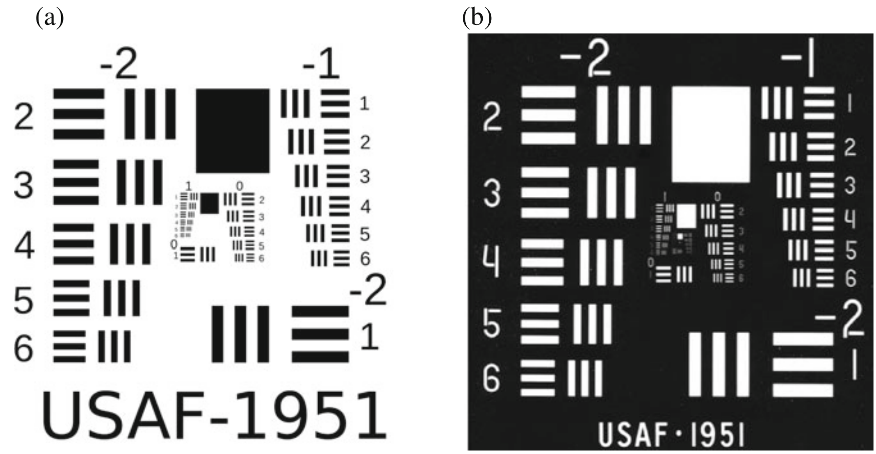

Fig. 2.2 Standard-resolution of USAF target, **a** and **b** are the negative and positive plates

the same linear polarizations. The noncollinear configuration used in the experiment significantly reduces the noise from the scattering of the write or read light.

We used two photomultiplier tubes (PMTs) (Hamamatsu, H10721) to detect the intensities of probe fields in the time domain respectively and used a time-resolution camera (CCD, 1024 × 1024, iStar 334 T series, Andor) to monitor theirs spatial structure before and after storage. The CCD can work in high-speed triggered mode only switching to external trigger DDG mode, actually we apply one trigger with respective to single pulse. By adjusting a quarter-wave plate (QWP) before the MOT, the write or read and probe fields were assigned opposite circular polarization. Using a QWP after the MOT, the fields were later reversed to have orthogonal linear polarization, thus be beneficial to sort probe and R (or W) fields. These polarization configuration not only can satisfy the EIT atomic energy configuration, but also can be used to reduce the cross-talk between probe beams and W, R, and R' beams.

2.1.1.3 4-F Imaging Setup

In demonstrating image quantum memory, we should measure the two-dimensional structured profile of light pulse before and after storage. In order for that, we use a standard method of 4-F imaging system shown in Fig. 2.3, we also give a simple theoretical description of such 4-F imaging system. Figure 2.3 shows a simplified diagram, which consists of three planes of a mask plane, a transform plane, an image plane, and two optical elements of lenses (lens 1 and lens 2). $U_{Input}(x, y)$ stands for the function of the image at the mask plane, $U_T(\xi, \eta)$ is at the transformed function by the lens, and $U_{Output}(x', y')$ is at the image plane. x, y, ξ, η, x' and y' represent two-dimensional coordinates of each plane respectively.

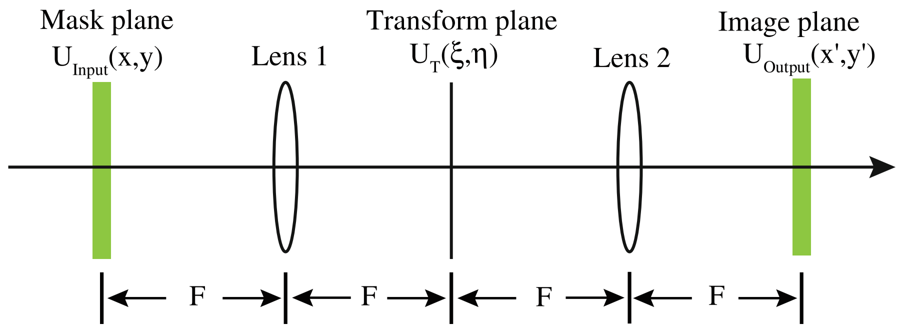

Fig. 2.3 4-F imaging system configuration for measurement spatial structure

Through lens 1 with a focal length of F, the diffracted image at the transform plane can be expressed as

$$U_T(\xi,\eta) \propto \int\int U_{Input}(x,y)exp(-i\overrightarrow{k}_{p,Input}\frac{x\xi+y\eta}{F})dxdy \tag{2.1}$$

Considering the phase matching of the EIT storage processes with same $\overrightarrow{k}_{p,Input}$ direction for output vector $\overrightarrow{k}_{p,Output}$ if not considering the nonlinear distortion of image, we obtain the retrieved diffracted image at the transform plane

$$U'_T(\xi,\eta) \propto \int\int U_{Input}(x,y)exp(-i\overrightarrow{k}_{p,Output}\frac{x\xi+y\eta}{F})dxdy \tag{2.2}$$

where the phase matching condition $\overrightarrow{k}_{p,Output} = \overrightarrow{k}_{p,Input}$ in storage process is considered. The inverse Fourier transform of above equation is

$$U_{Input}(x,y) \propto \int\int U'_T(\xi,\eta)exp(i\overrightarrow{k}_{p,Output}\frac{x\xi+y\eta}{F})d\xi d\eta \tag{2.3}$$

After passing through lens 2, with focus length of F, the image at the image plane can be expressed as

$$U_{Output}(x',y') \propto \int\int U'_T(\xi,\eta)exp(i\overrightarrow{k}_{p,Output}\frac{x\xi+y\eta}{F})d\xi d\eta \tag{2.4}$$

We can obtain the relation $U_{output}(x,y) \propto U_{Input}(-x,-y)$. This illustrates the output is a conjugate image to the input image with a high fidelity. In addition, if there is a difference between the vector modes of $\overrightarrow{k}_{p,Input}$ and $\overrightarrow{k}_{p,Output}$, we also can explore the diffusion and decoherence in quantum memory [36]. In some pratical applications, people maybe search methods to avoid the distortion between input and output images, such as eliminating atomic diffusion, and medium dispersion in light and matter interaction.

2.1.1.4 Multiplexing Image Storage

In order to capture the stored image with fast pulse and the retrieved image, we use a electric signal with TTL pulse to trigger ICCD, and turn the detection window (we set 2 μs) to cover the pulses of probe beams completely. In this way, there is no signal detected if the probe pulses and the detection window of ICCD are not matched. The W, R field and R' field are 3 mm in diameter and cover probe beams completely. If we use the R field as read light, the retrieved signals have a wavelength of 795 nm. The signals detected by PMTs are shown in Fig. 2.4a. The storage efficiency of probe 1 is $\eta_1 = 0.098$; the storage efficiency of probe 2 is $\eta_2 = 0.023$. Here the storage efficiency is defined as the ratio between the areas under the retrieved probe

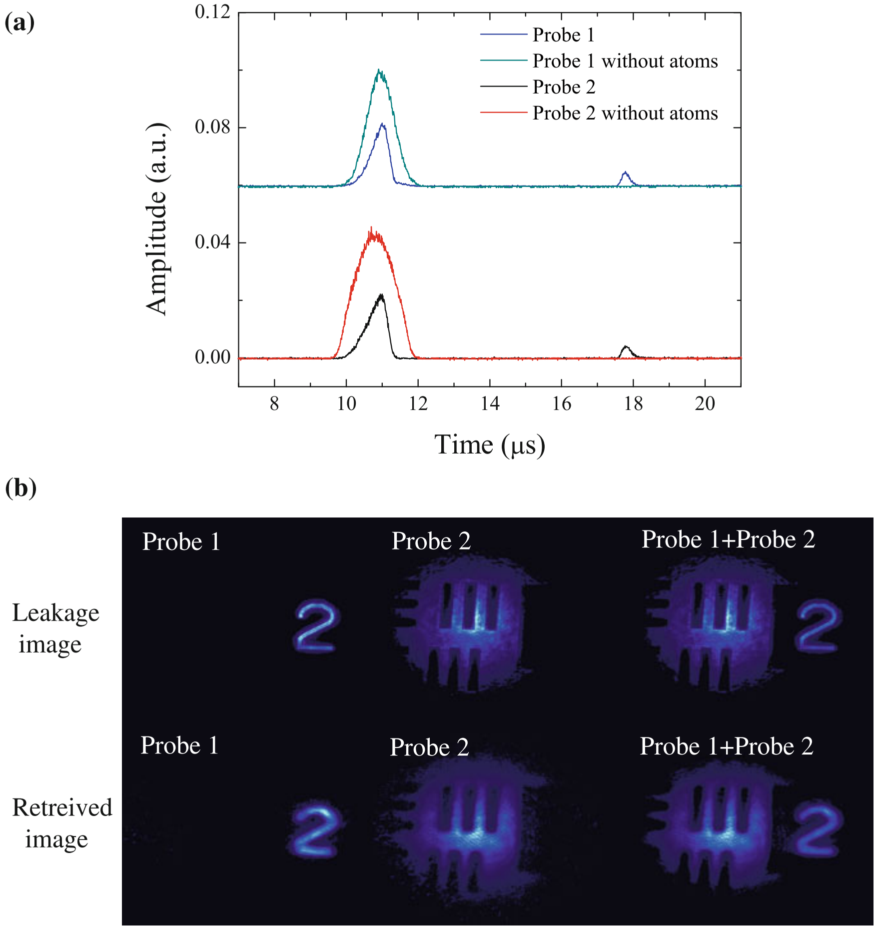

Fig. 2.4 **a** The intensities of the leakage and retrieved probe fields recorded by two PMTs. The green dotted line (top) is probe 1 without atoms and the blue solid line (top) is the storage of probe 1. The red dotted line (bottom) is probe 2 without atoms and the black solid line (bottom) is the storage of probe 2. **b** The leakage and retrieved images monitored by ICCD. Each image is the sum of the 50 retrieved images. The exposure time of ICCD camera was 1.0 s. Probes 1 and 2 are stored for about 6.7 μs. The power of the W or R field is 100 μW and the R field is 140 μW

profile and the input probe's without atoms. Then, we change the PMTs to ICCD for detecting its' spatial profile. The retrieved images are measured in Fig. 2.4b. The left column corresponds to the storage of probe 1 and the middle column to the storage of probe 2. The case of probes 1 and 2 being simultaneously stored and retrieved is shown in the right column of Fig. 2.4b. There is almost no difference between the leakage images and the retrieved images. In order to know whether or not the memory can store multimode images well. We calculate the similarity *R* of the retrieved images compared with the leakage images in the case of probes 1 and 2 being simultaneously stored and retrieved using the following formula

$$R = \sum_m \sum_n A_{mn} B_{mn} / \sqrt{\sum_m \sum_n A_{mn}^2 \sum_m \sum_n B_{mn}^2} \tag{2.5}$$

where A_{mn} and B_{mn} are the gray scale intensities recorded for pixels m and n of the two images to be compared, which is calculated with a factor of 96%[17].

This process can be used to realize the function of a beam splitter in frequency domain, by which the superposition of the different images at different frequencies is obtained. The superposition state is consisting of the leaked part with wavelength of 795 nm and the retrieved part with the wavelength of 780 nm with the frequency conversion. It is worth illustrating that efficiency of the frequency conversion is much higher than that achieved through a four-wave mixing in an atomic system. The frequency conversion in this work is essentially a four-wave mixing, a process which is split into two delayed parts, with a long-lived coherence in the atoms connecting the storage and retrieval processes. The atoms are coherently prepared during the process of storage. It has been demonstrated previously that coherently prepared media may enhance nonlinear optical interaction [6, 32]. Therefore, the efficiency is much higher compared with other works. Although the wavelength difference between the input image and the converted image is only about 15 nm in our experiment,we could realize the frequency conversion of images between different wavelength bands by selecting suitable atomic energy levels or selecting a suitable atom. For example, if the energy level of 6p of the ^{85}Rb atom is considered, then the image could be transferred from a light in the near infrared band (795 nm) to a light in the ultraviolet band (420 nm) or vice versa. As the whole experimental system could be much simplified and miniaturized, thus the experiment can not only be done in a cold atomic ensemble, but also can be realized in a hot atomic ensemble.

In addition, the retrieved interference phenomenon is observed under the condition that the probes 1 and 2 have same frequency. This process shows the atomic ensemble quantum memory device can store multiplexing probes coherently. But this needs to be checked further for the true single photons, which is described in the following section. In addition, the multiplexing can be either temporal, spectral or spatial and etc. Importantly, exploiting this multimode capacity requires the ability to do a selective recall of any of the stored modes [39] (Fig. 2.5).

2.1.1.5 Down to Single Photon Level

For quantum information science, we need to store light at single photon level, thus, we gradually reduced the power of the probe fields with attenuation, and record the retrieved images of probes. The quantum efficiency of ICCD at 795 nm is ∼25%, which can work under single photon level with heralded mode (the trigger signal is the electric pulse from AFG 3252, this signal also trigger the AOM inserted in

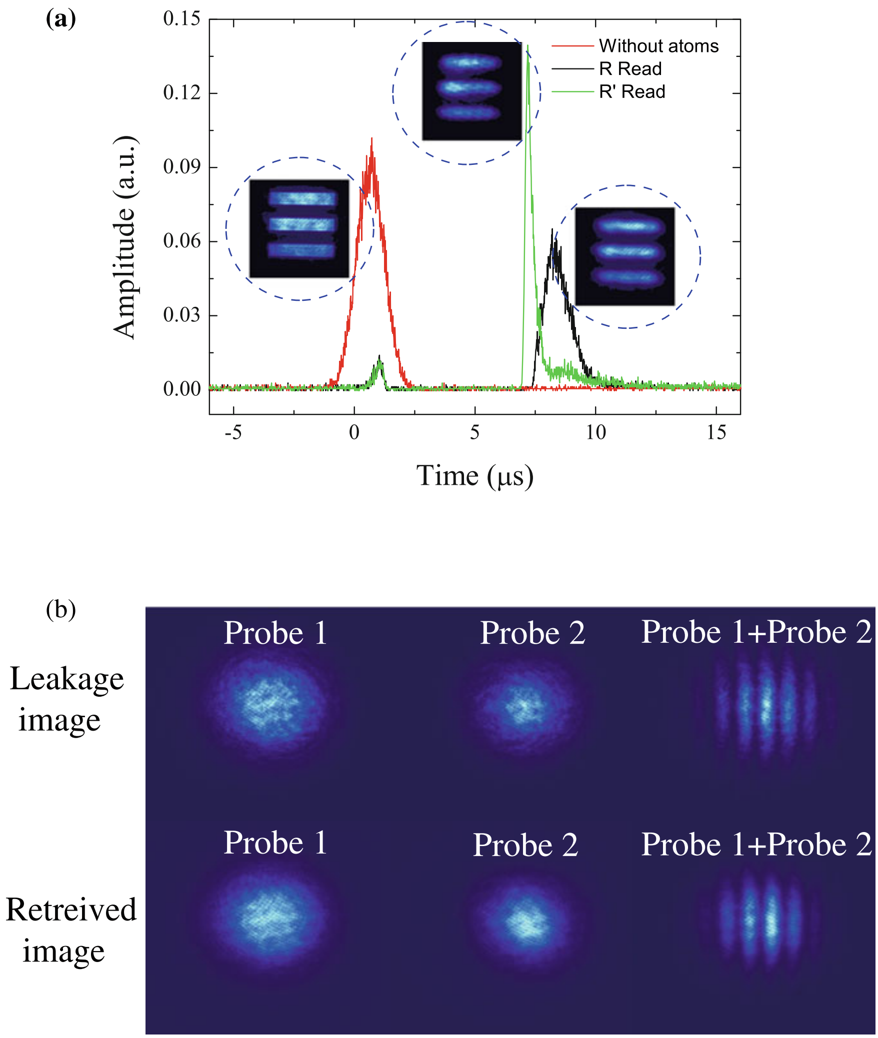

Fig. 2.5 **a** The stored collective spin excitation state can be read out by using different read fields R and R', with corresponding wavelengths of 795 and 780 nm. **b** The leaked and retrieved images under Probes 1 and 2 of same frequencies

optical path of probe field). Figure 2.6b–g corresponds to the storage of a pulse with 305, 162, 80, 40, 22, 10 and 5.3 photons, respectively. Even when storing the probe pulses with 1.2 photons, in Fig. 2.6h we can clearly observe the retrieved images. The composite images shown herein were obtained by omitting the background. The exposure time of the ICCD camera was 1.0 s.

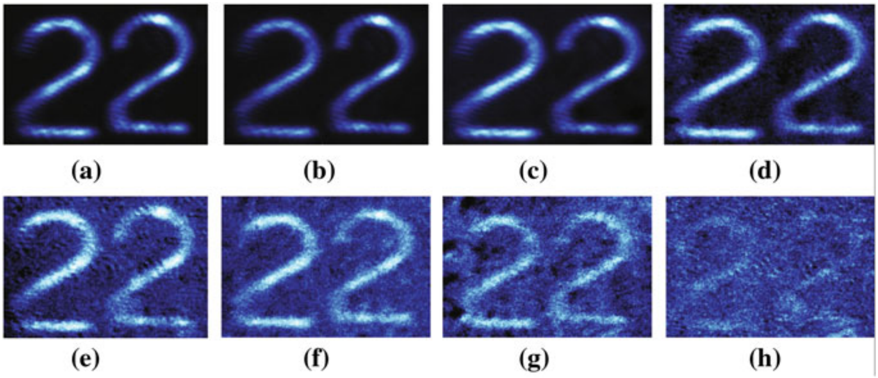

Fig. 2.6 Composite retrieved few- and single-photon images. The storage time for all images was 1.826 μs. In each panel, the left composite image was obtained from probe 1 and the right image from probe 2. In panels **a**–**c**, each composite image represents the sum of 50 retrieved images following storage of **a**: 305, **b**: 162, and **c**: 80 photons per pulse. In panels **d** and **e**, storage was 40 and 22 photons per pulse, respectively, and each picture is the sum of the 200 retrieved images. **f** Storage of 10 photons per pulse (sum of 500 retrieved images); **g** Storage of 5.3 photons per pulse (sum of 1000 retrieved images); **h** Storage of 1.2 photons per pulse (sum of 1000 retrieved images)

2.1.2 Image Storage with Heralded Single Photon

Storing true single photon carried by OAM or image information is essentially significant because this is a proof of for realizing high-dimensional quantum networks, in which a quantum memory that store high-dimensional state is needed. The previous works we have done as described in above section show there are no cross-talk between multiplexing K-space, and the near single photon level multimode quantum memory is verified under an obvious visibility. But for demonstrating quantum memory of true single photon carried by high-dimensional information, it is difficulty to prepare the single photons we needed, and precisely match the bandwidth of photons and the memory, and synchronize the time sequence of storage. Whether or not the spatial coherence of true single photon can be retained in storage is a challenging work and an interesting question. For this purpose, we construct an experiment including heralded single photon preparation, OAM encoding and OAM storage processes. The details are shown in the following subsections.

2.1.2.1 Experimental Preparation of Heralded Single Photon

2.1.2.2 Generation Single Photon

Generating heralded single photons are through SFWM in a cigar-shaped atomic ensemble, see Fig. 2.7a. SFWM process is based on a double-lambda configuration shown by the inset of Fig. 2.7a, where the states used were $|1\rangle$, $|2\rangle$, $|3\rangle$ and $|4\rangle$,

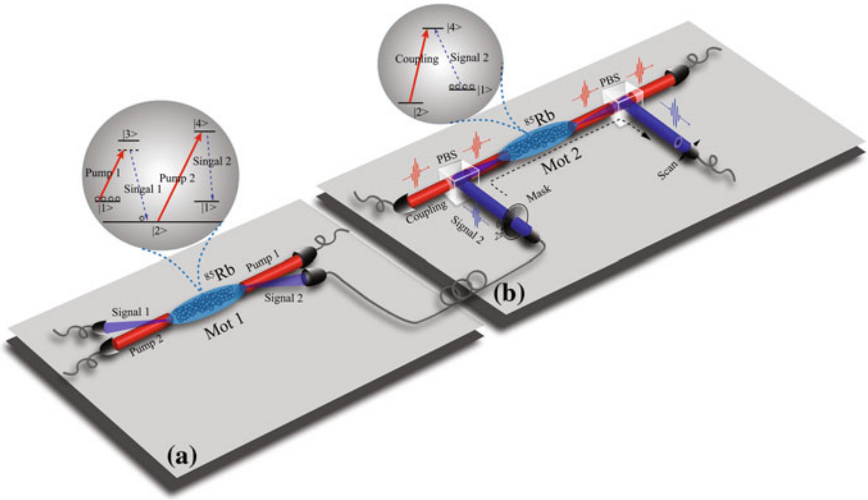

Fig. 2.7 Experimental setup for storing OAM state. **a** Simplified diagram depicting the generation of non-classical photon correlations using SFWM. MOT: magneto-optical trap. **b** Photon storage diagram. PBS: Glan-Taylor polarisation beam splitter with the extinction ratio of $10^5 : 1$. Inset in **a** and **b**: energy level diagrams for SFWM and EIT respectively

corresponding to energy levels $5S_{1/2}(F = 3)$, $5S_{1/2}(F = 2)$, $5P_{3/2}(F = 2)$ and $5P_{1/2}(F = 3)$ respectively. Pump 1 was from an external-cavity diode laser (DL100, Toptica), operating at wavelength 780 nm, with red-detuned at 79 MHz to the atomic transition of $5S_{1/2}(F = 3) \rightarrow 5P_{3/2}(F = 2)$. Pump 2, from another external-cavity diode laser (DL100, Toptica), operating at wavelength 795 nm, coupling the atomic transition $5S_{1/2}(F = 2) \rightarrow 5P_{1/2}(F = 3)$ resonantly. Under the orthogonal polarization of two pumps, signals 1 and 2 were also oppositely polarized due to the spin angular momentum conversation in SFWM process. The power of pumps 1 and pump 2 were 54 μW and 0.65 mW respectively. The *OD* of MOT 1 was about 8. Under conditions of phase matching and conversation of energy, the generated photons of signals 1 and 2 were non-classically correlated in the time domain. In the experiment, signal 1 and signal 2 photons were coupled into two single-mode fibers (SMF) with a 90 coupling efficiency. We performed our experiment with a repeat rate of 100 Hz. The atomic trapping time was 8 ms, the experimental window was 1.5 ms, and another 0.5 ms was used to prepare the initial state.

In each path of signal 1 and 2 fields, we insert interference filters (50 transmission) and home-made Fabry-Perot (FP) etalons (each path has two etalons, each FP had a transmission efficiency of 83% and a 500-MHz bandwidth) to reduce noise. Subsequently, signal-1 photons were detected by a single-photon detector (Avalanche diode, PerkinElmer SPCM-AQR-15-FC with efficiency.) whereas signal-2 photons were stored for followup experiments. After having been stored for a specified time, the retrieved signal-2 photon was detected by another single-photon detector (Avalanche diode, PerkinElmer SPCM-AQR-15-FC with efficiency.). Both of the outputs from both detectors were all TTL signal, which were converted into NIM signal and connected to a time-to-digital converter (Fast Comtec. P7888) with 1 ns bin-width to measure the cross-correlation function $g_{s1,s2}(\tau)$.

Usually classical light satisfied the following equation [28]:

$$R = \frac{[g_{s1,s2}(\tau)]^2}{g_{s1,s1}(0)g_{s2,s2}(0)} \leq 1 \tag{2.6}$$

where $g_{s1,s2}(\tau)$, $g_{s1,s1}(0)$, and $g_{s2,s2}(0)$ were the normalized second-order cross-correlation and auto-correlation of the photons respectively. The normalized $g_{s1,s2}(\tau)$ can be obtained by normalizing the true two-photon coincidence counts to the accidental two-photon coincidence counts $g_{s1,s2}(\infty)$. With $\tau = t_{s1} - t_{s2}$ the relative time delay between paired photons, the maximum $g_{s1,s2}(\tau)$ we obtained in the experiment was $g_{s1,s2}(\tau) = 200 \pm 4$ at $\tau = 19$ ns. Thus, the corresponding Cauchy-Schwarz inequality factor $R = 10000 \pm 400$ was much larger than 1 using the fact that $g_{s1,s1}(0)$, $g_{s2,s2}(0) \leq 2$ (photons from signals 1 and 2 exhibited photon statistics typical of thermal light). The Cauchy-Schwarz inequality is strongly violated, clearly demonstrating a non-classical correlation between photons. The full-width at half-maximum of the cross-correlation function was 32.5 ns, so we estimated that the frequency full bandwidth at half maxim of the photon was $\sim$30 MHz. The photon bandwidth could be tuned for example by changing the Rabi frequency of the pump beam [3].

Before storing single photon, we verified the single-photon property of the signal photon by performing the Hanbury-Brown and Twiss (HBT) experiment on signal 2 photon [7, 19]. Experimentally, we obtained an α value of 0.025 ± 0.005 for the signal photon. For an ideally prepared single-photon state, α tends to zero, for a classical field, $\alpha \geq 1$, based on the Cauchy-Schwarz inequality [7, 19]. A pure single photon has $\alpha = 0$ and a two-photon state has $\alpha = 0.5$. Therefore $\alpha < 1.0$ violates the classical limit and $\alpha < 0.5$ suggests the near-single-photon character. Here the anti-correlation parameter

$$\alpha = P_1 P_{123}/P_{12} P_{13}, \tag{2.7}$$

was given by the ratio of various photoelectric detection probabilities which were measured by the set of detectors $D1$, $D2$, and $D3$. P_1 was the trigger photon counts, P_{12} and P_{13} were the twofold coincidence counts between the trigger and the two separated signal photon (the signal was divided into two equal parts by a beam splitter, and detected by two single-photon detectors $D2$ and $D3$, not shown in Fig. 2.7) and P_{123} was the threefold coincidence counts between the three detectors $D1$, $D2$, and $D3$.

2.1.2.3 Quantum Storing Single Photon via EIT

The experimental storage of a single photon through EIT was implemented in another MOT 2, (Fig. 2.7b). The optical depth (OD) of MOT 2 was about 10. The bandwidth for storage was about ∼20 MHz. The coupling laser beam, from the same laser as the beam for pump 1, coupled the atomic transition of $5S_{1/2}(F = 2) \rightarrow 5P_{1/2}(F' = 3)$. The signal 1 was first detected, and the output electrical pulse from detector was used to trigger an arbitrary function generator (AFG 3252). This AFG 3252 is used to switch the coupling laser on and off with rising and falling edge of 15 ns. Thus, the coupling pulse is not overlapped with single 2 photon, in order for time synchronization, the signal 2 was first transmitted through 200 metres of single-mode fiber, and then was focused onto the atomic cloud in MOT 2. The Rabi frequency of the coupling laser was 4Γ, where Γ is decay rate of excited state $|4\rangle$. The angle between the coupling beam and probe was set to be 3°, this non-collinear configuration reduces the scattering noise from coupling laser. The retrieved signal was coupled into a single mode fiber and was detected by another detector.

We next stored single photons not carrying any spatial structure via EIT in the second atomic ensemble (see Fig. 2.7b). Cross-coincidence counts were measured between the trigger photon and the leaked signal photon and the retrieved signal photon (Fig. 2.8a). We also measured the efficiency of storage against storage time (Fig. 2.8b). The maximum efficiency obtained was ∼10%. We find that even after about 400 ns storage, a strong non-classical correlation between the retrieved signal photon and the trigger photon still persist.

Furthermore, we checked the single-photon nature of the signal photon after storage again by performing the HBT experiment with the trigger photon. An α value

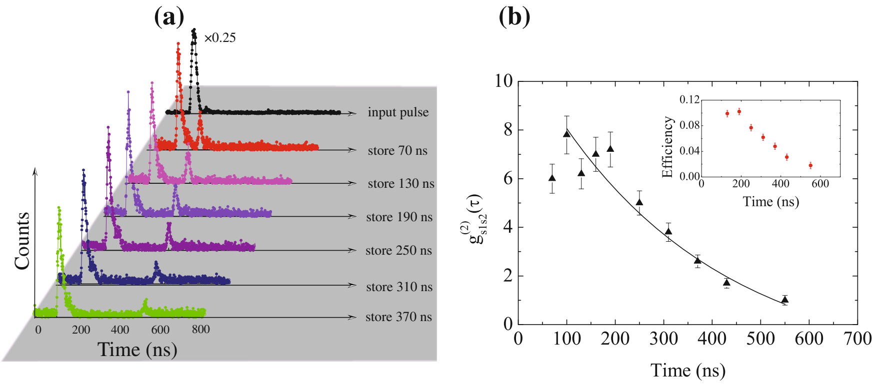

Fig. 2.8 Storage of a single photon. **c** Coincidence counts between the retrieved signal and the trigger as a function of storage time. **d** Cross-correlation function $g_{s1,s2}(\tau)$ between the retrieved signal and the trigger photons against the storage time. The solid line is the exponential fit $Ae^{-\tau/T} + g_0$ to $g^{(2)}_{s1s2}(\tau)$ (where $A = 13.3, T = 348, g_0 = -1.89$). The inset shows the efficiency function against storage time. Error bars represent one standard deviation

of 0.32 $\pm$ 0.08 was obtained for the retrieved signal photon having been stored for about 190 ns, confirming clearly that the single-photon nature is preserved during storage. In our experiment, α changed from 0.025 (before storage) to 0.32 (after storage), we estimated that the noise from the scattering of coupling contributed about 0.16 to α. More strict filtering could reduce this kind of noise further. The remaining contribution to α was mainly from the attenuation of the single photon during the storage, retrieval and the measurement. The noise generated through delayed four-wave mixing process could be negligible due to the large detuning of 3 GHz in our experimental energy level configuration and the small OD of the memory [9] in our system. In the HBT measurement, the detection system registers the particle-like property of the state irrespective of losses. For an ideal single photon, it can't be divided into two parts and detected by two different detectors simultaneously, therefore α goes to zero for a near perfect single photon state. The criterion shown in Ref. [15] shows that even for a state expressed as $\rho = p|0><0| + (1-p)|1><1|$ with $p > 0.5$, where p is the probability of the vacuum state caused by all losses of the single photon before it reaches the detection system, (in our experiment, $1-p$ corresponds to the storage efficiency) which has a positive Wigner function, but it cannot be expressed as a mixture of Gaussian states, is still a non-classical state.

2.1.2.4 Encode Single Photon with OAM

To store a single photon carrying spatial structure, we inserted a spiral phase plate (VPP-1c, RPC Photonics, transmission coefficient >95%) in the optical path along which the signal photon is transmitted. The signal photon now carried a donut-shape structure (see the CCD camera image in Fig. 2.9a taken after the light beam has traversed the plate; the power distribution curve along the transverse direction is given above); this signal has a well-defined OAM of 1 $\hbar$. After approximately 100

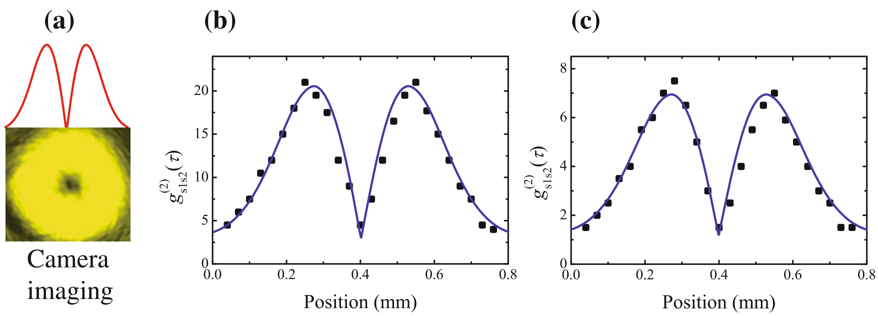

Fig. 2.9 Storage of a true single photon carrying an OAM. **a** Image of a laser beam after traversing the spiral phase plate. The red line is the power distribution curve along the transverse direction. **b** cross-correlation between input signal and trigger photons, obtained by scanning the transverse position of the input signal; **c** cross-correlation function between retrieved signal and the trigger photons. The solid lines in b and c are theoretical fits. All data are raw, without noise correction

ns in storage in MOT 2, the signal photon was retrieved and collected into a single-mode fiber; the tip of the fiber was scanned along the transverse direction. Before performing the storage experiment, we balanced the coupling efficiency of the fiber at different points along the transverse direction. During the experiment, we initially scanned the transverse position of the tip of the receiver fiber and measured the cross-correlation function between the input signal and the trigger photons, obtaining a donut-shape curve, as shown in Fig. 2.9b; see also Fig. 2.9a. Figure 2.9c shows the cross-correlation function, also donut-shaped, between the retrieved signal and the trigger photons. To compare Fig. 2.9b, c, we calculated image visibility and similarity. The former is obtained from $V = (g_{s1,s2,max} - g_{s1,s2,min})/(g_{s1,s2,max} + g_{s1,s2,min})$, where $g_{s1,s2,max}$ ($g_{s1,s2,min}$) are the maximal (minimal) cross-correlation values, was 0.9 for the input signal and 0.88 for the retrieved signal. We also analyzed the fidelity of the retrieved image by calculating the similarity according to Eq. 2.5. High similarity means high fidelity. The calculated similarity of the retrieved image was 0.996. In our calculation, m is fixed because we only scanned the tip of the fiber along the transverse direction.

Figure 2.9 provides clear experimental evidence that an image memory at the single-photon level can be realized using a cold atomic ensemble, the main features of the image had been preserved during storage. Moreover, the non-classical correlation between the trigger photon and the retrieved photon was retained. This point is crucial for establishing high-dimensional quantum repeaters. Dephasing between the two ground states induced by Earth's magnetic field had an effect during storage, which shortened the storage time and reduced the storage efficiency. It is theoretically predicted that the efficiency of the EIT-based memory could approach unity in an atomic ensemble at a high OD [18]. In our experiment, the memory OD is about 10, so we could improve the efficiency by increasing OD. The storage efficiency can be substantially improved by optimizing the pulse shape to match the EIT bandwidth [35, 46]. We could make the single-photon wave packet match the memory bandwidth to increase the storage efficiency. In Ref. [9], 78% storage efficiency is obtained via EIT in a cold atomic ensemble, where the techniques of matching the pulse shape to the EIT bandwidth and increasing OD of the atomic ensemble are applied. One main issue affecting the retrieved image quality was atomic diffusion, seen as softening at the edges of the image [11, 41]. This problem can be solved using a 4-f imaging system that Fourier transforms the image which is then stored, instead of the image itself, in the atomic ensemble. Thus, diffusion can be reduced significantly and the image can be stored for a much long time.

2.1.2.5 Storage Polarization Superposition State

To use our scheme in practice, we have to prove that photon coherence is preserved during storage. For this purpose, we performed two experiments. In the first, we experimentally checked whether or not we could store an arbitrary polarization state of the input signal photon. For that, we performed quantum storage process tomography [10] to construct the quantum state, aided by a Sagnac interferometer

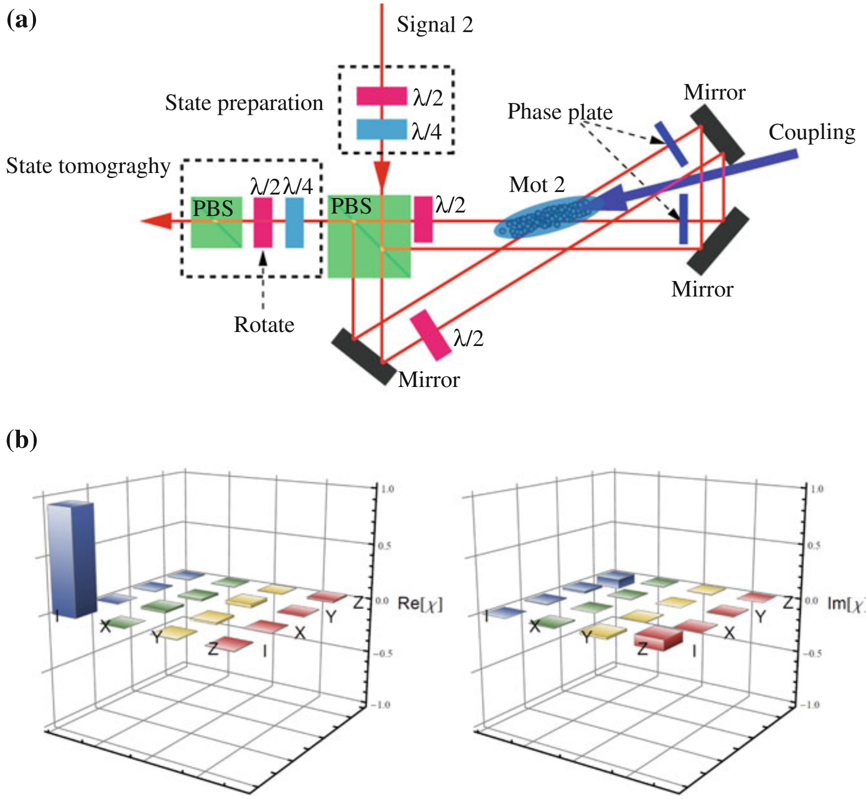

Fig. 2.10 Quantum process tomography of storing a polarization state of a true single photon. **a** Schematic of the simplified experimental setup demonstrating coherence of a single photon. $\lambda/2$ ($\lambda/4$): a HWP (a QWP). PBS: Glan-Taylor polarization beam splitter with the extinction ratio of $10^5 : 1$; **b** Calculated real and imaginary parts of the storage process matrix χ obtained from experimental data in the Pauli operator basis $\{\mathbf{I}, \mathbf{X}, \mathbf{Y}, \mathbf{Z}\}$. For an ideal quantum memory device, the χ matrix should be peaked only at $\{\mathbf{I}, \mathbf{I}\}$. All data are raw, without noise correction

(Fig. 2.10a). The advantage of Sagnac interferometer is that the relative phases between two optical paths are same due to the same phase difference afforded by external perturbation. Such symmetric configuration makes the system working in long-stabilized status. In this process, the two phase plates were removed from the interferometer, thus there are only polarized states. The whole setup consisted of three parts: state preparation of an arbitrary polarization state; storing the polarization state by using Sagnac interferometer , and quantum tomography for state analysis. In this experiment, the photon did not carry a spatial information, that is a Gaussian profile. Using such a configuration, two orthogonal polarizations, either forward or backward directed, of an input state were stored in the atomic ensemble. Figure 2.10b depicts the process matrix χ constructed according to experimental data. The calculated fidelity of the storage process were 0.94, 0.96, 0.98, and 0.96 for the four different input polarization states H, V, R, and D, respectively, where H and V stand for horizontal and vertical polarization, $R = (H - iV)\sqrt{2}$ right-circular polarization, and $D = (H + V)/\sqrt{2}$ diagonal polarization. In this process, the storage time was programmed for 100 ns. The experiment clearly demonstrates that photon coherence in polarization DOF is preserved during storage. Using the Sagnac interferometer here can avoid phase fluctuations between the two orthogonal polarization of the signal.

2.1.2.6 Storing OAM Superposition State

Most importantly, in the second experiment, we verified whether or not we could store an OAM superposition state of the input signal photon. For that, we inserted the two phase plate (VPP-2, RPC Photonics) into the two optical paths (see Fig. 2.10a) and the orientation of both phase plates should be opposite in order to make sure the superposition state of OAM, the photonic state of the input signal can be written as,

$$|\psi\rangle = \frac{1}{\sqrt{2}}(|H\rangle\,|l\rangle + |V\rangle\,|-l\rangle) \tag{2.8}$$

with OAM index $l = 2$ was prepared for storage. This state is exactly a hybrid entangled state between single photon's polarization, OAM and optical path DOFs. In general, it is called as a "classical" entangled state because it's not biparticle entangled state. Such state shows a non-locality between single photon's different DOFs, not the non-locality between a photon pair. The output state evolves into $|\psi_1\rangle = \frac{1}{\sqrt{2}}(|L\rangle\,|l\rangle + i\,|R\rangle\,|-l\rangle)$ with a 45° rotation after the retrieved signal passes a (QWP). Next, a half-wave plate (HWP) (see Fig. 2.10a) is used to rotate the photon polarization, and yields the output state,

$$|\psi_2\rangle = \hat{U}_{HWP}(\theta)\,|\psi_1\rangle \tag{2.9}$$

where $\hat{U}_{HWP}(\theta)$ is the transformational matrix of the half-wave plate with θ the angle of the fast axis with respect to the vertical axis. The output state can be written as:

$$|\psi_3\rangle = \frac{1}{\sqrt{2}}(e^{-i2\theta}\,|-l\rangle + ie^{i2\theta}\,|l\rangle) \tag{2.10}$$

Here, interference between two terms with opposite OAM state in Eq. 2.10 gives rise to a characteristic feature comprising four interference spots. Shifting the relative phase of the two terms causes this interference pattern to rotate. In our experiment, rotating the half-wave plate shifts the phase, i.e. changing θ continuously. In the actual experiment, we first used weak coherent light ($\sim 10^4$ photons per pulse) as the input signal. We set the angle of the HWP at $\theta = 22.5°$, 67.5°, 112.5° , and 157.5° respectively, and using a ICCD camera to monitor the spatial structure of input signal and retrieved signal. The results, given in Fig. 2.11, show theoretical simulations and experimental data are in good agreement.

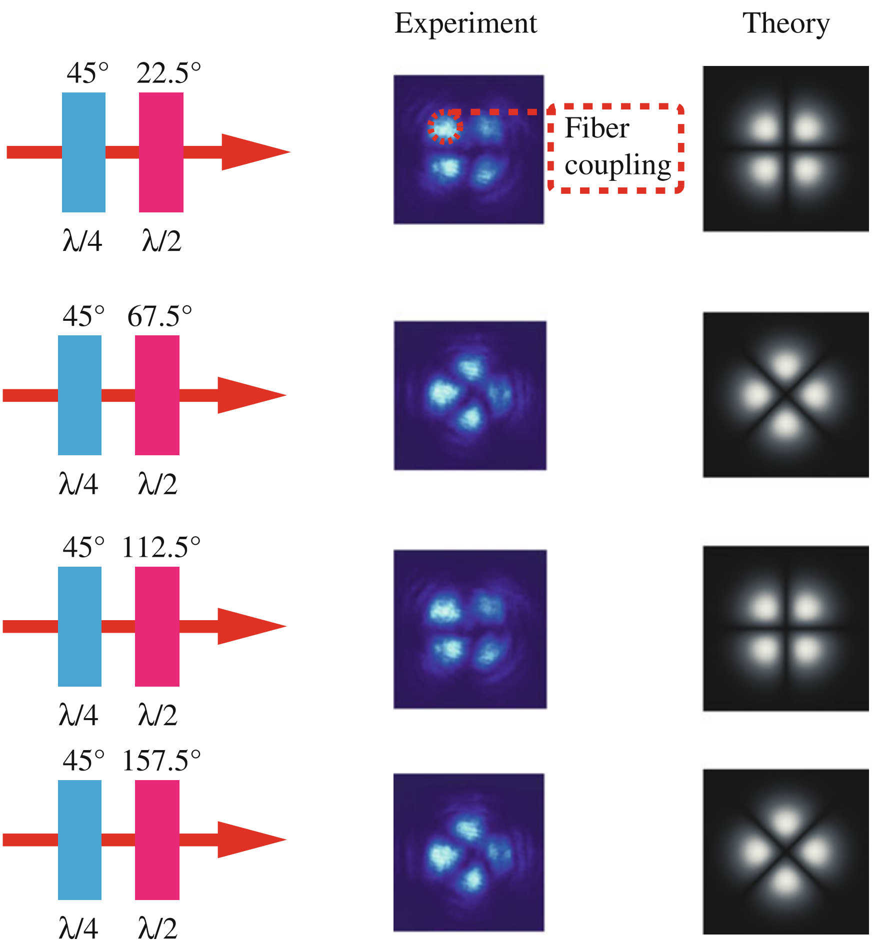

Fig. 2.11 Storing an OAM superposition state. **a** Rotated interference patterns at different angle settings of the HWP. The left column represents the experimental angle settings of the HWPs and the QWPs. The middle column is the experimental results and the right column is the theoretical simulations

Further more, we focused the photons in a single spot into a fiber (see Fig. 2.11) and detected these using a single photon detector (Avalanche diode, PerkinElmer SPCM-AQR-15-FC). From Eq. 2.10, we know that $|l\rangle$ and $|-l\rangle$ have an additional phase $2\theta+\pi/2$ and -2θ respectively. The detected intensity of the interference pattern will vary sinusoidally as $\mathrm{Sin}(4\theta)$ as the HWP angle changes. In this experiment, we used the true single photon (signal 2 photon, generated through SFWM in MOT 1) as the input signal. Storage time was programmed at 100 ns. The integrated coincidence counts per second in a 50-ns coincidence window with background noise subtracted showed a clear interference pattern against HWP plate angle (Fig. 2.12a) with a

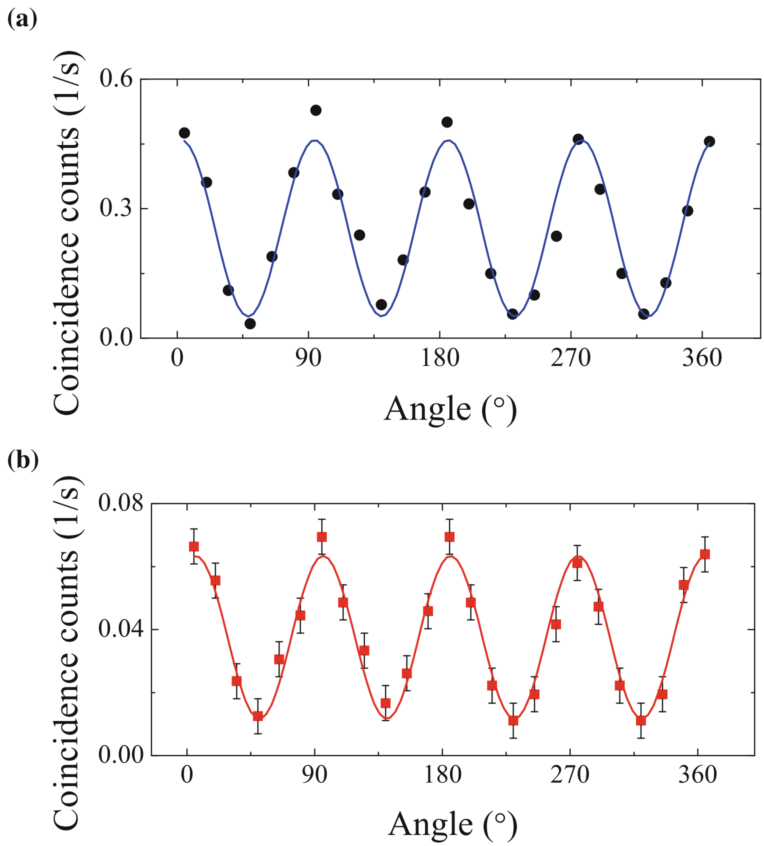

Fig. 2.12 **a** interference pattern of the input signal photon as a function of plate angle; **b** interference of retrieved signal with plate angle. Blue and red lines are fits of the Sinusoid .The background noise has been subtracted. Error bars represent ± one standard deviation, and are obtained based on the count statistics of single photons

visibility of 0.74 ± 0.1, the error being statistical arising mainly from noise from the scattering of coupling laser and the multi-photon events. Again, experimental and theoretical results agreed well. The results presented herein clearly demonstrate that coherence between two different OAM photon states is preserved during storage.

2.2 Research Summary

In this chapter, we demonstrated multimode quantum memory in K-vector, spatial and frequency domains in an atomic ensemble. The results show that multimode quantum memory maintains the multiplexing coherence of input probes, besides there are no obvious cross-talks between them, even the probes have same frequency. Further more, we have demonstrated quantum memory under single photon level, giving a first evidence of storing single photon carrying spatial information. Most importantly, our work shows that the coherence of input OAM superposition can be retained in the whole storage process. Although our work is a proof of principle, with a long way to go before being practical, it makes an important step towards realizing high-dimensional quantum memory. It accompanies recent progress in infrared-to-visible wavelength conversion [13] and long-distance fiber transmission of photons encoded in high-dimensional states [31], as well as the significant advances in quantum key distribution transmission between ground and air [34] and satellite [45]. All these results show that it is promising for establishing a high-dimensional quantum network in the future. Next, we will do some experiments related to the storage of a single photon carrying higher orbital angular momentum or a high dimensional superposition state in next chapter.

References

1. Abbas, M.M., T. Kostiuk, and K.W. Ogilvie. 1976. Infrared upconversion for astronomical applications. *Applied Optics* 15 (4): 961–970.
2. Afzelius, Mikael, Christoph Simon, Hugues De Riedmatten, and Nicolas Gisin. 2009. Multimode quantum memory based on atomic frequency combs. *Physical Review A* 79 (5): 052329.
3. Balić, Vlatko, Danielle A Braje, Pavel Kolchin, GY Yin, and Stephen E Harris. 2005. Generation of paired photons with controllable waveforms. *Physical Review Letters* 94 (18): 183601.
4. Bechmann-Pasquinucci, H., and Wolfgang Tittel. 2000. Quantum cryptography using larger alphabets. *Physical Review A* 61 (6): 062308.
5. Boyd, R.W., and C.H. Townes. 1977. An infrared upconverter for astronomical imaging. *Applied Physics Letters* 31 (7): 440–442.
6. Camacho, Ryan M., Praveen K. Vudyasetu, and John C. Howell. 2009. Four-wave-mixing stopped light in hot atomic rubidium vapour. *Nature Photonics* 3 (2): 103–106.
7. Chanelière, T., D.N. Matsukevich, S.D. Jenkins, S.Y. Lan, T.A. Kennedy, and A. Kuzmich. 2005. Storage and retrieval of single photons transmitted between remote quantum memories. *Nature* 438 (7069): 833.
8. Chen, Qun-Feng, Bao-Sen Shi, Yong-Sheng Zhang, and Guang-Can Guo. 2008. Entanglement of the orbital angular momentum states of the photon pairs generated in a hot atomic ensemble. *Physical Review A* 78 (5): 053810.
9. Chen, Yi-Hsin, Meng-Jung Lee, I-Chung Wang, Shengwang Du, Yong-Fan Chen, Ying-Cheng Chen, and A. Yu Ite. 2013. Coherent optical memory with high storage efficiency and large fractional delay. *Physical Review Letters* 110 (8): 083601.
10. Chuang, Isaac L., and Michael A. Nielsen. 1997. Prescription for experimental determination of the dynamics of a quantum black box. *Journal of Modern Optics* 44 (11–12): 2455–2467.
11. Ding, Dong-Sheng, Wu Jing-Hui, Zhi-Yuan Zhou, Yang Liu, Bao-Sen Shi, Xu-Bo Zou, and Guang-Can Guo. 2013. Multimode image memory based on a cold atomic ensemble. *Physical Review A* 87 (1): 013835.
12. Ding, Dong-Sheng, Wu Jing-Hui, Zhi-Yuan Zhou, Bao-Sen Shi, Xu-Bo Zou, and Guang-Can Guo. 2013. Multiple image storage and frequency conversion in a cold atomic ensemble. *Physical Review A* 87 (5): 053830.
13. Ding, Dong-Sheng, Zhi-Yuan Zhou, Bao-Sen Shi, Xu-Bo Zou, and Guang-Can Guo. 2012. Image transfer through two sequential four-wave-mixing processes in hot atomic vapor. *Physical Review A* 85 (5): 053815.

14. Djordjevic, Ivan B. 2011. Deep-space and near-earth optical communications by coded orbital angular momentum (oam) modulation. *Optics Express* 19 (15): 14277–14289.
15. Filip, Radim, and Ladislav Mišta Jr. 2011. Detecting quantum states with a positive wigner function beyond mixtures of gaussian states. *Physical Review Letters* 106 (20): 200401.
16. Gibson, Graham, Johannes Courtial, Miles J. Padgett, Mikhail Vasnetsov, Valeriy Pasï¿½1/2ï¿½1/2ko, Stephen M. Barnett, and Sonja Franke-Arnold. 2004. Free-space information transfer using light beams carrying orbital angular momentum. *Optics Express* 12 (22): 5448–5456.
17. Glorieux, Quentin, Jeremy B Clark, Alberto M. Marino, Zhifan Zhou, and Paul D. Lett. 2012. Temporally multiplexed storage of images in a gradient echo memory. *Optics Express* 20 (11): 12350–12358.
18. Gorshkov, Alexey, V., Axel André, Michael Fleischhauer, Anders S Sørensen, and Mikhail D. Lukin. 2007. Universal approach to optimal photon storage in atomic media. *Physical Review Letters* 98 (12): 123601.
19. Grangier, Philippe, Gerard Roger, and Alain Aspect. 1986. Experimental evidence for a photon anticorrelation effect on a beam splitter: a new light on single-photon interferences. *EPL (Europhysics Letters)* 1 (4): 173.
20. Grodecka-Grad, Anna, Emil Zeuthen, and Anders S. Sørensen. 2012. High-capacity spatial multimode quantum memories based on atomic ensembles. *Physical Review Letters*, 109(13): 133601.
21. He, Xiaodong, Xu Peng, Jin Wang, and Mingsheng Zhan. 2009. Rotating single atoms in a ring lattice generated by a spatial light modulator. *Optics Express* 17 (23): 21007–21014.
22. He, Xiaodong, Xu Peng, Jin Wang, and Mingsheng Zhan. 2010. High efficient loading of two atoms into a microscopic optical trap by dynamically reshaping the trap with a spatial light modulator. *Optics Express* 18 (13): 13586–13592.
23. Heinze, G., A. Rudolf, F. Beil, and T. Halfmann. 2010. Storage of images in atomic coherences in a rare-earth-ion-doped solid. *Physical Review A* 81 (1): 011401.
24. Higginbottom, Daniel B., Ben M. Sparkes, Milos Rancic, Olivier Pinel, Mahdi Hosseini, Ping Koy Lam, and Ben C Buchler. 2012. Spatial-mode storage in a gradient-echo memory. *Physical Review A* 86(2): 023801.
25. Hosseini, Mahdi. Ben M. Sparkes, Geoff Campbell, Ping K. Lam, and Ben C. Buchler. 2011. High efficiency coherent optical memory with warm rubidium vapour. Nature. *Communications* 2: 174.
26. Inoue, R., N. Kanai, T. Yonehara, Y. Miyamoto, M. Koashi, and M. Kozuma. 2006. Entanglement of orbital angular momentum states between an ensemble of cold atoms and a photon. *Physical Review A* 74 (5): 053809.
27. Kimble, H.J. 2008. The quantum internet. *Nature* 453: 19.
28. Kuzmich, A., W.P. Bowen, A.D. Boozer, A. Boca, C.W. Chou, L.-M. Duan, and H.J. Kimble. 2003. Generation of nonclassical photon pairs for scalable quantum communication with atomic ensembles. *arXiv preprint quant-ph/0305162*.
29. Leach, Jonathan, Barry Jack, Jacqui Romero, Anand K. Jha, Alison M. Yao, Sonja Franke-Arnold, David G. Ireland, Robert W. Boyd, Stephen M. Barnett, and Miles J. Padgett. 2010. Quantum correlations in optical angle- orbital angular momentum variables. *Science* 329 (5992): 662–665.
30. Li, Shujing, Xu Zhongxiao, Haiyan Zheng, Xingbo Zhao, Wu Yuelong, Hai Wang, Changde Xie, and Kunchi Peng. 2011. Coherent manipulation of spin-wave vector for polarization of photons in an atomic ensemble. *Physical Review A* 84 (4): 043430.
31. Löffler, W., T.G. Euser, E.R. Eliel, M. Scharrer, P. St, J. Russell, and J.P. Woerdman. 2011. Fiber transport of spatially entangled photons. *Physical Review Letters* 106 (24): 240505.
32. Lukin, M.D., P.R. Hemmer, and Marlan O. Scully. 2000. Resonant nonlinear optics in phase-coherent media. *Advances in Atomic, Molecular, and Optical Physics* 42: 347– 386.
33. Mair, A., A. Vaziri, G. Weihs, and A. Zeilinger. 2001. Entanglement of the orbital angular momentum states of photons. *Nature* 412 (6844): 313.

34. Nauerth, Sebastian, Florian Moll, Markus Rau, Christian Fuchs, Joachim Horwath, Stefan Frick, and Harald Weinfurter. 2013. Air-to-ground quantum communication. *Nature Photonics* 7 (5): 382–386.
35. Phillips, Nathaniel B., Alexey V. Gorshkov, and Irina Novikova. 2008. Optimal light storage in atomic vapor. *Physical Review A* 78(2): 023801.
36. Pugatch, Rami, Moshe Shuker, Ofer Firstenberg, Amiram Ron, and Nir Davidson. 2007. Topological stability of stored optical vortices. *Physical Review Letters* 98 (20): 203601.
37. Sangouard, Nicolas, Christoph Simon, Bo Zhao, Yu-Ao Chen, Hugues De Riedmatten, Jian-Wei Pan, and Nicolas Gisin. 2008. Robust and efficient quantum repeaters with atomic ensembles and linear optics. *Physical Review A* 77 (6): 062301.
38. Shuker, M., O. Firstenberg, R. Pugatch, A. Ron, and N. Davidson. 2008. Storing images in warm atomic vapor. *Physical Review Letters* 100 (22): 223601.
39. Simon, Christoph, Hugues De Riedmatten, Mikael Afzelius, Nicolas Sangouard, Hugo Zbinden, and Nicolas Gisin. 2007. Quantum repeaters with photon pair sources and multimode memories. *Physical Review Letters* 98 (19): 190503.
40. Veissier, Lucile, Adrien Nicolas, Lambert Giner, Dominik Maxein, A.S. Sheremet, Elisabeth Giacobino, and Julien Laurat. 2013. Reversible optical memory for twisted photons. *Optics Letters* 38 (5): 712–714.
41. Vudyasetu, Praveen, K., Ryan M. Camacho, and John C. Howell. 2008. Storage and retrieval of multimode transverse images in hot atomic rubidium vapor. *Physical Review Letters* 100 (12): 123903.
42. Wang, Hai, Shujing Li, Xu Zhongxiao, Xingbo Zhao, Lijun Zhang, Jiahua Li, Wu Yuelong, Changde Xie, Kunchi Peng, and Min Xiao. 2011. Quantum interference of stored dual-channel spin-wave excitations in a single tripod system. *Physical Review A* 83 (4): 043815.
43. Wu, Jinghui, Yang Liu, Dong-Sheng Ding, Zhi-Yuan Zhou, Bao-Sen Shi, and Guang-Can Guo. 2013. Light storage based on four-wave mixing and electromagnetically induced transparency in cold atoms. *Physical Review A* 87 (1): 013845.
44. Wu, Liu Yang, Shi Bao-Sen Jing-Hui, and Guo Guang-Can. 2012. Realization of a two-dimensional magneto-optical trap with a high optical depth. *Chinese Physics Letters* 29 (2): 024205.
45. Yin, Juan, Yuan Cao, Yu-Huai Li, Sheng-Kai Liao, Liang Zhang, Ji-Gang Ren, Wen-Qi Cai, Wei-Yue Liu, Bo Li, Hui Dai, et al. 2017. Satellite-based entanglement distribution over 1200 kilometers. *Science* 356 (6343): 1140–1144.
46. Zhou, Shuyu, Shanchao Zhang, Chang Liu. J.F. Chen, Jianming Wen, M.M.T. Loy, George Ke Lun Wong, and Shengwang Du. 2012. Optimal storage and retrieval of single-photon waveforms. *Optics Express* 20 (22): 24124–24131.

Chapter 3
Storing High-Dimensional Quantum States in a Cold Atomic Ensemble

Abstract The reversible transfer of a high-dimensional quantum state between a true single photon, an information carrier, and a matter used as a quantum memory with high fidelity and reliability could enhance the channel capacity significantly in addition to overcoming distance limitations of quantum communication schemes through transmission losses. In the Chap. 2, we have introduced how we demonstrated single photon storage encoded with two-dimensional OAM degree of freedom. Due to the infinity Hilbert space spanned by OAM degree of freedom, photon encoded in OAM space can extend to high-dimensional state. Quantum memories have been realized with different physical systems, such as atomic ensembles and solid systems etc., many of them only realize the storage and retrieval of the single photons spanned in a two-dimensional space for example, orthogonal polarizations, therefore only a quantum bit could be stored there. In this Chapter, I will introduce an experimental realization of a quantum memory storing a heralded photon lived in a three-dimensional space spanned by OAM via EIT in a cold atomic ensemble. We reconstruct the storage process density matrix with fidelity of 85.3% by the aid of a 4-F imaging system experimentally. The ability to store a high-dimensional quantum state with high fidelity is very promising for building a high-dimensional quantum network.

3.1 Research Motivations on Storing High-Dimensional State

A main goal of quantum communication is the development of a quantum network through which users can exchange quantum information in quantum regime. Such a network would consist of spatially separated quantum memories used to store and manipulate information, and quantum channels through which different quantum memories could be connected, as described in Chap. 1 in details. Photons are robust and efficient carriers of quantum information because of the high speed and the weak decoherence during their transmission in channel. The reversible transfer of quantum information between a photon and a quantum memory with high fidelity and

D.-S. Ding, *Broad Bandwidth and High Dimensional Quantum Memory Based on Atomic Ensembles*, Springer Theses, https://doi.org/10.1007/978-981-10-7476-9_3

reliability is the prerequisite for realizing a long-distance quantum communication and a quantum network [20, 22].

Different physical systems such as atomic ensembles, or cryogenically cooled doped crystals are used as quantum memories [4, 5, 7, 9, 14, 17, 26, 31, 32]. Usually quantum information is encoded in a two-dimensional space spanned for example by orthogonal polarizations of a photon, photonic pulse splitted into time-bin or two different paths along which a photon transmits. By this way, each photon could carry at most a quantum bit (qubit) information. If a photon could live in a high-dimensional space, for example, spanned by the inherently infinite-dimensional OAM degree of freedom, then the information carried by each photon could be increased significantly, (from a qubit to $log_2 d$ bits (hereafter called a qudit, for three-dimensional called as qutrit state), where, d is the number of orthogonal basis vectors of the Hilbert space in which the photon lives.). The channel capacity of the network and the transmission efficiency could be also improved greatly [21]. etc. Therefore quantum communication research with an information carrier lived in a high-dimensional space becomes a hot topic and attracts much attention recently, some works using for example a photonic high-dimensional time-bin state [10] or an OAM state [8, 15, 23] have been reported.

Quantum repeaters are indispensable for increasing transmission distance and improving quantum information processing efficiency [2], among which a quantum memory is the key component. If we could transfer a high-dimensional quantum information from a true single photon to a quantum memory and vice-visa with high fidelity and reliability, we could have the potential solution in enhancing the channel capacity significantly in addition to overcoming distance limitations of quantum communication schemes through transmission losses, then a high-dimensional quantum network can be expected. Therefore many groups and researchers are devoted to performing the storage of a light carrying OAM or image [11, 12, 18, 19, 27, 29, 30]. Although, Refs. [13, 25] reported on the storage of a light imprinted an OAM state at single-photon-level, but the photon still encode in a two-dimensional subspace, not taking the advantages of the own of OAM, thus carrying at most a qubit information. Therefore whether or not there exists a quantum memory which could store a photonic qudit is an open question and how to construct such a quantum memory is still a big challenge if it exists.

In this chapter, we introduce an experiment of quantum storing single photon carrying the OAM state up to three dimension. Herein, we will show how we encode the qutrit state, and decode it after storage. We reconstruct the storage process density matrix of a three-dimensional state (qutrit) by the quantum process tomography with fidelity of 85.3% by the aid of a 4-f imaging system, proving the feasibility of storing a qutrit in this kind of memory. In addition, I elaborate how to achieve quantum memory of higher-dimensional OAM state, in which there is an inevitable problem of unbalanced storage efficiency for distinct OAM modes.

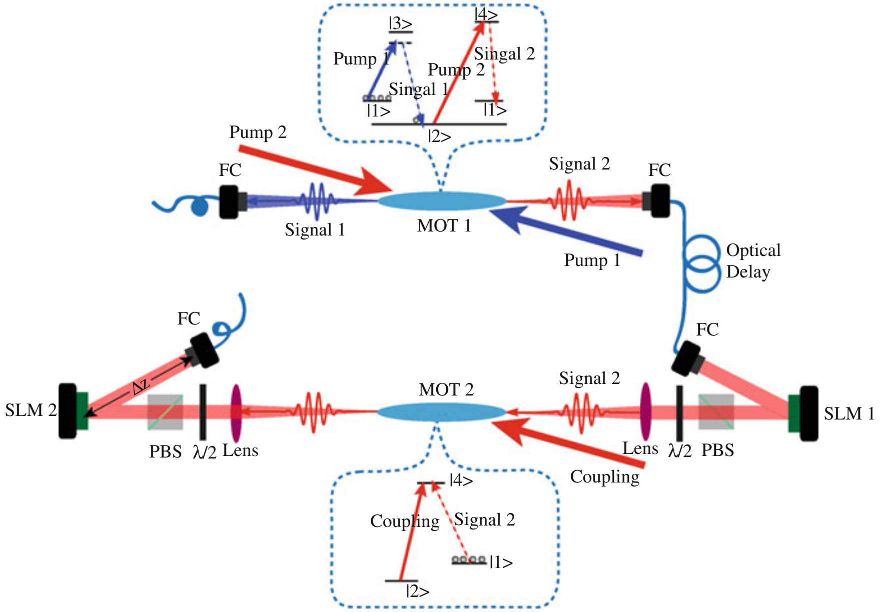

Fig. 3.1 Simplified experimental setup. **a** Simplified diagram depicting the generation of heralded single photon using SFWM and the storage of single photon encoding with high-dimensional state by SLM. MOT: magneto-optical trap; Lens: lens with focus length of 300 mm; FC: fibre coupler; SLM: spatial light modulator; PBS: polarisation beam splitter; $\lambda/2$: half-wave plate. Inset: energy level diagrams for SFWM and EIT respectively

3.1.1 Three-Dimensional OAM State Storage

The single photon used in the experiment was prepared using SFWM in a two-dimensional MOT 1 shown in Fig. 3.1. The experimental setup used for preparation of the single photon is the same as Ref. [13], as discussed in Chap. 2. The generated signal 1 and signal 2 are called as trigger and signal in the following. Through matching the bandwidths between signal and the memory, and time sequence synchronization between signal and trigger photons, we have realized quantum memory of heralded single photon with Gaussian beam. We demonstrated the storage of single photons via EIT scheme in MOT 2, the bandwidth for storage was about ∼30MHz.

Similarly, we characterized the non-classical correlation between photons in a pair and the single-photon property of the signal photon using the method and procedure given in Chap. 2. We further improved the whole system by turning the *OD* of the atomic ensemble and the power of the coupling laser, we obtain an α (anti-correlation parameter) value of 0.006 for the signal before storage and of 0.08 for the retrieved signal from MOT 2. Both α values go to zero, confirming clearly that the single-photon nature is preserved during storage. The storage data on cross-correlation function between signal and trigger photons are given in Fig. 3.2.

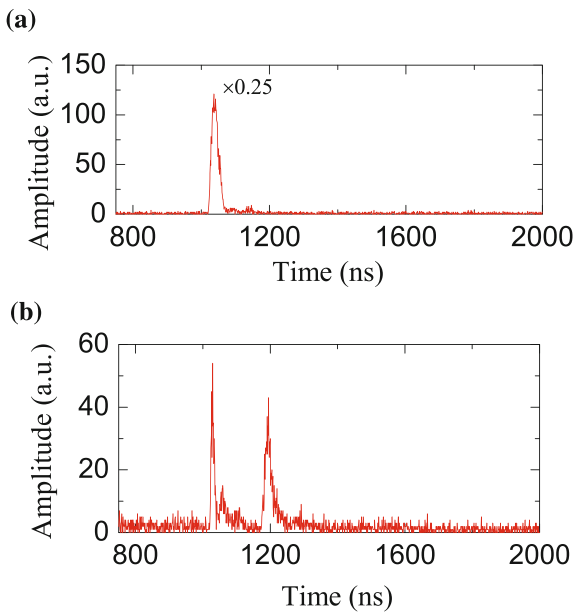

Fig. 3.2 **a** The measured cross-correlation between the input signal and the trigger. **b** The measured cross-correlation function between the retrieved signal and the trigger after a programmed storage time

3.1.1.1 Qutrit Encoding by Spatial Light Modulator

The ability to perform wave-front modulation in $2D$ space is of great importance in optical micro-manipulation, optical trapping, and quantum communications, etc. Encoding photons with OAM structure has many methods, such as using spiral phase plate, hologram grating, Q-plate, spatial light modulator (SLM) and so on. Certainly, there are many methods based on light and matter interaction, such as using cavity or a fibre, but these are not described in this thesis. For spiral phase plate, a Gaussian beam propagating through spiral phase plate becomes LG mode beam, the efficiency is very high depending on the transmission efficiency of plate. See Fig. 3.3a, different oriented phase singularities are used to create donut beams. The action of a spiral phase plate on a Gaussian state is shown in the following

$$|0\rangle \rightarrow |l\rangle \tag{3.1}$$

where l denotes the winding number of light or the index of the OAM beam.

For hologram grating, the positive/negative OAM beams are distributed in positive/negative diffracted light. In practical, there are higher-order diffracted light with $|\pm 2l\rangle$, $|\pm 3l\rangle$, $|\pm 4l\rangle$...., but these terms are in low efficiency thus can be ignored in practical. The hologram grating gives an action on Gaussian beam by the following relation

$$|0\rangle \rightarrow \eta_1\,|l\rangle + |0\rangle + \eta_1\,|-l\rangle \tag{3.2}$$

where η_1 is defined as the efficiency of generating first-order diffracted light. Generally, the OAM modes are depending on the number of the forked interference fringe. The more the number of forked fringe, the higher the quanta of OAM modes.

Q-plate is a device for generating LG mode beam depending on the polarization of input light, the right/left circularly polarized light through Q-plate become left/right circularly polarization and $l = -2q/2q$ OAM beams see Fig. 3.3c, in which q belongs to a half integer associated with the Q-plate. Consider a photon in the Gaussian mode and a superposition of left-handed and right-handed circular polarization $(|L'\rangle + |R'\rangle)/\sqrt{2}$. The action of a Q-plate on this state is given by

$$\frac{1}{\sqrt{2}}(|L', 0\rangle + |R', 0\rangle) \rightarrow \frac{1}{\sqrt{2}}(|R', -2\mathrm{q}\rangle + |L', 2q\rangle) \tag{3.3}$$

Note that the change in the OAM is twice the value of q. Generally, Q-plate is always used to demonstrate hybrid-entanglement, hyper-entanglement, spin orbital conversion experiments and spin orbital interactions [1, 3, 24] in quantum information science. Interestingly, Q-plate can be used to demonstrate quantum random walk [33], in which the setup is proposed by making use of a ring interferometer, containing a QWP and a Q-plate. This setup enables one to perform an arbitrary number of quantum walk steps.

SLM is a crystal material, each pixel of SLM can be programmed by a computer, that can modulate the wave-front of light with arbitrary structure. It is capable of converting data from electronic sheet into a spatially modulated coherent wave-front. Compared with hologram grating, spiral phase plate and Q-plate, SLM can be used to encode photons into an arbitrary structured pure state without changing its' place, while the phase plate introduced above need change position to project a superposition state.

In our experiment, SLM 1, MOT 2 and SLM 2 and two lenses compose a 4-f imaging system (see Fig. 2.3 in Chap. 2 for more details): SLM1 as a mask plane, the atomic ensemble in MOT 2 is the Fourier plane and the SLM 2 represents the image plane. Due to the conjugate properties between the mask plane and the image plane, the selected measurement vectors need to be converted to be the conjugate of the corresponding input states. In order to illustrate the imaging process, we give the phase distributions in mask, Fourier and image planes respectively in Fig. 3.4. The columns (1) show the different phase distributions imaged on the SLM 1, the columns (2) represents the phase distributions in Fourier plane by imaging the phase distribution on SLM 1. The columns (3) are the selected eigenvectors for measurement programmed on SLM 2. These phase structures are modulated by two spatial light modulators, SLM 1 and SLM 2.

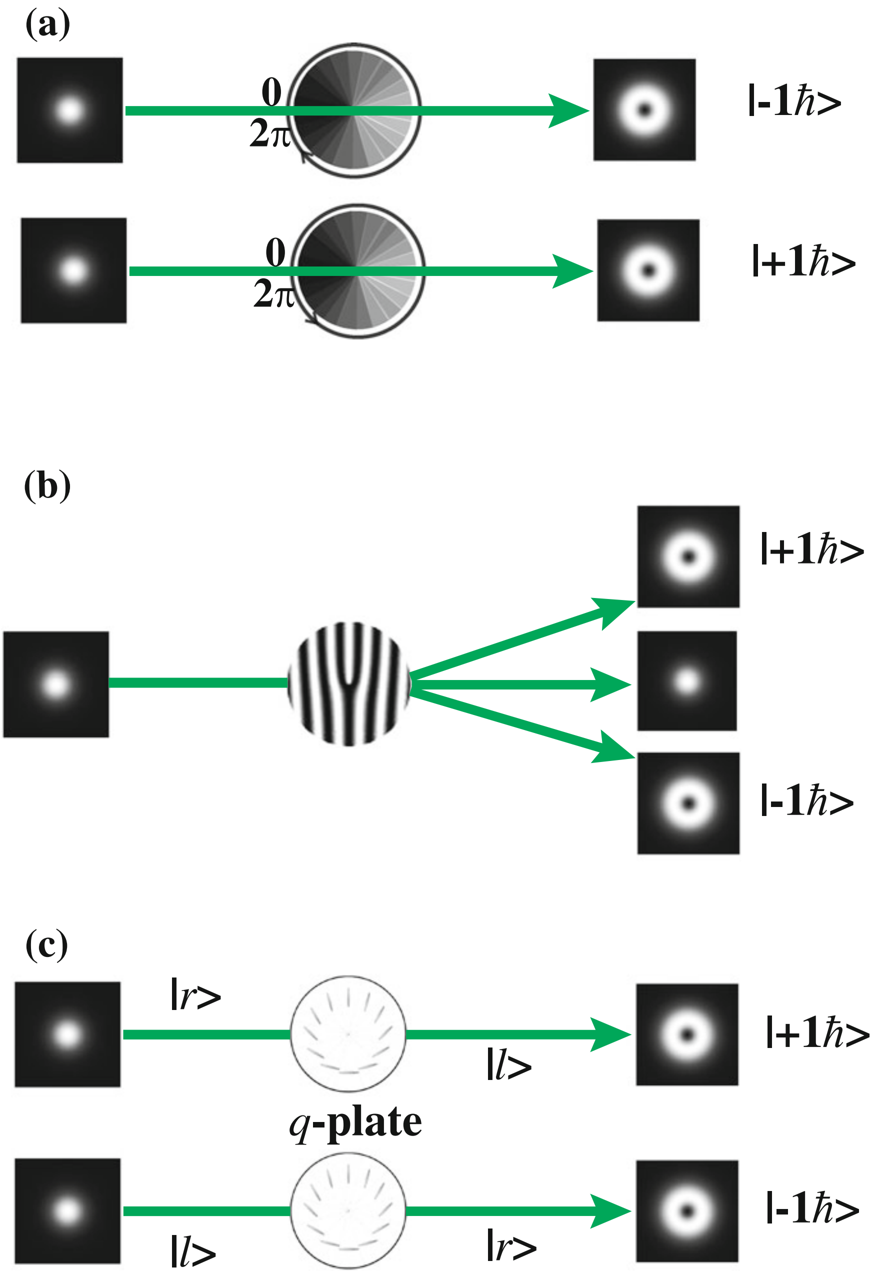

Fig. 3.3 **a** Phase singularities to create donut beams. $\pm l$ OAM beams are generated by passing through the front and back of a spiral phase plate. **b** Forked hologram grating generates ± 1 order diffracted beams with $\pm l$ OAM. **c** Q-plate for preparing different OAM beams with different circularly polarization beams

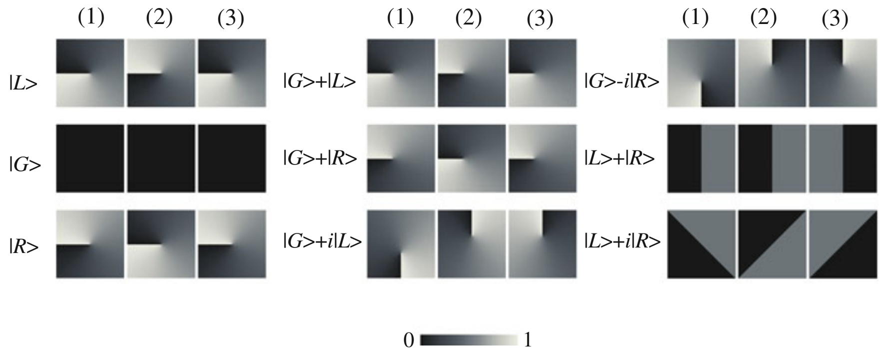

Fig. 3.4 The phase distributions in mask, Fourier and image planes. The column **1** shows the phase distributions imaged on the SLM 1; the column **2** represents the phase distributions in Fourier plane; the column **3** is the selected eigenvector for measurement programmed on SLM 2

3.1.1.2 High-Dimensional Quantum Tomography

In discrete-variable quantum information science, storing a state and retrieving it later can be regarded as a state linearly transfer process. This process can be represented by a quantum process matrix χ. The output state $\varepsilon(\rho)$ can be written as:

$$\varepsilon(\rho) = \sum_{m,n=1}^{9} \chi_{mn}\lambda_m \hat{\rho} \hat{\lambda}_n^{\dagger} \tag{3.4}$$

where $\hat{\lambda}_m$ is a basis for operator acting on input state ρ. The matrix χ can be obtained by measuring the output state $\varepsilon(\rho)$. The complete operators for reconstructing matrix χ of a photonic qutrit are given:

$$\lambda_1 = \begin{pmatrix} 1 & 0 & 0 \\ 0 & 1 & 0 \\ 0 & 0 & 1 \end{pmatrix}, \lambda_2 = \begin{pmatrix} 0 & 1 & 0 \\ 1 & 0 & 0 \\ 0 & 0 & 0 \end{pmatrix}, \lambda_3 = \begin{pmatrix} 0 & -i & 0 \\ -i & 0 & 0 \\ 0 & 0 & 0 \end{pmatrix},$$

$$\lambda_4 = \begin{pmatrix} 1 & 0 & 0 \\ 0 & -1 & 0 \\ 0 & 0 & 0 \end{pmatrix}, \lambda_5 = \begin{pmatrix} 0 & 0 & 1 \\ 0 & 0 & 0 \\ 1 & 0 & 0 \end{pmatrix}, \lambda_6 = \begin{pmatrix} 0 & 0 & -i \\ 0 & 0 & 0 \\ -i & 0 & 0 \end{pmatrix},$$

$$\lambda_7 = \begin{pmatrix} 0 & 0 & 0 \\ 0 & 0 & 1 \\ 0 & 1 & 0 \end{pmatrix}, \lambda_8 = \begin{pmatrix} 0 & 0 & 0 \\ 0 & 0 & -i \\ 0 & -i & 0 \end{pmatrix}, \lambda_9 = \begin{pmatrix} 1 & 0 & 0 \\ 0 & 1 & 0 \\ 0 & 0 & -2 \end{pmatrix} / \sqrt{3}.$$

The input states are:

$$|\Psi_1\rangle = \begin{pmatrix} 1 \\ 0 \\ 0 \end{pmatrix}, |\Psi_2\rangle = \begin{pmatrix} 0 \\ 1 \\ 0 \end{pmatrix}, |\Psi_3\rangle = \begin{pmatrix} 0 \\ 0 \\ 1 \end{pmatrix}, |\Psi_4\rangle = \begin{pmatrix} 1 \\ 1 \\ 0 \end{pmatrix}, |\Psi_5\rangle = \begin{pmatrix} 0 \\ 1 \\ 1 \end{pmatrix},$$

$$|\Psi_6\rangle = \begin{pmatrix} i \\ 1 \\ 0 \end{pmatrix}, |\Psi_7\rangle = \begin{pmatrix} 0 \\ 1 \\ i \end{pmatrix}, |\Psi_8\rangle = \begin{pmatrix} 1 \\ 0 \\ 1 \end{pmatrix}, |\Psi_9\rangle = \begin{pmatrix} 1 \\ 0 \\ i \end{pmatrix}.$$

In our experiment, these states corresponds OAM states of $|\mathrm{L}\rangle$, $|\mathrm{G}\rangle$, $|\mathrm{R}\rangle$, $(|\mathrm{G}\rangle + |\mathrm{L}\rangle)/\sqrt{2}$, $(|\mathrm{G}\rangle + |\mathrm{R}\rangle)/\sqrt{2}$, $(|\mathrm{G}\rangle + i\,|\mathrm{L}\rangle)/\sqrt{2}$, $(|\mathrm{G}\rangle - i\,|\mathrm{R}\rangle)/\sqrt{2}$, $(|\mathrm{L}\rangle + |\mathrm{R}\rangle)/\sqrt{2}$, $(|\mathrm{L}\rangle + i\,|\mathrm{R}\rangle)/\sqrt{2}$ respectively, where $|\mathrm{L}\rangle$, $|\mathrm{G}\rangle$, and $|\mathrm{R}\rangle$, are photonic states with OAM of $-\hbar$, 0, $+\hbar$ respectively. By storing these nine input states in MOT 2 respectively and measuring the corresponding retrieved output state in 9 basis vectors represented by the operators $\hat{\mu}_i \otimes \hat{\mu}_j$, where $i, j = 1, 2, ...9$, $\hat{\mu}_i = |\Psi_i\rangle\,\langle\Psi_i|$. We can reconstruct the quantum storage process matrix χ according to Eq. 3.4. The fidelity of this quantum process can be calculated by the equation of

$$F = Tr(\sqrt{\sqrt{\chi}\,\chi_{ideal}\sqrt{\chi}})^2 \tag{3.5}$$

where χ_{ideal} is the ideal quantum storage process density matrix.

During choosing 9 basis vectors, we need consider the conjugate properties between the mask plane and the image plane, the vectors for measurement need to be converted to be the conjugate to the corresponding input state (see 3.4). Another thing we wanted to point out was that the stored image in the atomic ensemble was the Fourier transformation of the input OAM state (the stored state is the intensity structures like Fig. 3.5), the phase distributions at the image plane or the measurement plane were the Fourier transformations of the OAM states in a donut structure, so if we wanted to obtain the retrieved OAM state of the input photon correctly, we had to Fourier transform the measured phase distribution of the retrieved photon, which was realized through a far-field diffraction by setting the single-mode fibre coupler used for collecting the retrieved photons to be 2.5 m away from the SLM 2 (Fig. 3.1) in our experiment. In this process, the Fresnel diffraction could be ignored and the Fraunhofer diffraction was predominant. If demonstrating a 4-f imaging process more precisely, we need to consider the short-focus lens fabricated in fiber collimator. This has been resolved in Chap. 5, where the more precisely 4-f imaging system is constructed for performing high-dimensional entanglement measurement.

By inputting 9 input states $|\Psi_{1\sim 9}\rangle$ respectively and measuring each retrieved signal in these 9 basis vectors, and integrating coincidence counts in a 50-ns coincidence window with background noise subtracted in each measurement, we obtained a set of 81 data points and reconstructed the quantum process density matrix for our quantum memory system [6, 28]. The results were shown in Fig. 3.6a and b, where Fig. 3.6a was the real part of the density matrix and Fig. 3.6b corresponded to the imaginary part. Compared with the ideal quantum storage process density matrix, the fidelity of the obtained density matrix was of 85.3%.

3.1.1.3 Storing Photonic Qutrit State

Storing single photon carrying a three-dimensional OAM state (we called qutrit state after) includes three processes: encoding qutrit state, storing and decoding qutrit state. We performed the experiments of storing two special photonic qutrit states

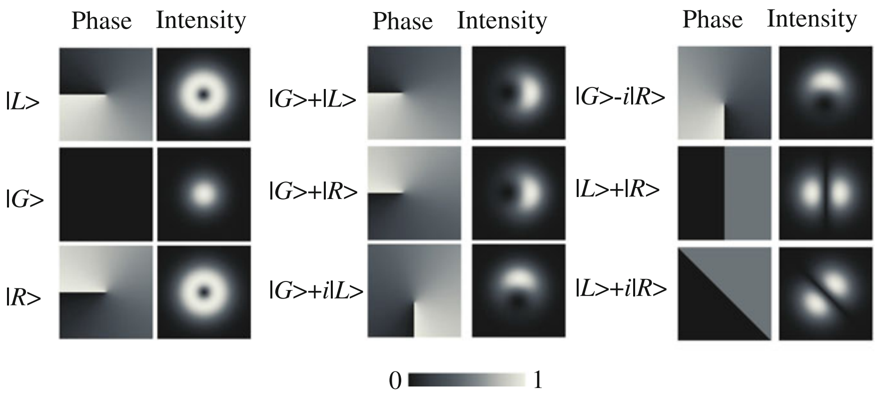

Fig. 3.5 The intensity (left panel of each pair) and the phase (right panel) distributions of input OAM states

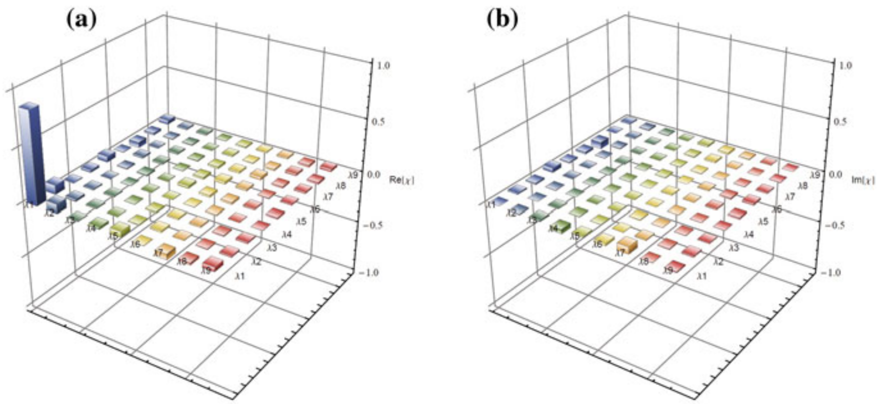

Fig. 3.6 **a** and **b** are the real and imaginary parts of reconstructed quantum storage process density matrix

of $\Psi_1 = (|\mathrm{L}\rangle + |\mathrm{G}\rangle + |\mathrm{R}\rangle)/\sqrt{3}$ and $\Psi_2 = (|\mathrm{L}\rangle - |\mathrm{G}\rangle + |\mathrm{R}\rangle)/\sqrt{3}$ as an example. In principle, we can create an arbitrary photonic qutrit state and demonstrate the storage. The phase structures and the intensity distributions of these two states were given in Figs. 3.7a and b. The qutrit states we prepared like a phase structure of two-dimensional OAM state $(|\mathrm{L}\rangle + |\mathrm{R}\rangle)/\sqrt{2}$ with positive and negative displacement along transverse direction. The intensity of these two states are asymmetric compared with state $(|\mathrm{L}\rangle + |\mathrm{R}\rangle)/\sqrt{2}$ shown in Fig. 3.5.

Through projecting these two states on nine basis vectors defined before, we obtained the nine coincidence counts respectively, reconstructed the density matrix of the retrieved state using them, shown in Fig. 3.8(a–d), where Fig. 3.8a and c were the real parts of retrieved photonic qutrit states, Fig. 3.8b and d corresponded to the imaginary parts respectively. We calculated the fidelity of the reconstructed density matrix by comparing with the ideal density matrix, which were 77%±3% for state Ψ_1

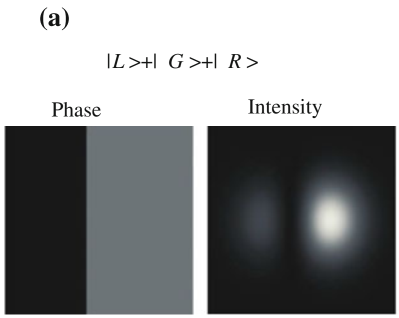

Fig. 3.7 **a** The phase (left panel of each pair) and the intensity (right panel) distributions of the photonic qutrit states $\Psi_1 = (|L\rangle + |G\rangle + |R\rangle)/\sqrt{3}$ and $\Psi_2 = (|L\rangle - |G\rangle + |R\rangle)/\sqrt{3}$

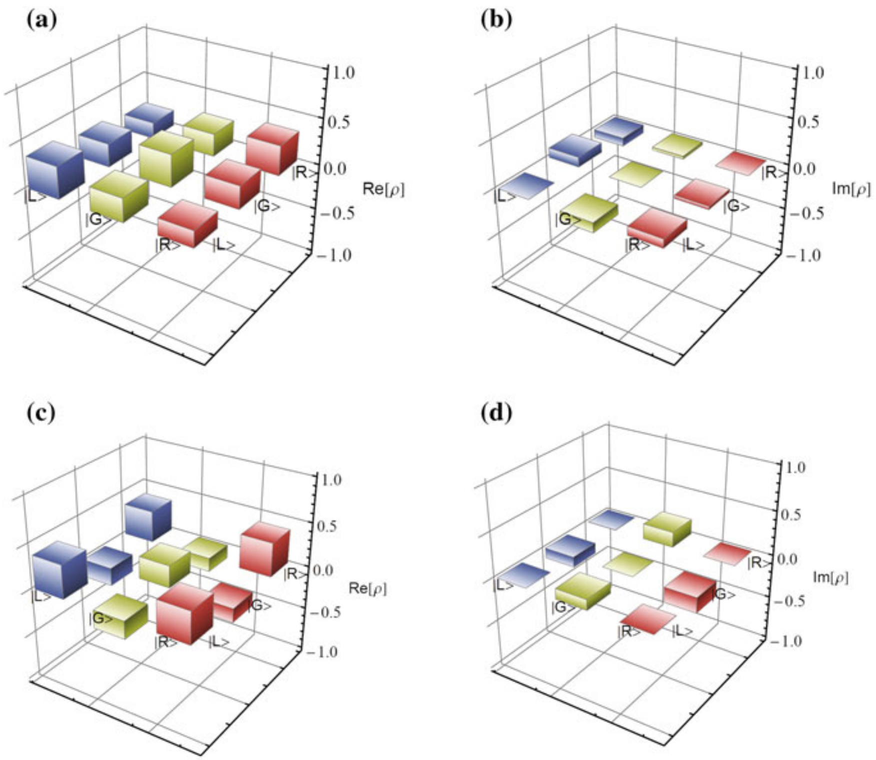

Fig. 3.8 **a** and **b** are the real and imaginary parts of the reconstructed density matrix of the retrieved photonic qutrit $|\Psi_1 = (|L\rangle + |G\rangle + |R\rangle)/\sqrt{3}$. **c** and **d** are the real and imaginary parts of the reconstructed density matrix of the retrieved photonic qutrit $\Psi_2 = (|L\rangle - |G\rangle + |R\rangle)/\sqrt{3}$

and 80%±2% for state Ψ_2 respectively through reconstructing the quantum storage process density matrix. The low fidelity are caused by the OAM state preparation and measurement, and the fluctuation noise in the storage process.

3.1.2 Towards Higher-Dimensional OAM State Storage

For realizing the high-dimensional quantum networks, and implementing quantum communication based on high-dimensional space, it is necessary to perform a quantum memory of higher-dimensional state where the channel capacity is enhanced significantly. Such a memory could also be checked by using the storage process tomography as used before. In such a process, the storage of a photon carrying a single-eigenstate OAM mode $|l\rangle$ or a photon carrying the superposition of two OAMs $|l_1\rangle + e^{i\theta_{12}} |l_2\rangle$ is performed (where l, l_1, and l_2 are the quanta of OAM mode, θ_{12} is the relative phase between l_1, and l_2 OAM mode), and then a storage process matrix could be reconstructed. So here we check the storage of a single eigenstate OAM or an OM-superposition-carrying photon. In order to simplify the experiment, we use the weak coherent light as the input signal instead; the input signal and retrieved signal are recorded by a high-resolution CCD camera ICCD, which can work at a single-photon level to measure the memory efficiency on different OAM states.

Through recording input and the retrieved intensity of different OAMs, we calculate the memory efficiency. The results are given in Fig. 3.9. The efficiency of memory decreases along with the increment of OAM quanta. This result gives us a hint that such a state $|l_1\rangle + e^{i\theta_{12}} |l_2\rangle$ with large difference quanta of l_1, and l_2 might be distorted during quantum memory due to unbalanced efficiency. As stated before, the profile of OAM at the center of the atomic ensemble is the transformed donut distribution from the phase structure, the OAM mode with quanta of l has a waist of $w(z) = \sqrt{l+1}w_0(z)$, where $w_0(z)$ is the beam waist of a Gaussian light. Thus there is a large difference in storage efficiency due to the different beam waists among the small index of OAM modes, for example, for $l = 7$, the beam waist is about two times than that with $l = 1$. If for $l = 100$, there is large difference between $l = 100$ and $l = 1$.

However, at high quanta of with adjacent OAM modes (for $l = 100$, $\sqrt{100+1} \approx \sqrt{100}$), there is little difference between the beam waists, thus resulting in a small difference in memory efficiency. The second thing is that we need to know whether the relative phase θ between l_1 and l_2 changes or not during the storage. In the EIT quantum memory scheme, the frequency of the photonic state l_1 and l_2 is the same; the relative phase does not change due to the same evolution of l_1 and l_2 , memorized as atomic spin waves when the angle between the coupling and signal beams is much greater than the direction angle of the signal beam.

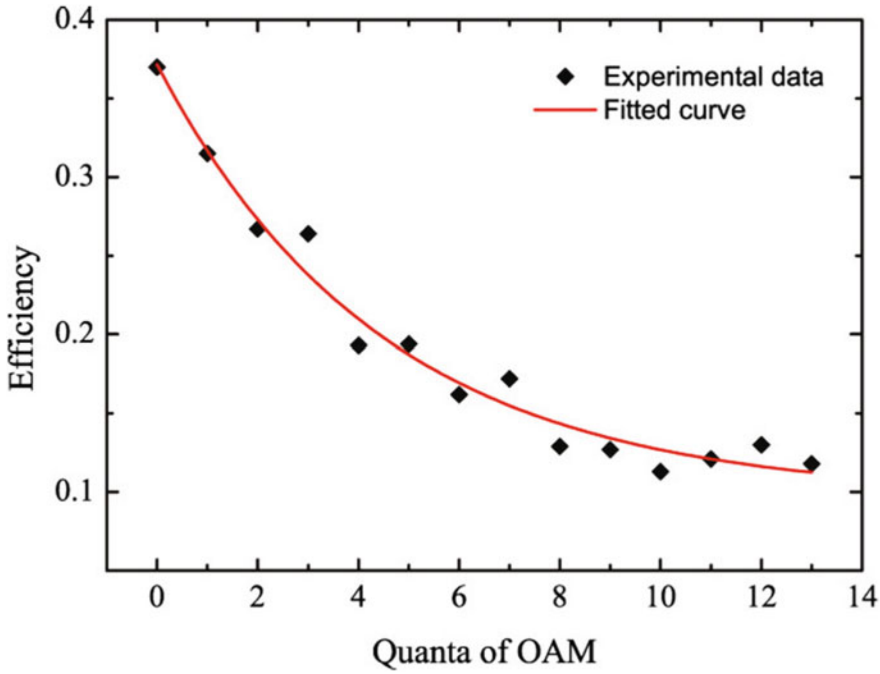

Fig. 3.9 The efficiency of quantum memory of different OAM states. The blue solid line is the fitted curve by a formula $y = Ae^{-x/T} + y_0$, where $A = 0.27$, $T = 4.4$, and $y_0 = 0.01$

3.2 Research Summary

In conclusion, we have realized the experimental demonstration of a quantum storing a true single photon encoded with a three-dimensional quantum state, and experimentally gave a challenge of our quantum memory device for storing the high-dimensional state with large index of OAM, which has the different memory efficiencies for different OAM states. Although our work provides a proof of principle of storing a photonic qutrit, it is the first step towards realizing a high-dimensional quantum memory. Moreover, for extension to the reconstruction of quantum process density matrices corresponding to high-dimensional OAM states ($d \geq 4$) in accordance with Ref. [6], many experimental parameters should be considered:

(1) The big challenge we face in the experimental demonstrations is further improvements in technique, such as how to achieve a higher signal-to-noise ratio and how to stabilize the system over long periods. This is because we will have to take more data.

(2) We must achieve the same efficiency of different OAM states in the process of storing high-dimensional states in the future. How to achieve a balanced memory efficiency between different OAM modes is a technique challenge.

(3) Reference [16] states that the number of dimensions per photon in practice was limited by several factors, such as the Fresnel number and the optical depth of the atomic ensemble, the angle of the signal field and the control field, etc. The requires further investigation.

References

1. Yu Bliokh, K., F.J. Rodríguez-Fortuño, Franco Nori, and Anatoly V. Zayats. 2015. Spin-orbit interactions of light. *Nature Photonics* 9 (12): 796–808.
2. Briegel, H.-J., Wolfgang Dür, Juan I. Cirac, and Peter Zoller. 1998. Quantum repeaters: the role of imperfect local operations in quantum communication. *Physical Review Letters* 81 (26): 5932.
3. Chen, Lixiang, and Weilong She. 2009. Increasing shannon dimensionality by hyperentanglement of spin and fractional orbital angular momentum. *Optics letters* 34 (12): 1855–1857.
4. Cho, Young-Wook, and Yoon-Ho Kim. 2010. Atomic vapor quantum memory for a photonic polarization qubit. *Optics express* 18 (25): 25786–25793.
5. Choi, K.S., H. Deng, J. Laurat, and H.J. Kimble. 2008. Mapping photonic entanglement into and out of a quantum memory. *Nature* 452 (7183): 67–71.
6. Chuang, Isaac L. 1997. Prescription for experimental determination of the dynamics of a quantum black box. *Journal of Modern Optics* 44 (11–12): 2455–2467.
7. Clausen, Christoph, Félix Bussieres, Mikael Afzelius, and Nicolas Gisin. 2012. Quantum storage of heralded polarization qubits in birefringent and anisotropically absorbing materials. *Physical review letters* 108 (19): 190503.
8. Dada, Adetunmise C., Jonathan Leach, Gerald S. Buller, Miles J. Padgett, and Erika Andersson. 2011. Experimental high-dimensional two-photon entanglement and violations of generalized bell inequalities. *Nature Physics* 7 (9): 677–680.
9. De Riedmatten, Hugues, Mikael Afzelius, Matthias U. Staudt, Christoph Simon, and Nicolas Gisin. 2008. A solid-state light-matter interface at the single-photon level. *Nature* 456 (7223): 773–777.
10. De Riedmatten, Hugues, Ivan Marcikic, Hugo Zbinden, and Nicolas Gisin. 2002. Creating high dimensional entanglement using mode-locked lasers. *Quantum Information and Computation* 2 (6): 425–433.
11. Ding, Dong-Sheng, Wu Jing-Hui, Zhi-Yuan Zhou, Yang Liu, Bao-Sen Shi, Xu-Bo Zou, and Guang-Can Guo. 2013. Multimode image memory based on a cold atomic ensemble. *Physical Review A* 87 (1): 013835.
12. Ding, Dong-Sheng, Wu Jing-Hui, Zhi-Yuan Zhou, Bao-Sen Shi, Xu-Bo Zou, and Guang-Can Guo. 2013. Multiple image storage and frequency conversion in a cold atomic ensemble. *Physical Review A* 87 (5): 053830.
13. Dong-Sheng, Ding, Zhi-Yuan Zhou, Bao-Sen Shi, and Guang-Can Guo. 2013. Single-photon-level quantum image memory based on cold atomic ensembles. *Nature communications*, 4.
14. England, D.G., P.S. Michelberger, T.F.M. Champion, K.F. Reim, K.C. Lee, M.R. Sprague, X.M. Jin, N.K. Langford, W.S. Kolthammer, J. Nunn, et al. 2012. High-fidelity polarization storage in a gigahertz bandwidth quantum memory. *Journal of Physics B: Atomic, Molecular and Optical Physics* 45 (12): 124008.
15. Fickler, Robert, Radek Lapkiewicz, William N. Plick, Mario Krenn, Christoph Schaeff, Sven Ramelow, and Anton Zeilinger. 2012. Quantum entanglement of high angular momenta. *Science* 338 (6107): 640–643.
16. Grodecka-Grad, Anna, Emil Zeuthen, and Anders S Sørensen. 2012. High-capacity spatial multimode quantum memories based on atomic ensembles. *Physical review letters*, 109(13):133601.

17. Gündoğan, Mustafa, Patrick M. Ledingham, Attaallah Almasi, and Matteo Cristiani. 2012. Quantum storage of a photonic polarization qubit in a solid. *Physical review letters* 108 (19): 190504.
18. Heinze, Georg, Christian Hubrich, and Thomas Halfmann. 2013. Stopped light and image storage by electromagnetically induced transparency up to the regime of one minute. *Physical review letters* 111 (3): 033601.
19. Higginbottom, Daniel B, Ben M Sparkes, Milos Rancic, Olivier Pinel, Mahdi Hosseini, Ping Koy Lam, and Ben C Buchler. 2012. Spatial-mode storage in a gradient-echo memory. *Physical Review A*, 86(2):023801.
20. Kimble, H.J. 2008. The quantum internet. *Nature* 453: 19.
21. Leach, Jonathan, Barry Jack, Jacqui Romero, Anand K. Jha, Alison M. Yao, Sonja Franke-Arnold, David G. Ireland, Robert W. Boyd, Stephen M Barnett, and Miles J Padgett. 2010. Quantum correlations in optical angle-orbital angular momentum variables. *Science* 329 (5992): 662–665.
22. Lvovsky, Alexander I., Barry C. Sanders, and Wolfgang Tittel. 2009. Optical quantum memory. *Nature photonics* 3 (12): 706–714.
23. Mair, A., A. Vaziri, G. Weihs, and A. Zeilinger. 2001. Entanglement of the orbital angular momentum states of photons. *Nature* 412 (6844): 313.
24. Marrucci, Lorenzo, Ebrahim Karimi, Sergei Slussarenko, Bruno Piccirillo, Enrico Santamato, Eleonora Nagali, and Fabio Sciarrino. 2011. Spin-to-orbital conversion of the angular momentum of light and its classical and quantum applications. *Journal of Optics* 13 (6): 064001.
25. Nicolas, A., L. Veissier, L. Giner, E. Giacobino, D. Maxein, and J. Laurat. 2014. A quantum memory for orbital angular momentum photonic qubits. *Nature Photonics* 8 (3): 234–238.
26. Reim, K.F., P. Michelberger, K.C. Lee, J. Nunn, N.K. Langford, and I.A. Walmsley. 2011. Single-photon-level quantum memory at room temperature. *Physical Review Letters* 107 (5): 053603.
27. Shuker, M., O. Firstenberg, R. Pugatch, A. Ron, and N. Davidson. 2008. Storing images in warm atomic vapor. *Physical review letters* 100 (22): 223601.
28. Thew, R.T., Kae Nemoto, Andrew G. White, and William J Munro. 2002. Qudit quantum-state tomography. *Physical Review A* 66 (1): 012303.
29. Vudyasetu, Praveen K., Ryan M. Camacho, and John C. Howell. 2008. Storage and retrieval of multimode transverse images in hot atomic rubidium vapor. *Physical review letters* 100 (12): 123903.
30. Jinghui, Wu, Yang Liu, Dong-Sheng Ding, Zhi-Yuan Zhou, Bao-Sen Shi, and Guang-Can Guo. 2013. Light storage based on four-wave mixing and electromagnetically induced transparency in cold atoms. *Physical Review A* 87 (1): 013845.
31. Zhang, Han, Xian-Min Jin, Jian Yang, Han-Ning Dai, Sheng-Jun Yang, Tian-Ming Zhao, Yu. Jun Rui, Xiao Jiang He, Fan Yang, et al. 2011. Preparation and storage of frequency-uncorrelated entangled photons from cavity-enhanced spontaneous parametric downconversion. *Nature Photonics* 5 (10): 628–632.
32. Zhou, Zong-Quan, Wei-Bin Lin, Ming Yang, Chuan-Feng Li, and Guang-Can Guo. 2012. Realization of reliable solid-state quantum memory for photonic polarization qubit. *Physical review letters* 108 (19): 190505.
33. Goyal, Sandeep K., Filippus S. Roux, Andrew Forbes, and Thomas Konrad. 2013. Implementing QuantumWalks Using Orbital Angular Momentum of Classical Light. *Physical review letters* 110: 263602.

Chapter 4
Quantum Storage of 2-D OAM Entanglement in an Atomic Ensemble

Abstract Photonic entangled source is the indispensable component in quantum communication and network, which plays a vital role in quantum information science. Constructing a quantum memory which can store photonic entanglement and release is essential for building up network in quantum regime [15, 21, 31, 34]. Quantum storing of photonic entanglement encoded in spin orbital momentum (polarization degree of freedom), or optical paths had been reported in many physical system [6–8, 36, 43, 50]. however there are little progress in storing photonic entanglement in OAM space. Due to the infinite dimensional space spanned by OAM degree of freedom, the photons carrying OAM state shows prospective for dimensional-space based information processing [2, 19, 47], thus enabling the high-capacity communications [46]. In this chapter, for demonstrating OAM entanglement storage, we realize a quantum memory under a far off-resonant two-photon transition, in a cold atomic ensemble. The measured density matrix before and after storage gives a fidelity of $90.3\% \pm 0.8\%$, all results clearly show the preservation of OAM entanglement during storage.

4.1 Research Motivations on Storing Photonic OAM Entanglement

Building up a quantum network in future needs distributing of quantum entangled photons over long distance and establishing quantum correlation between adjacent network nodes. The significant concept of quantum repeater is introduced [4] for resolving the exponential scaling of the error rate with the channel length, which combines entanglement swapping and quantum memory to efficiently extend the achievable distance of quantum communication. During the last years, important progresses have been made towards the realization of an efficient and coherent quantum memory based on gas and solid atomic ensemble [3, 5, 16, 51, 52], photons encoded in a two-dimensional space spanned for example by orthogonal polarizations or different paths had been stored [6–8, 36, 43, 50]. Moreover, many groups and researchers are active in storing light encoded using an OAM space in different physical systems [12–14, 22, 24, 25, 38, 39, 44, 45, 48]. Photon with OAM

D.-S. Ding, *Broad Bandwidth and High Dimensional Quantum Memory Based on Atomic Ensembles*, Springer Theses, https://doi.org/10.1007/978-981-10-7476-9_4

could be regarded helices with left and right handedness twisted to varying degrees [2, 19]. Due to the inherent infinite dimension of OAM space [11, 17, 33], a light encoded in OAM space could offer the high channel capacity. Therefore, the preparation of an OAM entangled state plays a vital role in quantum information and communication fields, and usually was realized by using the spontaneous parametric down-conversion in a crystal [35] or spontaneous Raman scattering (SRS) in an atomic ensemble [27, 28] experimentally.

Building up a quantum network based on OAM involves the coherent interaction [31] between OAM entangled photons and the matter, so storing an entanglement of OAM state is critical for establishing a quantum memory for photonic states encoded in OAM space. The present implemented memory protocols include EIT [23], far off-resonant two-photon transition (FORTPT) [40] (also called as Raman scheme), CRIB [37], and AFC [1], photon echo [26], optomechanical storage [18] and off-resonant Faraday [30]. Of which, FORTPT protocol has some interesting features, such as the ability to store a broadband pulse towards high-speed quantum memories, the insensitivity to inhomogeneous broadening, etc. [41, 42]. Since Zeilinger's group observed the entangled properties of OAM [35] in 2001 year, there has been no any report about quantum storing OAM entanglement via any protocol in any physical systems until we have realized OAM entanglement storage described in this Chapter. Experimentally realizing the storage of the OAM entanglement is a big challenge, because such storage includes the generation OAM entanglement, the storage of OAM entanglement and the encode and project of OAM entanglement.

In this chapter, the first experimental realization of a quantum memory for an OAM entanglement in 2-D subspace was reported. For preparing photonic OAM entangled source, the entanglement between signal 1 photon and the collective spin excited state of the atomic ensemble in MOT 1 was firstly established by nonlinear SRS process referenced from the previous methods [27, 28]. After this preparation process, we send this entanglement into another atomic ensemble for quantum storage by using FORTRT scheme. The signal 1 photon is far-detuned from the atomic transition so that we only use the Raman memory scheme to match the frequency between signal 1 and the memory. If using EIT scheme to perform the memory, it is hard to achieve quantum correlation between signal 1 and the collective spin excited state of atomic ensemble in MOT 1, because the nonlinear SRS process would generate more multi photon events under resonance. Otherwise, it is hard to achieve the storage of signal 1 photon before the entanglement between signal 1 and the collective spin excited state in MOT 1 is collapsed. Only by using Raman scheme, an OAM entanglement can be stored without collapse and the OAM entanglement is established between two atomic ensembles. All results we obtained clearly show the preservation of the OAM entanglement in our gas memory system.

4.2 Experimental Results

Before describing the main results on storing OAM entanglement, we need to emphasize some key points on entanglement storage. The quantum memory can be called as a linear state transfer process. In the process of storage, the photonic entangled state can not be collapsed. There should not be any destructive measurement until the operation of storage has been done. For our purpose on storing OAM entangled state, there are two methods for this: one is preparing OAM entangled photon pair by using SRS process in atomic ensemble, then make a delay for both of photons, one photon is delayed and another is stored; another method is preparing quantum correlation between single photon and collective spin excited state, before the photon has been stored and retrieved, the collective spin excited state cannot be readout for measurement. In this Chapter, we use the later method to perform storing OAM entanglement in principle.

4.2.1 *Details for Experimental Setup and Time Sequence*

The layout of our experiment was given by Fig. 4.1. There are four atomic states used for demonstrating OAM entanglement storage. The states |1> and |2> correspond to

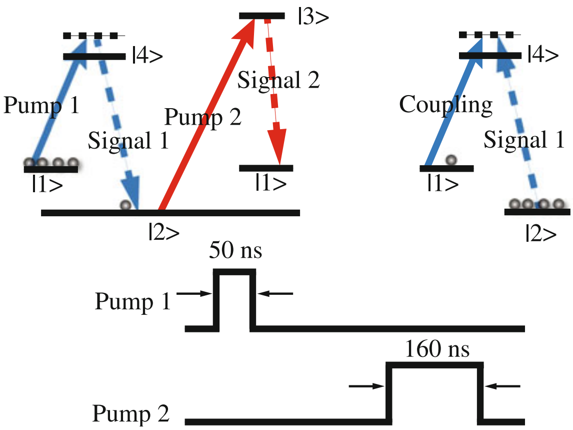

Fig. 4.1 Simplified energy level diagram of the SRS and Raman memory scheme.The pump 1 laser is from an ECDL (DL100, Toptica) with the wavelength of 795 nm, and is blue-detuned to the atomic transition of $5S_{1/2}(F = 3) \rightarrow 5P_{1/2}(F' = 3)$ with a value of +70 MHz. The pump 2 laser is from another ECDL (DL100, Toptica) with the wavelength of 780 nm which couples the atomic transition of $5S_{1/2}(F = 2) \rightarrow 5P_{3/2}(F' = 3)$. The powers of pump 1 and pump 2 are 0.5 mW and 4 mW respectively. The coupling laser is from the same laser with pump 1 and is also blue-detuned to atomic transition of $5S_{1/2}(F = 3) \rightarrow 5P_{1/2}(F' = 3)$ with a value of +70 MHz. In this configuration, the coupling and signal 1 photon can satisfy the condition of Raman two-photon atomic transition

two metastable levels $5S_{1/2}(F = 3)$ and $5S_{1/2}(F = 2)$ of ^{85}Rb atom respectively, |3> and |4> are the excited levels of $5P_{3/2}(F' = 3)$ and $5P_{1/2}(F' = 3)$ respectively. By using a series of AOMs, the pump 1 and pump 2 are modulated into pulse modes with a width of 50 ns and 160 ns respectively, and a rising edge of 30 ns. The rising time of pulse is dependent on the beam waist in the inserted AOM, the smaller the beam waist, the smaller the rising/falling edge of the modulated pulse. The delayed time between the pump 1 pulse and the pump 2 pulse is programed to be 260 ns for the process of storage.

In the experiment, pump 1 was applied firstly for generating an anti-Stokes photon at 795 nm called signal 1 by a non-collinear SRS process in an optically thick cold ensemble, which was trapped in a two-dimensional MOT (MOT 1) [49]. By using a series of mirrors and lenses (a 4-F imaging system was consisted, the plane in the center of MOT 1 is transformed to be in the center of MOT 2), the generated signal 1 photon was delivered into the second cold atomic ensemble in MOT 2 for subsequent storage. A coupling laser pulse with orthogonal polarization to signal 1 was used to store the signal 1 via Raman scheme. The coupling power is set to be 12 mW. After the signal 1 photon was retrieved from MOT 2, the pump 2 laser was switched on for converting the collective spin excited state of the atomic ensemble in MOT 1 to a Stokes photon at 780 nm called signal 2. The delayed time between the pump 1 pulse and the pump 2 pulse is larger than the storage time in MOT 2, otherwise the stored state is not an entangled state (Fig. 4.2).

4.2.2 *Storing a Product Non-classical State*

4.2.2.1 The Experimental Procedure and Details

Firstly, we built a non-classical correlation between signal 1 and collective spin excited state in MOT 1 by SRS process. Then through storing signal 1 photon by using Raman protocol in MOT 2, we established the non-classical correlation in time domain between atomic ensembles in MOT 1 and MOT 2. In this case, the delayed time between the pump 1 and pump 2 pulses was programmed to be 260 ns. In our experiment, before the pump 2 was applied, we added a coupling laser to store the generated signal 1 photon via Raman in MOT 2 for a while for ensuring the storage of non-classical correlation. Then we checked the non-classical correlation between collective spin excited states in MOT 1 and MOT 2 by reading them out to measure the cross-correlation function, which was given by Fig. 4.3. In this implementation, the beam profile of signal 1/2 were not projected with any OAM structure, both of them were Gaussian profile. The detailed information on photon generation, storage and verification were given in the following.

The optical depth (OD) of MOT 1 measured was about 8. The OD of MOT 2 was 20. There was an angle of 3° between the signal 1 and coupling laser for reducing the scattering noise from the coupling laser, due to the large scattering photons making the subsequent filtering difficulty. After a programmed storage time, the signal 1 photon

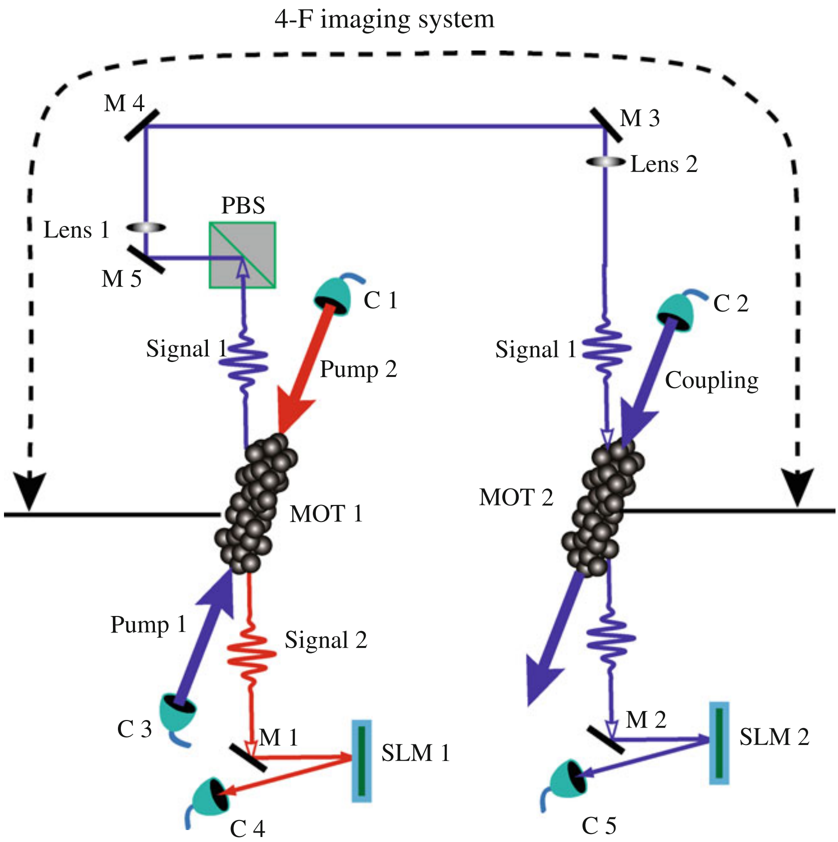

Fig. 4.2 **b** Simplified diagram depicting the storage of entanglement of OAM state. The waist of signal 1 at MOT 2 was 63 μm. MOT: magneto-optical trap; $\lambda l/2$: half-wave plate. Lens 1 and Lens 2 consisted of a 4-F imaging system. C: fibre coupler; M: mirror; SLM: spatial light modulator; PBS: polarisation beam splitter

was retrieved and reflected by a SLM (SLM 2, HOLOEYE, PLUTO. The active area is of 15.36 mm × 8.64 mm, the pixel pitch size is 8 μm, and with a resolution of 1920 × 1080. The reflectivity is of 60%.) and then coupled into a single mode fibre (with an overall efficiency of 30%, including the loss of lens, mirrors, mirror of the MOT 2 and the coupling efficiency of the single mode fibre). After the signal 1 photon was retrieved from MOT 2, the pump 2 laser, which counter-propagated through MOT 1 with pump 1, was switched on for converting the collective spin excited state of the atomic ensemble in MOT 1 to signal 2. Pump 1 and pump 2 had the opposite linear polarizations. The signal 1 and signal 2 counter-propagated and the angle between the signal 1 and pump 2 beams was set to be 3° in order to reduce the scattering noise from the pump lasers. The signal 2 photons were input onto the surface of another

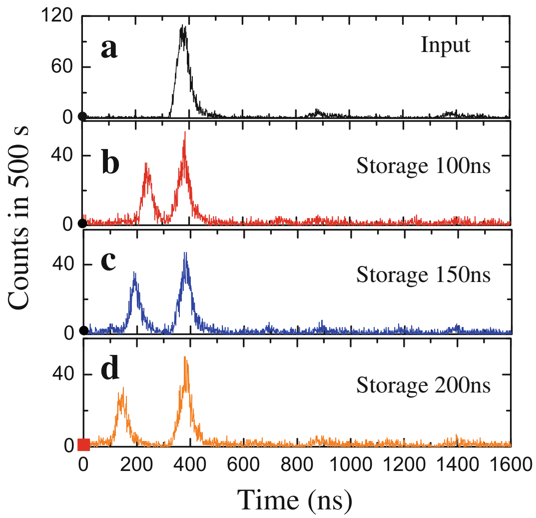

Fig. 4.3 The measurement of cross-correlated function $g_{s1,s2}(\tau)$ in the process of storage. **a** cross-correlated function $g_{s1,s2}(\tau)$ between signal 1 and signal 2 photons with a delayed time of 260 ns between pump 1 and pump 2. **b**, **c** and **d** were the time-correlated function $g_{s1,s2}(\tau)$ between signal 2 photon and the retrieval signal 1 photon with storage time of 100 ns, 150 ns and 200 ns respectively. **e** showed the collected noise without the input signal, which is mainly from the scattering light of coupling laser. The signal 1 acted as trigger photon, and the signal 2 acted as stop signal. The spatial modes of both signal 1 and signal 2 were Gaussian. All data were raw, without noise correction

spatial light modulator (SLM 1), and the reflected photons were coupled into another single mode fibre with a coupling efficiency of 80%.

Both photons were detected by two single photon detectors 1 and 2 respectively (PerkinElmer SPCM-AQR-15-FC, with an efficiency of 60%), whose outputs were converted to NIM signal and connected to a time-to-digital converter (Fast Comtec P7888) with 1 ns bin width for coincidence measurement. The signal 1 acted as trigger photon, and the signal 2 acted as stop signal. The pump 2 was filtered by an interference filter (with a transmission rate of 95%) for reducing the fluorescence noise from diode laser. Several FP etalons with a bandwidth of 500 MHz each were inserted into the optical routes of signal 1 and signal 2 for reducing the noises further, the overall transmission rates were 50% and 60% respectively. The experiment was performed with a repeat rate of 100 Hz. In each cycle, the time for atomic trapping was 8 ms, the experimental window was 1.5 ms, and another 0.5 ms was used to initialize the atomic state.

4.2.2.2 Measurement of Cauchy-Schwarz Inequality and Anti-correlation Parameter

By this way, we built up the non-classical correlation between two MOTs. We could demonstrate this non-classical correlation in time domain by mapping the spin excited states in two ensembles to two photons and checking their correlation. After had retrieved signal 1 photon in MOT 2, we used the pump 2 laser to map the collective spin excited state of the atomic ensemble in MOT 1 to signal 2 photon. We measured the cross-correlation function $g_{s1,s2}(\tau)$ against the storage time, the results were shown in Fig. 4.3. We first proved the existence of a non-classical correlation between these two photons by demonstrating a strong violation of the Cauchy-Schwarz inequality [5]. If $R > 1$ from Eq. 2.6, the light is non-classical correlated. Where $g_{s1,s2}(\tau)$, $g_{s1,s1}(0)$, and $g_{s2,s2}(0)$ are the normalised second-order cross-correlation and auto-correlation of the photons respectively. The normalized $g_{s1,s2}(\tau)$ can be obtained by normalizing the true two-photon coincidence counts to the accidental two-photon coincidence counts $g_{s1,s2}(\infty)$. (Since the time-correlated function in pulse-mode was comb-like peak structure, $g_{s1,s2}(\tau)$ was calculated by the ratio between the coincidence rate in the first peak and that in the second one (not the first one is reasonable).) With $\tau = t_{s1} - t_{s2}$, the relative time delay between paired photons, the maximum $g_{s1,s2}(\tau)$ obtained was $g_{s1,s2}(\tau) = 24$ at $\tau = 380$ ns with the storage time of 150 ns. Thus, $R = 144$, was much larger than 1 using the fact that $g_{s1,s1}(0) = g_{s2,s2}(0) \approx 2$ (photons from signals 1 and 2 exhibited photon statistics typical of thermal light, they are all mixed state for their own), the Cauchy-Schwarz inequality was strongly violated, clearly demonstrating the preservation of non-classical correlation during the storage.

Through HBT [5] experiment, we also characterized the single photon property of the signal 1 photon by checking an anti-correlation parameter α given by 2.7, which were of 0.074 ± 0.012 before storage and 0.29 ± 0.02 after 150 ns-long storage. For an ideally prepared single-photon state, α tends to zero, for a classical field, $\alpha \geq 1$, based on the Cauchy-Schwarz inequality. Both went to zero confirmed clearly the preservation of the single-photon nature in storage. The experimental results also clearly demonstrated the successful storage of a true-single-photon via Raman in an atomic ensemble. The degradation of after storage is mainly from the noise from the scattering of coupling laser, the stricter filtering could reduce it further.

The state stored in the memory is a non-classical state between two atomic ensembles, actually it is a product photonic polarized state between signal 1 photon and the atomic state in MOT 1. If the delayed time between pump 1 and pump 2 laser pulses is much smaller than the storage time, it is thus a heralded process of storing a single photon. The following section describes an experiment on storing OAM product state due to the storage of collapsed entangled state.

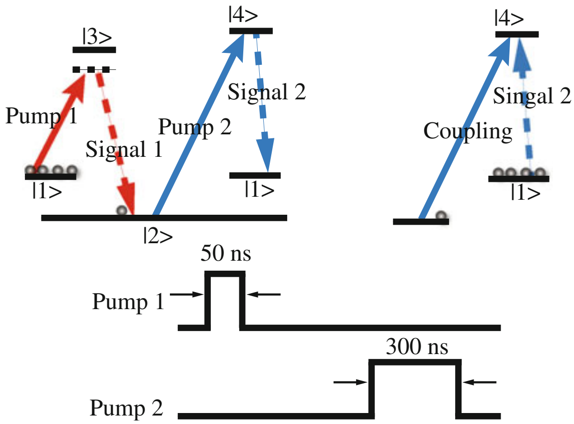

Fig. 4.4 The states$|1>$ and $|2>$ correspond to two metastable levels, $5S_{1/2}(F=3)$ and $5S_{1/2}(F=2)$, of ^{85}Rb respectively, and $|3>$ and $|4>$ are the excited levels $5P_{3/2}(F'=2)$ and $5P_{1/2}(F'=3)$ respectively

4.2.3 Storing Collapsed OAM Entangled State

This subsection described here was to explain the significance of delay time between two pump lasers. The more details are given in the following:

The pump 1 beam was from an ECDL (DL100, Toptica) with a wavelength of 780 nm, and is red-detuned to the atomic transition $5S_{1/2}(F=3) \rightarrow 5P_{3/2}(F'=2)$ with a value of 50 MHz. The pump 2 beam is from another ECDL (DL100, Toptica) with a wavelength of 795 nm, which couples the atomic transition $5S_{1/2}(F=2) \rightarrow 5P_{1/2}(F'=3)$. Pumps 1 and 2 were modulated into pulse mode with a width of 50 ns and 300 ns respectively, and a rising edge of 30 ns (Fig. 4.4).

Then we set the delay time between pumps 1 and 2. In this case, the non-classical correlation between signal 1 photons and the collective atomic spin-excited state of the ensemble was established before pump 2 was applied, and it decayed with the delay time of pump 2 applied. This was verified by mapping the collective spin-excited state of the ensemble to the signal 2 photon, and checking the non-classical correlation between signal 1 and signal 2 photons. However, the signal 1 was detected first, the non-classical property was the feature between electric signal from signal 1 and the collective spin excited state in MOT 1. This state was the projected state when it was collapsed. When pump 2 was applied, the collective spin-excited state was mapped into the signal 2 photon and used for subsequent storage in MOT 2 via EIT.

In this case, we also checked the nature of entanglement by measuring the density matrix and CHSH inequality which were described in more details. The reconstructed density matrix provided a fidelity of 83.9% $\pm$ 3.2% compared with the reconstructed density matrix ρ_{input} before storage. The visibility of the two-photon interference was larger than 70.7%. Although these data we obtained violated the limit of the entanglement, but this was not real storing OAM entanglement. This process can be regarded as many-times storage process with different projected state of signal 1. If there were enough optical delay for the signal 1 in free space, the problem shown in above could be resolved completely.

4.2.4 Storing OAM Entangled State

In the following experiment, the storage process was the real quantum memory of OAM entanglement because the entangled state was not measured before the storage had been done.

4.2.4.1 The Mechanism of OAM Entanglement

We focused on the main part of this work: establishing an OAM entanglement in two atomic ensembles by storing signal 1 photon in MOT 2. How to generate OAM entanglement becomes a problem for our experiment, through Ref. [27, 28], we know that we can create OAM entanglement between photon pairs from a cold atomic ensemble. Due to the momentum conservation in the SRS process (including linear momentum, spin angular momentum and orbital angular momentum), the total momentum of photons and the atomic ensemble after Raman excitation is equal to that before excitation. The SLMs act as spatial post-selection tool instead of mirrors for the following measurements. In the experiment, we built up the OAM entanglement between the anti-Stokes photon and the collective spin excited state of the atomic ensemble in one cold atomic ensemble in MOT 1 by SRS firstly. The initial OAM is zero due to the input Gaussian beam of pump 1 and pump 2 laser beams, there is an OAM correlation between signal 1 and the collective excited state in MOT 1. This entanglement was specified by the formula of [27, 28]

$$|\psi\rangle = \sum_{l=-\infty}^{l=\infty} c_l |l\rangle_{s1} \otimes |-l\rangle_{a1} \tag{4.1}$$

this is a high-dimensional entangled state. Where subscripts s1 and a1 labeled the signal 1 photon and the atomic ensemble in MOT 1 respectively, $|c_l|^2$ is the photonic excitation probability, $|l\rangle$ is the OAM eigenmode with quanta of l. By storing signal 1 photon in the atomic ensemble in MOT 2, the OAM information with signal 1 can be transferred to atomic state, finally, an OAM entangled state between two atomic ensembles was established. We could demonstrate this OAM entanglement by mapping the spin excited states in two ensembles to two photons and checking their entanglement. But in order to simplify the experiment, shorten the measurement time, here we only experimentally demonstrated the storage of the OAM entanglement post-selected in a two-dimensional subspace ($|l>$ and $|-l>$ basis), thus the photonic entanglement state becomes to be $|\Psi> = (|l>|l> + |-l>|-l>)/\sqrt{2}$.

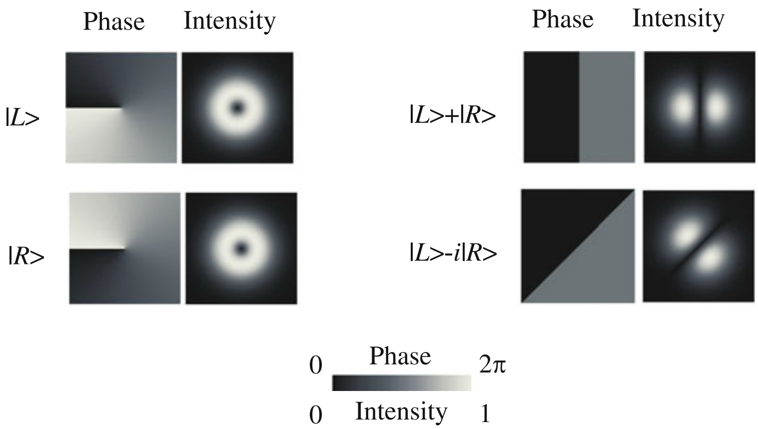

Fig. 4.5 The four OAM states for reconstructing density matrix. The phase (left panel of each pair) and the intensity (right panel) distributions of four OAM states. All images in figure are without transformed, in practical the images we used are the transformed due to same optical components, such as mirrors and lens

4.2.4.2 Entangled State Tomography

In order to characterize the obtained state, two-qubit state tomography [29] was performed to reconstruct the density matrix of state. We experimentally demonstrated the storage of the OAM entanglement post-selected in a two-dimensional subspace by using SLMs. We considered the quanta of OAM $l = \pm 1\ \hbar$. The OAM photons was entangled in an expression of $|\Psi>= (|L>|L> + |R>|R>)/\sqrt{2}$, where $|L>$, and $|R>$ were states corresponding to a well-defined OAM of 1 $\hbar$ and $-1\ \hbar$ respectively. To reconstruct the density matrix of the entangled OAM state, both photons were input to two SLMs respectively, where four states of $|\psi_{1\sim4}>(|L>, |R>, (|L> + |R>)/\sqrt{2}, (|L> -i|R>)/\sqrt{2})$ shown by Fig. 4.5 were programmed onto the SLM 1 and SLM 2 by two computers. The reflected photons from SLMs were collected into two single-mode fibers respectively. We measured each correlated coincidence, obtained a set of 16 data and used them to reconstruct the density matrix.

In the experiment, we set the delayed time of the applied pump 2 to be 260 ns. Before pump 2 was applied, the OAM entanglement between signal 1 photon and the ensemble in MOT 1 was established, which could be verified by mapping the OAM of the ensemble in MOT 1 to signal 2 photon, and checking OAM entanglement between signal 1 and signal 2 photons. By projecting signal 1 and signal 2 photons on basis vectors of $|L>, |R>, (|L> -i|R>)/\sqrt{2}, (|L> + |R>)/\sqrt{2}$ by using two SLMs, we obtained corresponding 16 coincidence rates, then used them to reconstruct the density matrix of the state. Figure 4.6a, b were the corresponding real and imaginary parts of the reconstructed density matrix. By using the formula of $F_1 = \mathrm{Tr}(\sqrt{\sqrt{\rho_{input}}\rho_{ideal}\sqrt{\rho_{input}}})^2$, we calculated the fidelity of the reconstructed density matrix by comparing it with the ideal density matrix, which was of 91.0% ± 1.8%. Where ρ_{ideal} was the density matrix corresponding to the ideal OAM entangled state of $|\Psi>=(|L>|L>+|R>|R>)/\sqrt{2}$, ρ_{input} was the reconstructed density matrix for the input OAM entangled state. Next we sent the signal 1 photon to MOT 2 for subsequent storage via Raman scheme. After a programmed storage time of 150 ns, the signal 1 was retrieved by switching on the coupling light again. Then we applied the pump 2 to map the spin excited state of the ensemble in MOT 1 to signal 2 photon. We measured the time-correlated function between the signal 2 photon and the retrieved signal 1 photon, reconstructed the density matrix according to the measured coincidence rates. The real/imaginary part of the reconstructed density matrix of the OAM entanglement was shown by Fig. 4.6c, d. The fidelity of the density matrix calculated was 84.6% ± 2.6% by comparing it with the ideal density matrix ρ_{ideal}, and was 90.3% ± 0.8% compared with the reconstructed density matrix ρ_{input} before storage by using the formula of $F_2 = \mathrm{Tr}(\sqrt{\sqrt{\rho_{output}}\rho_{input}\sqrt{\rho_{output}}})^2$, where ρ_{output} was the reconstructed density matrix after storage.

4.2.4.3 CHSH Inequality and Two-Photon Interference

In order to check the CHSH inequality and observe two-photon interference, we defined the different sector states by setting different angle phase distributions onto the SLMs shown by Fig. 4.7b, and measured the corresponding coincidence rate with these states. Using these coincidence rates, we calculated the CHSH inequality in the cases of before and after storage. In experiment, the conjugate properties owing to the 4-F imaging system used had been considered when the signal 2 was input onto SLM 2. The details can be referred to Chap. 3. There were one and five mirrors (shown in Fig. 4.1 four mirrors plus a PBS) mounted in optical routes of signal 2 and signal 1 photons respectively. Thus, our system was symmetrical because of the odd-numbered mirror in each optical route (herein one mirror may change the OAM state $|L>/|R>$ to its' reversed state $|R>/|L>$). If the mirror 2 (M2) was removed, the entangled measurement will be of $|\Psi>=(|L>|R>+|R>|L>)/\sqrt{2}$. Another point was that the 4-F imaging system was constructed by lens 1 and lens 2, which induced the inverted imaging in the signal 1 photon due to the conjugation.

We further characterized the degree of entanglement after storage through checking the Bell's inequality, which was the symmetrized version called CHSH inequality [9, 10, 20]. For our experiment, the CHSH parameter S was referenced by Ref. [32] as:

$$S = E(\theta_A, \theta_B) - E(\theta_A, {\theta_B}') + E({\theta_A}', \theta_B) + E({\theta_A}', {\theta_B}') \tag{4.2}$$

where θ_A, θ_B were the angles of the phase distributions on the surfaces of SLMs which were defined in Fig. 4.7. $E(\theta_A, \theta_B)$ can be calculated from the coincidence rates at particular orientations,

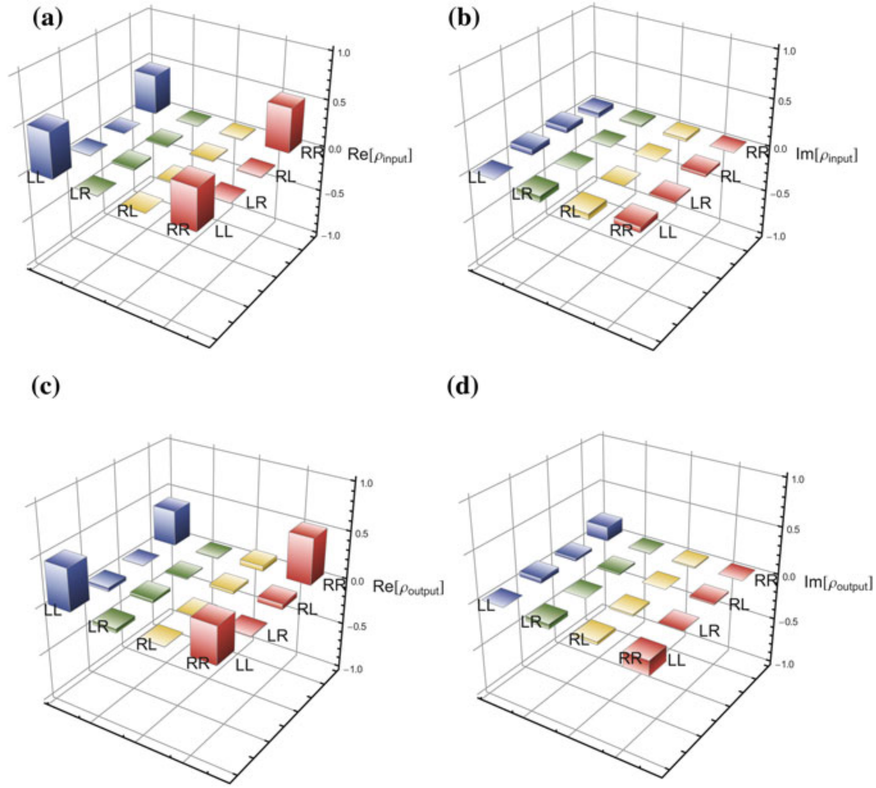

Fig. 4.6 The reconstructed density matrices before and after storage. **a** and **b** are the real and imaginary parts of the reconstructed density matrix of the state before storage respectively. **c** and **d** correspond to the real and imaginary parts of the reconstructed density matrix of the state after storage respectively. The background noise has been subtracted. The background noise was estimated by repeating the experiment without input signal 1 photon to MOT 2. The measurement time for each data was 500 s in **a** and **b** and 1000 s in **c** and **d**

$$E(\theta_A, \theta_B) = \frac{C(\theta_A, \theta_B) + C(\theta_A + \frac{\pi}{2}, \theta_B + \frac{\pi}{2}) - C(\theta_A + \frac{\pi}{2}, \theta_B) - C(\theta_A, \theta_B + \frac{\pi}{2})}{C(\theta_A, \theta_B) + C(\theta_A + \frac{\pi}{2}, \theta_B + \frac{\pi}{2}) + C(\theta_A + \frac{\pi}{2}, \theta_B) + C(\theta_A, \theta_B + \frac{\pi}{2})} \tag{4.3}$$

In our experiment, we selected $\theta_A = 0$, $\theta_B = \pi/8$, $\theta_{A\prime} = \pi/4$, $\theta_{B\prime} = 3\pi/8$. The calculated S was of $S = 2.48 \pm 0.04$ before storage and $S = 2.41 \pm 0.06$ after storage. The inequality is violated when the values of S are greater than 2 and the violation of inequality means that there exists the entanglement between photons. These results experimentally obtained clearly showed that the CHSH inequality was violated even after a programmed storage time, demonstrating the preservation of the OAM entanglement during the storage.

Moreover, we checked the two-photon interference. As we knew that if the visibility of the two-photon interference was $>70.7\%$, then CHSH inequality would be

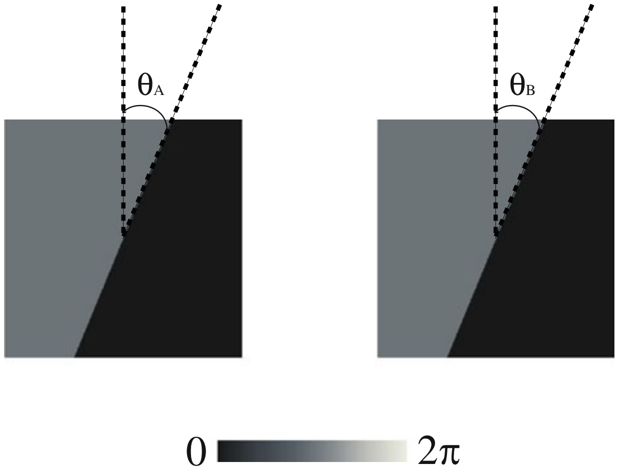

Fig. 4.7 The different sector states corresponding to the different OAM superposition states defined by different angles θ_A, θ_B. The dark area represents the zero phase, while the gray color is the phase of π

violated, proving the entanglement existed between two photons. In this experiment, we fixed the phase angle of SLM 1 to be $\theta_A = 0^\circ$ or 45° respectively, measured the coincidence rate at different angles of θ_B of the SLM 2. The storage time was set to be of 150 ns. The experimental results were shown by Fig. 4.8, visibility was 85.2% $\pm$ 3.0% at $\theta_A = 0^\circ$ and 86.8% $\pm$ 3.3% at $\theta_A = 45^\circ$, both were larger than 70.7%, clearly proved the preservation of the OAM entanglement in storage again.

In experiment, the error bar of our measurement was estimated from Poisson statistics and using Monte Carlo simulations. The details are the following: we assume our experimental data follows the Poisson distribution. For each data point, we assume 50 random numbers by using Mathematics software, which are in the Poisson distribution. The errors of visibility and fidelity are then estimated by the square root of the variance of the 50 values.

4.3 Research Summary

In conclusion, the first experimental realization of storing OAM entanglement via Raman in an atomic ensemble is introduced in details. The fidelity of the reconstructed density matrices in a post-selected two-dimensional subspace before and after storage were 91% and 84% respectively compared with the ideal density matrix. In addition, the violations of CHSH inequality were experimentally demonstrated before and after storage. Besides, we also realized the first experimental storage of a true-single-photon state via Raman in an atomic ensemble, and also provided experimental evidence that an image memory at single-photon level can be realized via Raman

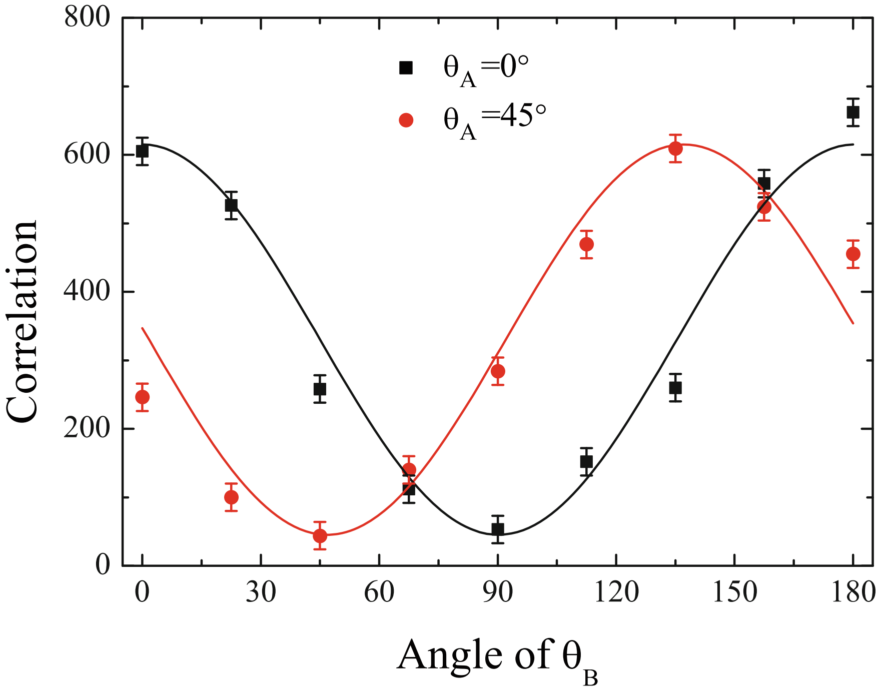

Fig. 4.8 The measured coincidence rate at $\theta_A = 0^{\circ}$ and 45° with different θ_B. The red (blue) curve represents the correlated coincidence rate with the orientations of $\theta_A = 0$ (45°). The background noise has been subtracted. Error bar is ± 1 standard deviation. The background noise was estimated by repeating the experiment without input signal 1 photon to MOT 2. The measurement time for each data was 1000 s

too. It is very promising to demonstrate GHz-bandwidth quantum memory for storing photonic OAM entanglement and increase the bandwidth of Raman protocol in cold atomic medium. This work reported herein clearly demonstrates the workability of building up a high-dimensional quantum communication system in the future.

References

1. Afzelius, Mikael, Christoph Simon, Hugues De Riedmatten, and Nicolas Gisin. 2009. Multimode quantum memory based on atomic frequency combs. *Physical Review A* 79 (5): 052329.
2. Allen, Les, Marco W. Beijersbergen, R.J.C. Spreeuw, and J.P. Woerdman. 1992. Orbital angular momentum of light and the transformation of laguerre-gaussian laser modes. *Physical Review A* 45 (11): 8185.
3. Appel, Jürgen, Eden Figueroa, Dmitry Korystov, M. Lobino, and A.I. Lvovsky. 2008. Quantum memory for squeezed light. *Physical Review Letters* 100 (9): 093602.
4. Briegel, H.-J., Wolfgang Dür, Juan I. Cirac, and Peter Zoller. 1998. Quantum repeaters: the role of imperfect local operations in quantum communication. *Physical Review Letters* 81 (26): 5932.

5. Chanelière, T., D.N. Matsukevich, S.D. Jenkins, S.Y. Lan, T.A. Kennedy, and A. Kuzmich. 2005. Storage and retrieval of single photons transmitted between remote quantum memories. *Nature* 438 (7069): 833.
6. Choi, K.S., H. Deng, J. Laurat, and H.J. Kimble. 2008. Mapping photonic entanglement into and out of a quantum memory. *Nature* 452 (7183): 67–71.
7. Chou, C.W., H. de Riedmatten, D. Felinto, S.V. Polyakov, S.J. van Enk, and H.J. Kimble. 2005. Measurement-induced entanglement for excitation stored in remote atomic ensembles. *Nature* 438 (7069): 828–832.
8. Clausen, C., I. Usmani, F. Bussières, N. Sangouard, M. Afzelius, H. de Riedmatten, and N. Gisin. 2011. Quantum storage of photonic entanglement in a crystal. *Nature* 469 (7331): 508–511.
9. Clauser, John, F., and Michael A. Horne. 1974. Experimental consequences of objective local theories. *Physical Review D* 10 (2): 526.
10. Clauser, John, F., Michael A. Horne, Abner Shimony, and Richard A. Holt. 1969. Proposed experiment to test local hidden-variable theories. *Physical Review Letters* 23 (15): 880.
11. Dada, Adetunmise, C., Jonathan Leach, Gerald S. Buller, Miles J. Padgett, and Erika Andersson. 2011. Experimental high-dimensional two-photon entanglement and violations of generalized bell inequalities. *Nature Physics* 7 (9): 677–680.
12. Ding, Dong-Sheng, Wu Jing-Hui, Zhi-Yuan Zhou, Yang Liu, Bao-Sen Shi, Xu-Bo Zou, and Guang-Can Guo. 2013. Multimode image memory based on a cold atomic ensemble. *Physical Review A* 87 (1): 013835.
13. Ding, Dong-Sheng, Wu Jing-Hui, Zhi-Yuan Zhou, Bao-Sen Shi, Xu-Bo Zou, and Guang-Can Guo. 2013. Multiple image storage and frequency conversion in a cold atomic ensemble. *Physical Review A* 87 (5): 053830.
14. Ding, Dong-Sheng, Zhi-Yuan Zhou, Bao-Sen Shi, and Guang-Can Guo. 2013. Single-photon-level quantum image memory based on cold atomic ensembles. *Nature Communications*, 4.
15. Duan, L.M., M.D. Lukin, J.I. Cirac, and P. Zoller. 2001. Long-distance quantum communication with atomic ensembles and linear optics. *Nature* 414 (6862): 413.
16. Eisaman, M.D., A. André, F. Massou, M. Fleischhauer, et al. 2005. Electromagnetically induced transparency with tunable single-photon pulses. *Nature* 438 (7069): 837.
17. Fickler, Robert, Radek Lapkiewicz, William N. Plick, Mario Krenn, Christoph Schaeff, Sven Ramelow, and Anton Zeilinger. 2012. Quantum entanglement of high angular momenta. *Science* 338 (6107): 640–643.
18. Fiore, Victor, Yong Yang, Mark C. Kuzyk, Russell Barbour, Lin Tian, and Hailin Wang. 2011. Storing optical information as a mechanical excitation in a silica optomechanical resonator. *Physical Review Letters* 107 (13): 133601.
19. Franke-Arnold, Sonja, Les Allen, and Miles Padgett. 2008. Advances in optical angular momentum. *Laser & Photonics Reviews* 2 (4): 299–313.
20. Freedman , Stuart J., and John F. Clauser. 1972. Experimental test of local hidden-variable theories. *Physical Review Letters* 28 (14): 938.
21. Alberto Galindo and Miguel Angelo Martin-Delgado. 2002. Information and computation: Classical and quantum aspects. *Reviews of Modern Physics* 74 (2): 347.
22. Glorieux, Quentin, Jeremy B. Clark, Alberto M. Marino, Zhifan Zhou, and Paul D. Lett. 2012. Temporally multiplexed storage of images in a gradient echo memory. *Optics Express* 20 (11): 12350–12358.
23. Hau, Lene Vestergaard, Stephen E. Harris, Zachary Dutton, and Cyrus H. Behroozi. 1999. Light speed reduction to 17 metres per second in an ultracold atomic gas. *Nature* 397 (6720): 594.
24. Heinze, G., A. Rudolf, F. Beil, and T. Halfmann. 2010. Storage of images in atomic coherences in a rare-earth-ion-doped solid. *Physical Review A* 81 (1): 011401.
25. Higginbottom, Daniel B., Ben M. Sparkes, Milos Rancic, Olivier Pinel, Mahdi Hosseini, Ping Koy Lam, and Ben C. Buchler. 2012. Spatial-mode storage in a gradient-echo memory. *Physical Review A* 86(2):023801.

26. Hosseini, Mahdi, Ben M. Sparkes, Geoff Campbell, Ping K. Lam, and Ben C. Buchler. 2011. High efficiency coherent optical memory with warm rubidium vapour. *Nature Communications* 2: 174.
27. Inoue, R., N. Kanai, T. Yonehara, Y. Miyamoto, M. Koashi, and M. Kozuma. 2006. Entanglement of orbital angular momentum states between an ensemble of cold atoms and a photon. *Physical Review A* 74 (5): 053809.
28. Inoue, R., T. Yonehara, Y. Miyamoto, M. Koashi, and M. Kozuma. 2009. Measuring qutrit-qutrit entanglement of orbital angular momentum states of an atomic ensemble and a photon. *Physical Review Letters* 103 (11): 110503.
29. James, Daniel F.V. Paul G. Kwiat, William J. Munro, and Andrew G. White. 2001. Measurement of qubits. *Physical Review A* 64 (5): 052312.
30. Julsgaard, B., J. Sherson, J.I. Cirac, J. Fiurásek, and E.S. Polzik. 2004. Experimental demonstration of quantum memory for light. *Nature* 432 (7016): 482–486.
31. Kimble, H.J. 2008. The quantum internet. *Nature* 453: 19.
32. Leach, J., B. Jack, J. Romero, M. Ritsch-Marte, R.W. Boyd, A.K. Jha, S.M. Barnett, S. Franke-Arnold, and M.J. Padgett. 2009. Violation of a bell inequality in two-dimensional orbital angular momentum state-spaces. *Optics Express* 17 (10): 8287–8293.
33. Leach, Jonathan, Barry Jack, Jacqui Romero, Anand K. Jha, Alison M. Yao, Sonja Franke-Arnold, David G. Ireland, Robert W. Boyd, Stephen M. Barnett, and Miles J. Padgett. Quantum correlations in optical angle-orbital angular momentum variables. *Science* 329 (5992): 662–665.
34. Lvovsky, Alexander I., Barry C. Sanders, and Wolfgang Tittel. 2009. Optical quantum memory. *Nature Photonics* 3 (12): 706–714.
35. Mair, A., A. Vaziri, G. Weihs, and A. Zeilinger. 2001. Entanglement of the orbital angular momentum states of photons. *Nature* 412 (6844): 313.
36. Moehring, D.L., P. Maunz, S. Olmschenk, K.C. Younge, D.N. Matsukevich, L.-M. Duan, and C. Monroe. 2007. Entanglement of single-atom quantum bits at a distance. *Nature* 449 (7158): 68.
37. Moiseev, S.A., and Stefan kröll. 2001. Complete reconstruction of the quantum state of a single-photon wave packet absorbed by a doppler-broadened transition. *Physical Review Letters* 87 (17): 173601.
38. Moretti, D., D. Felinto, and J.W.R. Tabosa. 2009. Collapses and revivals of stored orbital angular momentum of light in a cold-atom ensemble. *Physical Review A* 79 (2): 023825.
39. Nicolas, A., L. Veissier, L. Giner, E. Giacobino, D. Maxein, and J. Laurat. 2014. A quantum memory for orbital angular momentum photonic qubits. *Nature Photonics* 8 (3): 234–238.
40. Nunn, J., I.A. Walmsley, M.G. Raymer, K. Surmacz, F.C. Waldermann, Z. Wang, and D. Jaksch. 2007. Mapping broadband single-photon wave packets into an atomic memory. *Physical Review A* 75 (1): 011401.
41. Reim, K.F., P. Michelberger, K.C. Lee, J. Nunn, N.K. Langford, and I.A. Walmsley. 2011. Single-photon-level quantum memory at room temperature. *Physical Review Letters* 107 (5): 053603.
42. Reim, K.F., J. Nunn, V.O. Lorenz, B.J. Sussman, K.C. Lee, N.K. Langford, D. Jaksch, and I.A. Walmsley. 2010. Towards high-speed optical quantum memories. *Nature Photonics* 4 (4): 218–221.
43. Saglamyurek, Erhan, Jeongwan Jin, Varun B. Verma, Matthew D. Shaw, Francesco Marsili, Sae Woo Nam, Daniel Oblak, and Wolfgang Tittel. 2015. Quantum storage of entangled telecom-wavelength photons in an erbium-doped optical fibre. *Nature Photonics* 9 (2): 83–87.
44. Shuker, M., O. Firstenberg, R. Pugatch, A. Ron, and N. Davidson. 2008. Storing images in warm atomic vapor. *Physical Review Letters* 100 (22): 223601.
45. Vudyasetu, Praveen K., Ryan M. Camacho, and John C. Howell. 2008. Storage and retrieval of multimode transverse images in hot atomic rubidium vapor. *Physical Review Letters* 100 (12): 123903.
46. Wang, Jian, Jeng-Yuan Yang, Irfan M. Fazal, Nisar Ahmed, Yan Yan, Hao Huang, Yongxiong Ren, Yang Yue, Samuel Dolinar, Moshe Tur, et al. 2012. Terabit free-space data transmission employing orbital angular momentum multiplexing. *Nature Photonics* 6 (7): 488–496.

47. Weihs, G., and A. Zeilinger. 2001. Entanglement of the orbital angular momentum states of photon. *Nature* 412: 313–316.
48. Jinghui, Wu, Yang Liu, Dong-Sheng Ding, Zhi-Yuan Zhou, Bao-Sen Shi, and Guang-Can Guo. 2013. Light storage based on four-wave mixing and electromagnetically induced transparency in cold atoms. *Physical Review A* 87 (1): 013845.
49. Liu Yang, Wu, Shi Bao-Sen Jing-Hui, and Guo Guang-Can. 2012. Realization of a two-dimensional magneto-optical trap with a high optical depth. *Chinese Physics Letters* 29 (2): 024205.
50. Zhang, Han, Xian-Min Jin, Jian Yang, Han-Ning Dai, Sheng-Jun Yang, Tian-Ming Zhao, Yu. Jun Rui, Xiao Jiang He, Fan Yang, et al. 2011. Preparation and storage of frequency-uncorrelated entangled photons from cavity-enhanced spontaneous parametric downconversion. *Nature Photonics* 5 (10): 628–632.
51. Zhao, Bo, Yu-Ao Chen, Xiao-Hui Bao, Thorsten Strassel, Chih-Sung Chuu, Xian-Min Jin, Jörg Schmiedmayer, Zhen-Sheng Yuan, Shuai Chen, and Jian-Wei Pan. 2008. A millisecond quantum memory for scalable quantum networks. arXiv preprint arXiv:0807.5064.
52. Zhao, R., Y.O. Dudin, S.D. Jenkins, C.J. Campbell, D.N. Matsukevich, T.A.B. Kennedy, and A. Kuzmich. 2009. Long-lived quantum memory. *Nature Physics* 5(2).

Chapter 5
Quantum Storage of High-D OAM Entanglement in an Atomic Ensemble

Abstract In this Chapter, I focus on the key goal as described in the beginning, that is the realization of high-dimensional entanglement storage and establishment high-dimensional entanglement between two atomic states. Quantum states entangled in high-dimensional OAM space show more advantages that entangled in two-dimensional space, like photonic polarization DOF. They enable quantum communication with enhanced channel capacity, quantum-information processing in more efficient way, and be more feasible to close the detection loophole in the fundamental quantum physics of Bell test experiments, etc. Preparing high-dimensional OAM entangled state and establishing distant memories in high-dimensional OAM entanglement are significant for long-distance communication in high-space, but its experimental demonstration was lacking before this work has been implemented. Herein, we have experimentally established high-dimensional entanglement in OAM space between two atomic ensembles separated 1 m apart through the technique of Raman storing photonic OAM high-dimensional entangled state. We reconstructed the density matrix for a three-dimensional entanglement, and obtained an entanglement fidelity of 83.9 ± 2.9%. More importantly, we confirmed the successful preparation of a state entangled in more than three-dimensional space (up to seven-dimensional) using general and conditional entanglement witnesses. Achieving high-dimensional entanglement may represent a significant step towards a high-capacity quantum information processing, quantum communications in high-dimension.

5.1 Research Motivations on Storing High-Dimensional OAM Entanglement

Constructing quantum networks based on OAM DOF involves the preparation of high-dimensional OAM entangled photons and the realization of high-dimensional entangled memories. As we know, quantum entanglement distributed in distant nodes is significantly essential for realizing long-distance quantum communications [29]. By introducing a quantum repeater protocol, the problem of exponential scaling of the error rates with channel length in quantum communication can be overcome with entanglement storage, entanglement swapping and entanglement purification etc. [5].

D.-S. Ding, *Broad Bandwidth and High Dimensional Quantum Memory Based on Atomic Ensembles*, Springer Theses, https://doi.org/10.1007/978-981-10-7476-9_5

The repeaters for high-dimensional quantum communication network are based on many high-dimensional entangled memories modes, the long-distance communication can be realized through swapping operation between the adjacent entangled memories. Thus, establishing high-dimensional entangled memories with physical systems is a critical step.

Progresses have been made towards preparing high-dimensional OAM entangled states, including measuring a three-dimensional entanglement between a delayed atomic spin wave and a photon [28] through SRS, an 11-dimensional entanglement verified by checking high-dimensional Bell inequality [10], a high-dimensional image entanglement measured by a high-resolution and high efficient camera [17], and generation of a 100×100-dimension OAM entanglement [31] between two photons by SPDC. There are many progresses towards storing entangled photons with different DOF in different systems. Usually, the stored photons are encoded in a two-dimensional space such as for photonic polarization, which-path of photon propagating, and time-bin in time domain, resulting in information carried by a photon as a qubit. Recently, another photonic DOF, OAM [19, 32, 48], has attracted much interest and provides many potential applications because the OAM states of the photon could belong to a high-dimensional Hilbert space, which would enable encoding with inherent infinite DOF, thereby enhancing the capacity of channel and improving the efficiency of network significantly [14, 45].

In recent years, many groups have been exploring the realization of high-dimensional entangled memories with some successful characteristic [12, 13, 16, 21, 25, 27, 33, 34, 40, 43, 44, 46], but all these work has only displayed approaches to this goal. Until this work has been realized, all experimental works on establishing entangled memories using different physical systems have focused on the entanglement only in a two-dimensional space [7, 8, 11, 15, 38, 49]. The storage of a high-dimensional OAM state on demand in a physical system is a key for the realization of quantum repeaters for long-distance quantum communications, and the establishment of a high-dimensional OAM entanglement between distant quantum memories is a primary node of the high-dimensional quantum network. Trying to demonstrate this experiment in lab is the main motivation of this work.

A previous work [15] as described in Chap. 4 in details has reported the creation of a two-dimensional OAM entanglement between two atomic ensembles, but the realization of a high-dimensional entanglement between different quantum memories is non-trivial, and is not a straightforward extension of establishing a two-dimensional entanglement between two atomic ensembles. There are many challenges, especially in proving the exact nature of high-dimensional entanglement, determining the dimension of OAM entanglement, etc. Generally, we could characterize the storage with entanglement fidelity by comparing the density matrices before and after storage, which are reconstructed via a technique of quantum tomography. For a high-dimensional entangled state, the number of required measurements for reconstructing density matrix scales quadratically with dimension D. Therefore reconstructing the density matrices for a high-dimensional (>3) entangled state is impractical because the amount of data needed to be measured significantly increases. In addition, how to balance the distinct efficiencies in generating and storing the different OAM modes in high-dimension is also a challenge, which becomes more difficult for high dimension.

In this Chapter, we introduce the experimental demonstration of high-dimensional OAM entanglement between two quantum memories by using Raman storing photonic OAM high-dimensional entanglement, as a result, this makes a primary step towards building up a high-dimensional quantum network. In practical procedure, we entangled high-dimensional OAM states of a photon and a collective spin-excited state in first cold atomic ensemble by SRS [28], and then sent this photon to be stored in second cold atomic ensemble using the Raman scheme [36]. In this way, we established high-dimensional OAM entanglement between two atomic ensembles. We measured the entanglement by mapping the spin-excited states in the two ensembles to two photons and checked whether or not there is indeed an entanglement. We reconstructed the density matrices of the three-dimensional OAM entangled photons. All results obtained in my lab show there is exactly a high-dimensional OAM entanglement during the storage. By using an entanglement witness (called as general witness) to characterize the nature of the higher dimensional entanglement, concluding that there is at least a four-dimensional entanglement within the two memories. Through the dimensionality witness (called as conditional witness), we confirmed a seven-dimensional entanglement between these two memories.

5.2 Experimental Results

Before introducing the main results on storing high-dimensional OAM entanglement, it needs to explain the main challenges for our experiment. First, it is not easy to balance the distinct efficiencies in storing the different OAM modes. This is not a problem in the two-dimensional case because any two OAM modes with the same value but opposite sign serve as a two-dimensional space, because same OAM mode has same storage efficiency. Another big difference is that a series of 4-F imaging systems are designed subtly and constructed meticulously in this Chapter to detect the high-dimensional entanglement, instead of the direct projection on SLM for the low azimuthal index of $\pm 1\ \hbar$ in Ref. [15]; otherwise, we could not obtain the correct results for reconstructing the density matrix and calculating the witness. We believe these are the main reasons why there have been no reports of experimental progress until that time. Indeed on one important aspect, i.e., the storage of a high-dimensional OAM state on demand in any physical system and the establishment of a high-dimensional OAM entanglement between different quantum memories, storing high-dimensional OAM entanglement definitely represents primary progress and a significant step forward in the field of quantum information science.

5.2.1 Experimental Details

The experimental media are optically thick atomic ensembles of Rubidium 85 (^{85}Rb) trapped in two MOTs [47], separated 1 m apart but working independently. The schematic of the energy levels involved and the experimental setup are shown in Fig. 5.1a and b. Through inputting Gaussian pulse modes with a pulse width of 30 ns, we prepared an OAM entanglement between the signal-1 photon and the collective spin-excited state of atomic ensemble in MOT 1 by SRS. In this process, the laser pulse of pump 1 was blue-detuned by 70 MHz to the atomic transition $|3>(5S_{1/2}(F=3)) \rightarrow |2>(5P_{1/2}(F'=3))$ and the signal-1 was blue-detuned by 70 MHz to atomic transition $|2>(5P_{1/2}(F'=3)) \rightarrow |1>(5S_{1/2}(F=2))$. As this is a SRS process that conserves momentum, the initial state of the system has zero linear and angular momentum, so that the resulting joint state of the signal 1 photon and the atomic spin-excited state has zero total linear and angular momentum, which induces OAM quantum correlations between them. The linear momentum correlation can be used to prepared multiplexing K-vectors entangled state as described in Chap. 6. The established OAM entanglement between photon and atoms is written as:

$$|\psi\rangle = \sum_{m=-\infty}^{m=\infty} c_m |m\rangle_{s1} \otimes |-m\rangle_{a1}$$

where $|m\rangle$ denotes the OAM state of the m quantum eigenmode; subscripts s1 and a1 refer to the signal-1 photon and the atomic ensemble in MOT 1, respectively; and is the excitation probability for different OAM modes. Next, the signal-1 photons are sent to be stored as a collective spin-excited state of the atomic ensemble trapped in MOT 2 using the Raman scheme [35]. Hence, the collective spin-excited state of two atomic ensembles in different MOTs are in a high-dimensional entanglement of

$$\left|\psi'\right\rangle = \sum_{m=-\infty}^{m=\infty} o_m |-m\rangle_{a1} \otimes |-m\rangle_{a2} \tag{5.1}$$

where $|o_m|^2$ is the amplitude probability for the different modes m, and subscript a2 refers to the atomic collective spin-excited states in MOT 2. The power of the coupling laser is 40 mW with a beam waist of 2 mm, corresponding to the Rabi frequency of 10.6 Γ (Γ is the decay rate of level $5P_{1/2}(F'=3)$). The storage time T2 in MOT 2 should not be larger than the storage time of the spin wave T1 in MOT 1 to demonstrate the storage of the entanglement as explained in Chap. 4, otherwise the stored state is a post-selected product state. In our experiment, the condition T2 = T1 = 100 ns is taken; i.e., the coupling laser and pump-2 laser are opened at the same time. Furthermore, we apply the method detailed in Ref. [15] to match the bandwidth between the signal-1 photons and the memory for high storage efficiency, and a storage efficiency of 26.8% is achieved experimentally. The memory efficiency is calculated as the ratio of coincidence counts for after and before storage. After a

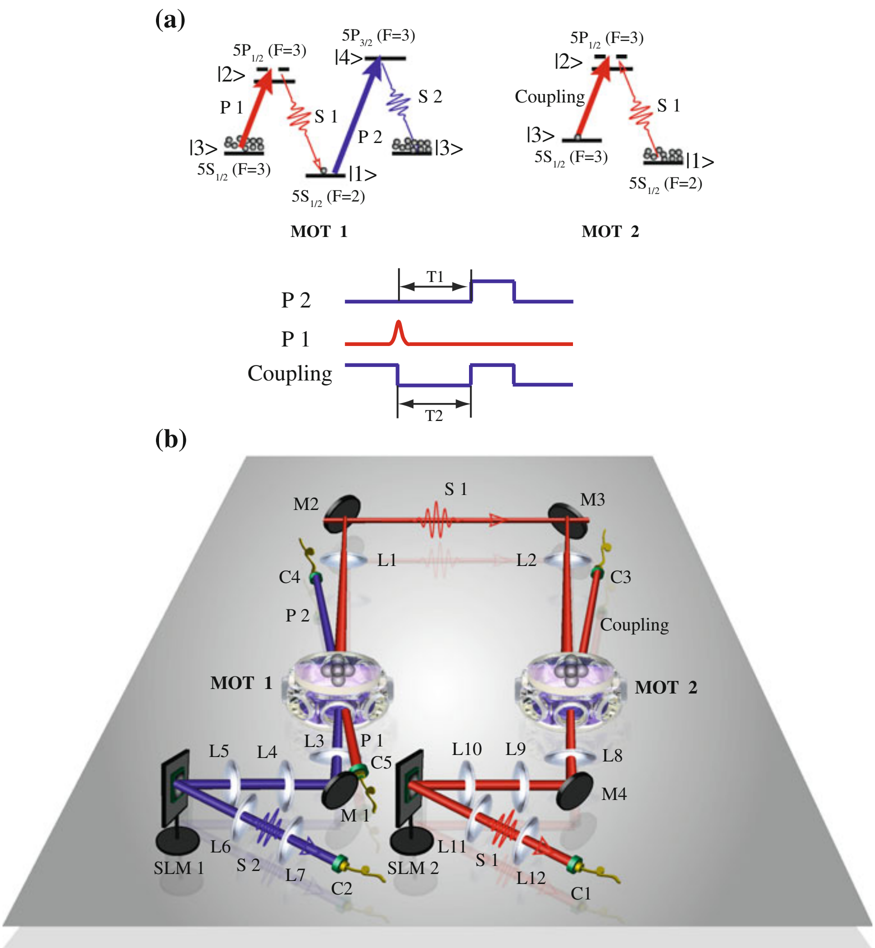

Fig. 5.1 **a** Energy level diagrams and the time sequence for creating and storing OAM entanglement. **b** Experimental setup. Lenses L1 and L2 are used to focus signal 1 on the center of MOT 2. L3, L4, and L5 are used to focus the phase structure of signal 2 on the center of MOT 1 onto the surface of SLM 2. L6 and L7 are used to couple the OAM mode of signal 2 to C2. There is an asymmetric optical path for coupling signal 1 into C1 in the right half of the figure. P 1/2: Pump 1/2; S 1/2: Signal 1/2; C: fiber coupler; M: mirror; L: lens

delayed time of 100 ns, we used the pump-2 laser with a square pulse of 250 ns width, resonant with the atomic transition |1> $(5S_{1/2}(F = 2)) \rightarrow |4 > (5P_{3/2}(F' = 3))$, to read the spin wave to generate the signal-2 photon, which corresponds to the atomic transition |4> $(5P_{3/2}(F' = 3)) \rightarrow |3 > (5S_{1/2}(F = 3))$. Simultaneously, we switched the coupling laser on to read the signal-1 photon out of the atomic ensemble in MOT 1. The delayed time is measured by comparing the peaks of the two-photon coincidence with and without delayed pumps 1 and 2. Pumps 1 and 2 have power

0.5 mW and 4 mW, respectively. Through checking the entanglement between the signal-1 and signal-2 photons in OAM space, we can verify the high-dimensional entanglement between the two atomic ensembles.

For the experimental configuration, a series of 4-F imaging systems are designed subtly to make the measurement easier and more feasible. The main idea of the design of 4-F imaging system is given by Fig. 5.2. In order to explain different measured results based on the imaging process, I assume the fiber tip is at the position of image plane. For this assumption, the lens 2 and the fiber tip form a commercial optical collimator as we usually used in lab. Due to the conjugate property between input image and the out image, the intensity measured at image plane should be a single peak profile. As a result, this configuration cannot distinguish the different OAM modes, because the transverse intensity distribution scanned by fiber tip is always a single peak. If the fiber tip is at transform plane, in which the OAM modes are transformed to be the intensity profile, the transverse distribution is the intensity profile of OAM eigenmode.

5.2.2 *High-D OAM Correlation*

Before checking the high-dimensional OAM entanglement, the correlations in the OAM space between the two ensembles before and after storage were first taken to measure by coincidence. The results are shown in Fig. 5.3 with panels (a)/(b) showing the OAM correlations between photons of signal 1 and signal 2 without/with storing signal 1. This also characterizes the correlations between the signal-1 photon and the atomic collective spin-excited state in MOT 1. The soft differences in OAM correlations shown in Fig. 5.3a arise from different OAM distributions in the nonlinear SRS process Fig. 5.3c. While the orthogonal characteristics between different OAM modes can be seen in non-diagonal elements of Fig. 5.3. Because the efficiencies are different in storing the various OAM modes $|m>$, the resulting correlation matrix after storage Fig. 5.3b has a little difference from that before storage Fig. 5.3a; this is similar to the result demonstrated using a weak coherent light [14]. The different storage efficiencies measured for different OAM modes m are shown in Fig. 5.3d.

There are many limiting factors for atomic storage time: such as residual magnetic field and atomic motion etc. In general, memory time can be improved by compensating the magnetic field or by using magnetic field-insensitive states. By reducing atomic motion by using optical lattice, a millisecond even hundred millisecond storage time could be achieved. In addition, the dynamic decoupling method can also be used to improve the storage time. Besides, in present experiment, the storage time is also limited by the experimental time sequence, which is performed within hundreds' nanoseconds. The storage time can be improved further through optimizing the time sequence.

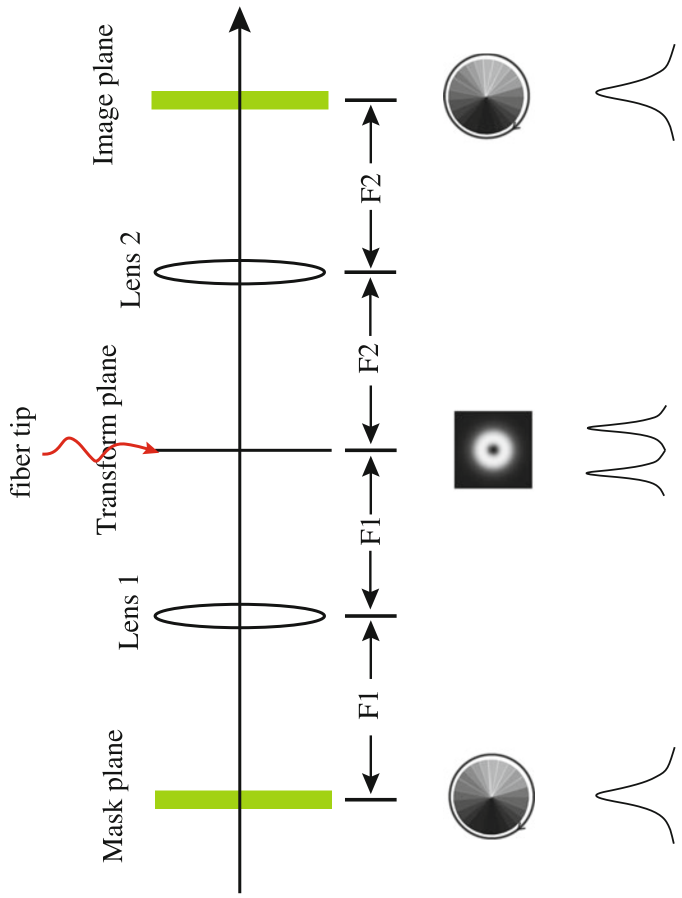

Fig. 5.2 Design of 4-F imaging system for high quanta OAM mode detection. F1 and F2 are focus length of lens 1 and 2 respectively. The spiral phase of OAM light can be transformed to its' conjugate spiral phase by using 4-F imaging system

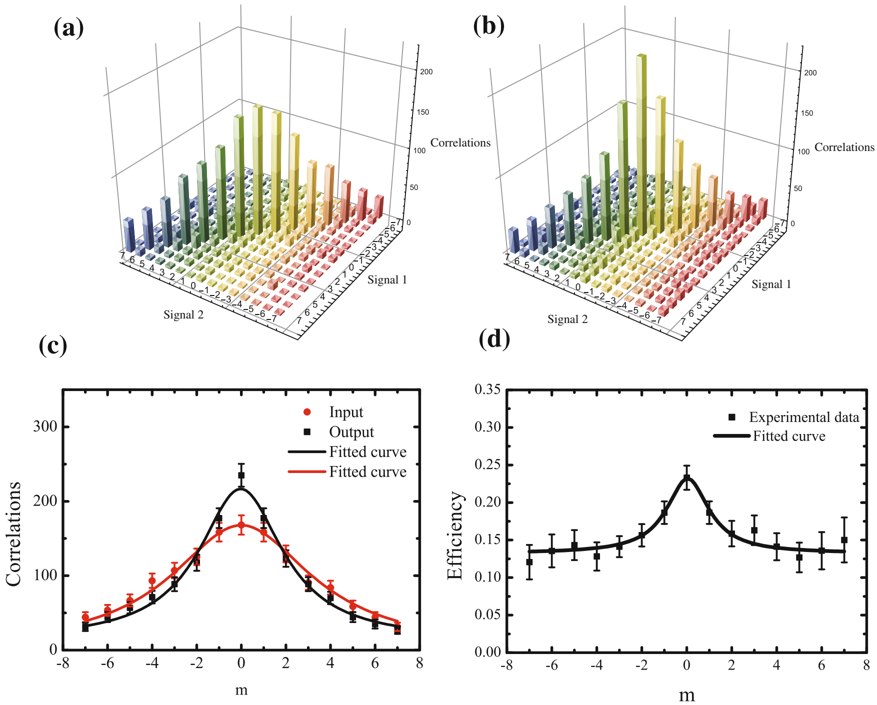

Fig. 5.3 OAM Correlation between signal 1 and signal 2 photons with $m = -7 \rightarrow 7$ before and after storage. **a** Coincidence rate before storage measured over an interval of 100 s. **b** Coincidence rate after storage measured over an interval of 600 s. **c** Distributions of the correlated OAM modes generated from SRS, where red dots and black squares represent datasets of input and output OAM correlations, respectively. Both correlations are fitted using fitting function with $y = y_0 + \frac{2A}{\pi}\frac{w}{4(x-x_c)^2+w^2}$ ($y_0 = 0$, $x_c = 0$, $w = 7.7$, $A = 2030$) and ($y_0 = 12.7$, $x_c = 0$, $w = 4.57$, $A = 1463$), respectively. (d) The efficiency of storing different OAM modes. The black curve is calculated using the same fitting function with fitted values ($y_0 = 0.132$, $x_c = 0$, $w = 2.274$, $A = 0.354$); w specifies the half-width at half-maximum of y. We identify w with the effective quantum spiral bandwidth. For panels (c) and (d), the correlation refer to the coincidences of signal 1 and 2 photons, the efficiency correspond to the ratio of the coincidences before and after storage. Error bars represent $\pm$ s.d

5.2.3 Three-Dimensional Entanglement

Next, we verified the entanglement with OAM dimension $d = 3$. We projected the signal-1 and signal-2 photons onto SLM 1 and SLM 2, respectively, which are programmed with nine different phase states $|\psi_{1\sim9}>$ corresponding to states $|L>$, $|G>$, $|R>$, $(|G>+|L>)/\sqrt{2}$, $(|G>+|R>)/\sqrt{2}$, $(|G>+i|L>)/\sqrt{2}$, $(|G>-i|R>)/\sqrt{2}$, $(|L>+|R>)/\sqrt{2}$, and $(|L>+i|R>)/\sqrt{2}$ [14, 42], where $|L>$, $|G>$, and $|R>$ are states corresponding to a well-defined OAM of -1, 0, and $+1$, respectively. With this projection, the mirrors and lens should be considered owing to its transformation in imaging processing. We reconstruct the density matrix before storage Fig. 5.4a and b by converting the spin-excited state in MOT 1 into a signal-2 photon. The signal-1 photon is then stored for a while in MOT 2 following a Raman protocol. This established the entanglement between the two atomic ensembles, for which the reconstructed density matrix is given in Fig. 5.4c and d. The difference between the states before and after storage is owing to the different storage efficiencies for the $|R>$ ($|L>$) mode and $|G>$ mode Fig. 5.3d. To check the entangled state before and after storage, we used pump 2 and the coupling lasers to read the atom–atom entangled state into the retrieved signal 1–signal 2 entangled state, then checked the entanglement between these two photons. The reconstructed density matrices are shown in Fig. 5.4a–d. Using the formula $\mathrm{F}_1 = \mathrm{Tr}(\sqrt{\sqrt{\rho_x}\rho_{ideal}\sqrt{\rho_x}})^2$, where x represents the input and output, ρ_{ideal} is the density matrix of the ideal three-dimensional OAM entangled state of $|\Psi_{ideal}> = (|R>_{a1}|R>_{a2} + |G>_{a1}|G>_{a2} + |L>_{a1}|L>_{a2})/\sqrt{3}$. The template for reconstructing the ideal OAM entangled state $|\Psi> = (|R>|L> + |G>|G> + |L>|R>)/\sqrt{3}$ can be referenced in the Section of appendix. We calculated the fidelity of the reconstructed density matrix before storage and after storage, which were $76.7 \pm 2.8\%$ and $71.7 \pm 2.8\%$, respectively. All error bars in this experiment were estimated using Poisson statistics and performing Monte Carlo simulations using Mathematica software. Both exceed the threshold of 2/3 [28, 39] for a maximally entangled state of Schmidt rank 3, which confirms the density matrix cannot be decomposed into an ensemble of pure states of Schmidt rank 1 or 2; i.e., the Schmidt number of the density matrix must be equal to or greater than 3 before and after storage. We calculated the fidelity of entanglement between input and output density matrix, which gives $83.9 \pm 2.9\%$.

In order to reconstruct a 3×3 density matrix, there needs 9 different modes $|\psi_{1\sim 9}>$ for projections at least, i.e., the density matrix of a 3D entanglement can be reconstructed by using the 9 OAM modes. If one use 15 modes including another 6 modes $(|G> - |L>)/\sqrt{2}$, $(|G> - |R>)/\sqrt{2}$, $(|G> - i|L>)/\sqrt{2}$, $(|G> + i|R>)/\sqrt{2}$, $(|L> - |R>)/\sqrt{2}$, and $(|L> - i|R>)/\sqrt{2})$, the 3×3 density matrix can be reconstructed more precisely. The missing 6 modes are orthogonal with the 6 modes we used in our experiment. We omit these 6 modes in order to reduce the experimental time, due to the negligible effect on the final results.

5.2.4 High-Dimensional Entanglement

Finally, we focus on the main part of this study, specifically, quantum storage of high-dimensional OAM entanglement, and the establishment of a high-dimensional OAM entanglement between two memories. We known that, in principle, the density matrices of the higher-dimensional entangled state can be reconstructed using the above tomography method, but in practice, there are some experimental challenges in its physical realization. For example, for a d-dimensional entangled state, the amount of data needed is of order d^4, which makes the reconstruction of the density matrix

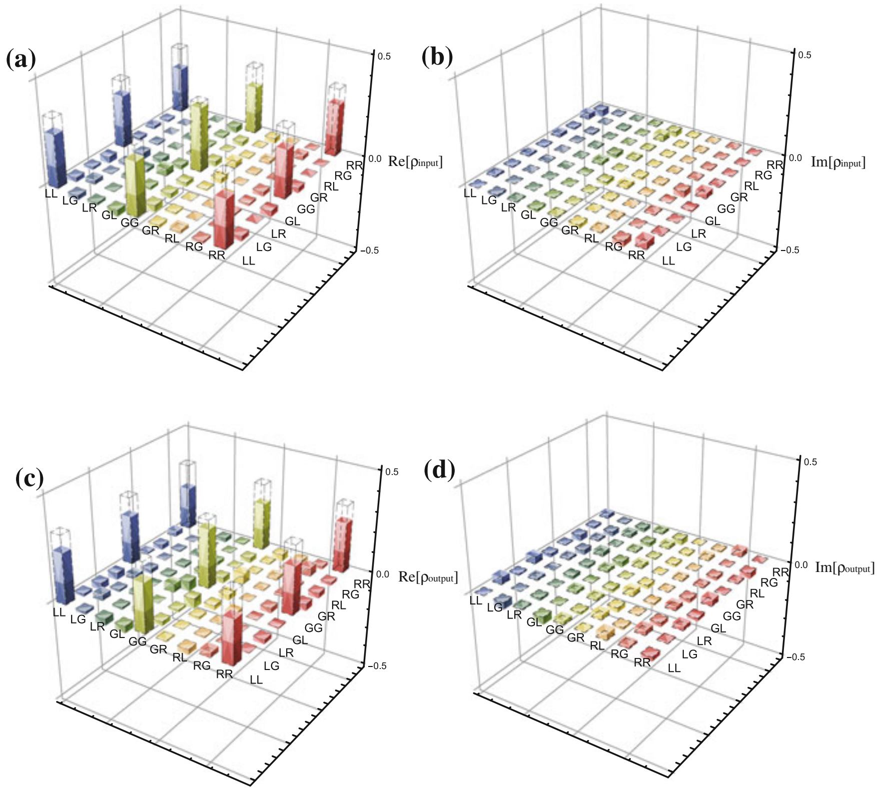

Fig. 5.4 Constructed density matrix of 3-dimensional OAM entanglement. **a** and **b** Real and imaginary parts before storage; **c** and **d** those after storage. The dotted bars added in each density matrix correspond to the expected value of the ideal density matrix

impractical. Basically, there are three methods to check whether or not a system is in high-dimensional entanglement:

(1) Using unbiased basis states that span the whole high-dimensional subspace [26, 41];

(2) Checking Bell inequalities in higher dimensional space directly [9, 37];

(3) Finding a violation that is stronger than allowed within a two-dimensional state space, thereby hinting at entanglement in (untested) higher dimensions.

Here, we used method (3) to characterize the high-dimensional entanglement, finding a bound that hinting high-dimensional entanglement. We used the entanglement witness [18, 24] to prove whether or no there is a high-dimensional entanglement, and the dimensionality witness [2, 6, 23] to characterize the dimensionality of the entanglement. These witnesses determine the level of entanglement using a minimum number of measurements. Due to the number of two-dimensional subspaces in any d-dimensional system is the binomial coefficient C_d^2. To calculate the witnesses, we only need to measure all states entangled in a two-dimensional OAM subspace; i.e., correlations in three mutually unbiased bases, including diagonal/anti-diagonal, left/right, and horizontal/vertical bases with total 6 measurements, need to be measured, with the amount of data needed being reduced to [1].

$$n = 6C_d^2 = 6\frac{D!}{2!(d-2)!} = 3d(d-1) \tag{5.2}$$

For example, in order to reconstruct the density matrix, the amount of data required to be measured for 3-D is 81 and 256 for 4-D. If we use the witness, then the amount of data needed is reduced significantly to be 18 and 36 respectively. It greatly shortens the experimental time as we wanted. The entanglement witness and dimensionality witness can be calculated from the sum of the visibility $M = V_x + V_y$ and $N = V_x + V_y + V_z$ respectively, in each 2×2 subspace, where the visibility are defined as $V_i = |\langle \sigma_i \otimes \sigma_i \rangle|$, $i = x, y, z$. Here, $\sigma_{\mathrm{x}}, \sigma_y, \sigma_z$ represent the measurements in the diagonal/anti-diagonal, left/right, and horizontal/vertical basis, respectively. The superposition is calculated by adding equal amounts of the two modes and the phase is calculated just from the argument of the resultant complex [20]. Figure 5.5a shows an example of mutually unbiased bases formed from the OAM modes $m = 5$ and $m = -1$, which can referenced by the mathematica program given in Appendix.

General Witness: We have derived the violation for high-dimensional entanglement through a reference [18]. To verify the general bound for entanglement, we construct a general two photon OAM separable state:

$$\left|\psi^{(2)}\right\rangle = |\psi_1\rangle \otimes |\psi_2\rangle \tag{5.3}$$

where

$$|\psi_1\rangle = a\,|LG_{l1}\rangle + b \cdot \mathrm{e}^{i\theta_1}\,|LG_{l2}\rangle$$

$$|\psi_2\rangle = c\,|LG_{l1}\rangle + d \cdot \mathrm{e}^{i\theta_2}\,|LG_{l2}\rangle$$

here $a, b, c, d, \theta_1, \theta_2$ are real, $a^2 + b^2 = 1$, $c^2 + d^2 = 1$. $|LG_{l1,l2} >$ presents the quantum state of OAM with azimuthal index of $l1$ and $l2$. $|\psi_1\rangle$ and $|\psi_2\rangle$ is a general pure state of two photons. The two-photon entanglement is bounded by a witness:

$$W = V_{D/A} + V_{R/L} \tag{5.4}$$

where $V_{D/A}$ and $V_{R/L}$ corresponds the visibilities under the diagonal/anti-diagonal, left/right OAM basis. The calculation of witness can be written as:

$$W = 4abcdCos(\theta_1 - \theta_2) \tag{5.5}$$

Thus, the maximum value of the witness W is 1 for $a = b = c = d = 1/\sqrt{2}$, $\theta_1 = \theta_2$. If the sum of the visibilities is bigger than 1, the measured state of two photons is non-separable, that is in entanglement. The witness W is calculated as 2 under two-photon maximally entanglement, where the states and cannot be written as a separable state.

For an arbitrary separable state within a d-dimensional subspace, for example OAM space, a product state of a $(d-1)$-dimensional maximum entangled state and a single state expressed by

$$\psi_{system} = \psi_{d-1} \otimes \psi_1$$

would maximize the overall sum of the measured visibility. Because the allowed maximum visibility of entanglement in a two-dimensional subspace is 2 (that is $M = V_x + V_y = 2$, $V_x = V_y = 1$), the allowed maximum visibility can be calculated as $2C_{d-1}^2 = (d-1)(d-2)$ for a $(d-1)$-dimensional entanglement. The maximum visibility for the remaining separable state are $(d-1)$ with $(d-1)$ terms [18]. Hence, the maximum bound for high-dimensional entanglement can be directly obtained by $((d-1)(d-2) + (d-1))$:

$$M_d = (d-1)^2 \tag{5.6}$$

If there is a d-dimensional entanglement, the maximum bound of M_d should be violated. For a state comprising $m = 2, 1, 0, -1$, a four-dimensional entanglement, the maximum bound is $M_4 = 9$. The measured M' is 9.30 ± 0.06 and 9.19 ± 0.06 before and after storage. These values clearly suggest that there is at least a four-dimensional entanglement between these two distant memories.

Conditional Witness: By assuming the high-dimensional correlations between two readout photons

$$|\psi\rangle = \sum_{m=-\infty}^{m=\infty} c_m |m\rangle_{s1} \otimes |m\rangle_{s2},$$

as done in Ref. [31], we sum the visibilities N for each of σ_x, σ_y, σ_z bases to calculate a witness value W to determine the dimensionality of high-dimensional OAM entanglement. All experimentally measured visibilities N are shown in Fig. 5.5b and c, corresponding to quantities before and after storage respectively (left/right column). The conditional dimensional witness value can be expressed by:

$$W_d = 3\frac{D(D-1)}{2} - D(D-d) \tag{5.7}$$

where D is the number of OAM modes in the measurement. If $W > W_d$ satisfies, there is a high-D entanglement at least $d+1$-dimensions. In our experiment, the measured number of modes is 11 ($m = -5 \rightarrow 5$); the obtained W of 123.9 ± 0.8 for the input state and 112.8 ± 0.8 for the output state, these values violate the bound of 110 for an input of $d = 6$ and 99 for an output of $d = 5$, both by 17 standard deviations, implying that there strongly exists a six-dimensional entanglement between the two memories. The obtained W also violates the bound of 121 for an input of $d = 7$ and 110 for an output of $d = 6$, both by 3 standard deviations, demonstrating that there exists a seven-dimensional entanglement, and indeed a high-dimensional entanglement in our memories. According to the measurement for the dimension before and after storage, there is only one dimension lost in the storage process. The reasons caused this loss maybe come from the distinct storage efficiencies from the OAM filtering

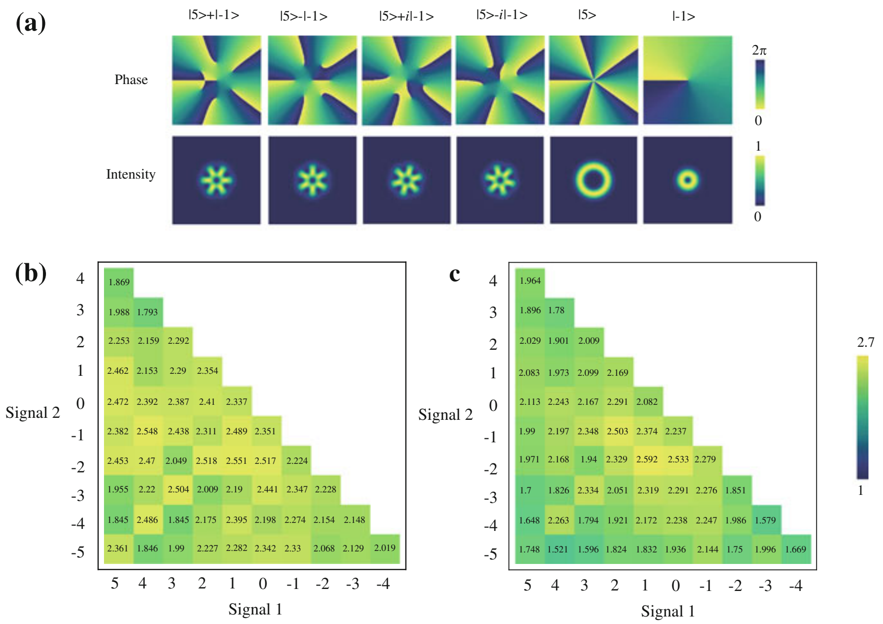

Fig. 5.5 **a** The diagonal/anti-diagonal, left/right, and horizontal/vertical bases in the phase and intensity spaces with OAM modes $m = 5$ and $m = -1$. The OAM superposition of LG_5 and LG_{-1} is calculated by adding equal amounts of the two modes and the phase is calculated from the argument of the resultant complex [20] with a function of $Arg(LG_5 + e^{i\theta} LG_{-1})$, where LG_5 and LG_{-1} are the amplitudes of OAM states with azimuthal index of 5 and -1, θ represents the relative phase between these two modes. See details in Appendix. **b** and **c** are the measured visibilities before and after storage under different basis. The sum of the visibilities in three arbitrary OAM modes of larger than six means the existence of two-dimensional entanglement

effect, which can be seen from Fig. 5.3d. Another reason maybe is the more noise from the memory process, which would decrease the visibility. In all experiments, entanglement is verified by checking the entangled photons readout from the atomic ensembles, and therefore is a-posteriori entangled state. Both signal photons are completely covered by the pump and coupling laser beams in our experiment, and hence it is reasonable to assume that the read-out efficiencies for different OAM modes are the same. Hence, the photonic entangled state can be regarded as a post-selected entangled state of the atomic ensembles.

In demonstrating 3-dimensional entanglement storage, the storage fidelity is affected by the distinct storing efficiencies Fig. 5.3d for different OAM modes [14], narrowing the spiral bandwidth of the OAM modes. We can improve the entanglement fidelity by purifying the entangled state [3, 17]. However, achieving a balanced efficiency in storing different OAM modes is a big challenge [22]. The main reasons affecting the entanglement dimension are the following:

1. the distinct efficiencies in storing the different OAM modes;
2. the noise associated with storage, which is mainly from the scattering from the coupling laser, resulting in a low signal-to-noise ratio (SNR);

3. the stability of the whole system over long experimental periods (the total measured time for the storage and retrieval processes was ~100 h).

To increase the OAM entanglement dimension, we believe four problems need to be solved:

- generating a maximal high-dimensional entanglement between the signal-1 photon and the spin wave using purification, as done in Ref. [10];
- balancing the storage efficiency for different OAM modes by for example smoothing the transverse distribution of the coupling laser beam in the cold atomic ensemble and the atomic density;
- reducing the background noise by using more strict filtering to achieve a better SNR;
- improving the working state of the whole system over long experimental periods.

We emphasize that achieving high-dimensional entanglement between different quantum memories is non-trivial, and is not a straightforward extension from establishing a two-dimensional entanglement between two atomic ensembles. There are many challenges both in its creation and verification. For distant memories entangled in two-dimensional space [15], the entanglement can be well characterized by reconstructing the density matrix and checking the Bell-type inequality. In contrast, characterizing a high-dimensional entanglement is more complex and difficult. As noted earlier, reconstructing the density matrices using the method for two-dimensional entanglement is impractical for a high-dimensional entanglement (>3) because the amount of data needed to be measured significantly increases. Therefore, we sought a different way to characterize it using the witness instead.

In addition, we note that the Ref. [50] reports a quantum storage of a 3 dimensional entanglement in solid crystal. Compared to that work, besides the media for memory is different, our work reports a higher-dimensional entanglement storage. Most importantly, the memory we achieved can work on-demand, this is the key point for realizing a long-distance quantum communication based on quantum repeater. A technique of two-level atomic frequency comb used in that work cannot work on-demand, the storage time is predetermined. There is another difference between these two works: we achieved the high-dimensional entanglement between two physical systems, is not the OAM entanglement between a delayed photon and the atomic excitation achieved in solid storage.

5.3 Research Summary

In summary, quantum memories entangled in high-dimensional OAM space between two 1-m-distant atomic ensembles were experimentally established for the first time. The density matrices for the three-dimensional entanglement were reconstructed, giving $83.9 \pm 2.9\%$ entanglement storage fidelity. For a higher-dimensional case, we proved that at least a four-dimensional entanglement existed between two memories using an general witness. In checking the dimension of the entangled memories, experimental data showed that there was a seven-dimensional entanglement within the two atomic-ensemble memories by using a conditional witness. Overcoming higher-dimensional OAM entanglement would be challenging, this is actually the next project in my lab. Maybe, it should start with high quanta of OAM entangled state storage, for example, realizing $l = \pm 20$ or $l = \pm 50$ entangled state for exploring the limitations for the high quanta of OAM modes.

Nowadays, light carried OAM cannot be transmitted in a commercial optical fibre, therefore the OAM-based quantum networks may be more suitable to work in free space system. Recently, Zeilinger's group has realized the distribution of OAM entanglement between two distanced sites separated by 3 km in Vienna in 2015 [30]. We also noted that light with OAM can transmit along some special designed fibers over kilometers [4]. Nowadays, many groups and people work in this field, therefore quantum network based on OAM may be realized in the future. The experiment to establish high-dimensional entangled memories is an important step towards high-dimensional quantum communications.

References

1. Agnew, M., J. Leach, and R.W. Boyd. 2012. Observation of entanglement witnesses for orbital angular momentum states. *The European Physical Journal D-Atomic, Molecular, Optical and Plasma Physics* 66 (6): 1–4.
2. Agnew, Megan, Jeff Z. Salvail, Jonathan Leach, and Robert W. Boyd. 2013. Generation of orbital angular momentum bell states and their verification via accessible nonlinear witnesses. *Physical Review Letters* 111 (3): 030402.
3. Charles H Bennett, Herbert J Bernstein, Sandu Popescu, and Benjamin Schumacher. 1996. Concentrating partial entanglement by local operations. *Physical Review A* 53(4):2046.
4. Bozinovic, Nenad, Yang Yue, Yongxiong Ren, Moshe Tur, Poul Kristensen, Hao Huang, Alan E. Willner, and Siddharth Ramachandran. 2013. Terabit-scale orbital angular momentum mode division multiplexing in fibers. *Science* 340 (6140): 1545–1548.
5. Briegel, H.-J., Wolfgang Dür, Juan I. Cirac, and Peter Zoller. 1998. Quantum repeaters: the role of imperfect local operations in quantum communication. *Physical Review Letters* 81 (26): 5932.
6. Bruß, Dagmar. 2002. Characterizing entanglement. *Journal of Mathematical Physics* 43 (9): 4237–4251.
7. Choi, K.S., H. Deng, J. Laurat, and H.J. Kimble. 2008. Mapping photonic entanglement into and out of a quantum memory. *Nature* 452 (7183): 67–71.
8. Clausen, C., I. Usmani, F. Bussières, N. Sangouard, M. Afzelius, H. de Riedmatten, and N. Gisin. 2011. Quantum storage of photonic entanglement in a crystal. *Nature* 469 (7331): 508–511.
9. Collins, Daniel, Nicolas Gisin, Noah Linden, Serge Massar, and Sandu Popescu. 2002. Bell inequalities for arbitrarily high-dimensional systems. *Physical Review Letters* 88 (4): 040404.
10. Adetunmise, C, Dada, Jonathan Leach, Gerald S Buller, Miles J Padgett, and Erika Andersson. 2011. Experimental high-dimensional two-photon entanglement and violations of generalized bell inequalities. *Nature Physics* 7 (9): 677–680.
11. Dai, Han-Ning, Han Zhang, Sheng-Jun Yang, Tian-Ming Zhao, Jun Rui, You-Jin Deng, Li Li, Nai-Le Liu, Shuai Chen, Xiao-Hui Bao, et al. 2012. Holographic storage of biphoton entanglement. *Physical Review Letters* 108 (21): 210501.

12. Ding, Dong-Sheng, Wu Jing-Hui, Zhi-Yuan Zhou, Yang Liu, Bao-Sen Shi, Xu-Bo Zou, and Guang-Can Guo. 2013. Multimode image memory based on a cold atomic ensemble. *Physical Review A* 87 (1): 013835.
13. Ding, Dong-Sheng, Wu Jing-Hui, Zhi-Yuan Zhou, Bao-Sen Shi, Xu-Bo Zou, and Guang-Can Guo. 2013. Multiple image storage and frequency conversion in a cold atomic ensemble. *Physical Review A* 87 (5): 053830.
14. Ding, Dong-Sheng, Wei Zhang, Zhi-Yuan Zhou, Shuai Shi, Jian-song Pan, Guo-Yong Xiang, Xi-Shi Wang, Yun-Kun Jiang, Bao-Sen Shi, and Guang-Can Guo. 2014. Toward high-dimensional-state quantum memory in a cold atomic ensemble. *Physical Review A* 90 (4): 042301.
15. Ding, Dong-Sheng, Wei Zhang, Zhi-Yuan Zhou, Shuai Shi, Guo-Yong Xiang, Xi-Shi Wang, Yun-Kun Jiang, Bao-Sen Shi, and Guang-Can Guo. 2015. Quantum storage of orbital angular momentum entanglement in an atomic ensemble. *Physical Review Letters* 114 (5): 050502.
16. Dong-Sheng Ding, Zhi-Yuan Zhou, Bao-Sen Shi, and Guang-Can Guo. 2013. Single-photon-level quantum image memory based on cold atomic ensembles. *Nature Communications*, 4.
17. Matthew, P Edgar, Daniel S Tasca, Frauke Izdebski, Ryan E Warburton, Jonathan Leach, Megan Agnew, Gerald S Buller, Robert W Boyd, and Miles J Padgett. 2012. Imaging high-dimensional spatial entanglement with a camera. *Nature Communications* 3: 984.
18. Robert Fickler, Mario Krenn, Radek Lapkiewicz, Sven Ramelow, and Anton Zeilinger. 2013. Real-time imaging of quantum entanglement. *Scientific Reports*, 3.
19. Franke-Arnold, Sonja, Les Allen, and Miles Padgett. 2008. Advances in optical angular momentum. *Laser & Photonics Reviews* 2 (4): 299–313.
20. Franke-Arnold, Sonja, and Jonathan Leach, Miles J Padgett, Vassilis E Lembessis, Demos Ellinas, Amanda J Wright, John M Girkin, Patrik Öhberg, and Aidan S Arnold. 2007. Optical ferris wheel for ultracold atoms. *Optics Express* 15 (14): 8619–8625.
21. Glorieux, Quentin, Jeremy B Clark, Alberto M Marino, Zhifan Zhou, and Paul D Lett. 2012. Temporally multiplexed storage of images in a gradient echo memory. *Optics Express* 20 (11): 12350–12358.
22. Anna Grodecka-Grad, Emil Zeuthen, and Anders S Sørensen. 2012. High-capacity spatial multimode quantum memories based on atomic ensembles. *Physical Review Letters* 109(13):133601.
23. Gühne, O., P. Hyllus, D. Bruß, A. Ekert, M. Lewenstein, C. Macchiavello, and A. Sanpera. 2002. Detection of entanglement with few local measurements. *Physical Review A* 66 (6): 062305.
24. Gühne, Otfried, and Géza Tóth. 2009. Entanglement detection. *Physics Reports* 474 (1): 1–75.
25. Heinze, G., A. Rudolf, F. Beil, and T. Halfmann. 2010. Storage of images in atomic coherences in a rare-earth-ion-doped solid. *Physical Review A* 81 (1): 011401.
26. Beatrix, C. 2013. Hiesmayr and Wolfgang Löffler. Complementarity reveals bound entanglement of two twisted photons. *New Journal of Physics* 15 (8): 083036.
27. Daniel B Higginbottom, Ben M Sparkes, Milos Rancic, Olivier Pinel, Mahdi Hosseini, Ping Koy Lam, and Ben C Buchler. 2012. Spatial-mode storage in a gradient-echo memory. *Physical Review A* 86(2):023801.
28. Inoue, R., T. Yonehara, Y. Miyamoto, M. Koashi, and M. Kozuma. 2009. Measuring qutrit-qutrit entanglement of orbital angular momentum states of an atomic ensemble and a photon. *Physical Review Letters* 103 (11): 110503.
29. Kimble, H.J. 2008. The quantum internet. *Nature* 453: 19.
30. Krenn, Mario, Johannes Handsteiner, Matthias Fink, Robert Fickler, and Anton Zeilinger. 2015. Twisted photon entanglement through turbulent air across vienna. *Proceedings of the National Academy of Sciences* 112 (46): 14197–14201.
31. Krenn, Mario, Marcus Huber, Robert Fickler, Radek Lapkiewicz, Sven Ramelow, and Anton Zeilinger. 2014. Generation and confirmation of a (100×100)-dimensional entangled quantum system. *Proceedings of the National Academy of Sciences* 111 (17): 6243–6247.
32. Mair, A., A. Vaziri, G. Weihs, and A. Zeilinger. 2001. Entanglement of the orbital angular momentum states of photons. *Nature* 412 (6844): 313.

33. Moretti, D., D. Felinto, and J.W.R. Tabosa. 2009. Collapses and revivals of stored orbital angular momentum of light in a cold-atom ensemble. *Physical Review A* 79 (2): 023825.
34. Nicolas, A., L. Veissier, L. Giner, E. Giacobino, D. Maxein, and J. Laurat. 2014. A quantum memory for orbital angular momentum photonic qubits. *Nature Photonics* 8 (3): 234–238.
35. Reim, K.F., P. Michelberger, K.C. Lee, J. Nunn, N.K. Langford, and I.A. Walmsley. 2011. Single-photon-level quantum memory at room temperature. *Physical Review Letters* 107 (5): 053603.
36. Reim, K.F., J. Nunn, V.O. Lorenz, B.J. Sussman, K.C. Lee, N.K. Langford, D. Jaksch, and I.A. Walmsley. 2010. Towards high-speed optical quantum memories. *Nature Photonics* 4 (4): 218–221.
37. Romero, Jacquiline, Jonathan Leach, Barry Jack, Stephen M Barnett, Miles J Padgett and Sonja Franke-Arnold. 2010. Violation of leggett inequalities in orbital angular momentum subspaces. *New Journal of Physics* 12 (12): 123007.
38. Saglamyurek, Erhan, Neil Sinclair, Eongwan Jin, Joshua A Slater, Daniel Oblak, Félix Bussières, Mathew George, Raimund Ricken, Wolfgang Sohler, and Wolfgang Tittel. 2011. Broadband waveguide quantum memory for entangled photons. *Nature* 469 (7331): 512–515.
39. Sanpera, Anna, Dagmar Bruß, and Maciej Lewenstein. 2001. Schmidt-number witnesses and bound entanglement. *Physical Review A* 63 (5): 050301.
40. Shuker, M., O. Firstenberg, R. Pugatch, A. Ron, and N. Davidson. 2008. Storing images in warm atomic vapor. *Physical Review Letters* 100 (22): 223601.
41. Christoph Spengler, Marcus Huber, Stephen Brierley, Theodor Adaktylos, and Beatrix C Hiesmayr. 2012. Entanglement detection via mutually unbiased bases. *Physical Review A* 86(2):022311.
42. Thew, R.T, Kae Nemoto, Andrew G White, and William J Munro. 2002. Qudit quantum-state tomography. *Physical Review A* 66 (1): 012303.
43. Veissier, Lucile, Adrien Nicolas, Lambert Giner, and Dominik Maxein, AS Sheremet, Elisabeth Giacobino, and Julien Laurat. 2013. Reversible optical memory for twisted photons. *Optics Letters* 38 (5): 712–714.
44. Praveen K, Vudyasetu, Ryan M Camacho, and John C Howell. 2008. Storage and retrieval of multimode transverse images in hot atomic rubidium vapor. *Physical Review Letters* 100 (12): 123903.
45. Wang, Jian, Jeng-Yuan Yang, Irfan M. Fazal, Nisar Ahmed, Yan Yan, Hao Huang, Yongxiong Ren, Yang Yue, Samuel Dolinar, Moshe Tur, et al. 2012. Terabit free-space data transmission employing orbital angular momentum multiplexing. *Nature Photonics* 6 (7): 488–496.
46. Jinghui, Wu, Yang Liu, Dong-Sheng Ding, Zhi-Yuan Zhou, Bao-Sen Shi, and Guang-Can Guo. 2013. Light storage based on four-wave mixing and electromagnetically induced transparency in cold atoms. *Physical Review A* 87 (1): 013845.
47. Liu Yang, Wu, Shi Bao-Sen Jing-Hui, and Guo Guang-Can. 2012. Realization of a two-dimensional magneto-optical trap with a high optical depth. *Chinese Physics Letters* 29 (2): 024205.
48. Alison M Yao and Miles J Padgett. 2011. Orbital angular momentum: origins, behavior and applications. *Advances in Optics and Photonics* 3(2):161–204.
49. Zhang, Han, Xian-Min Jin, Jian Yang, Han-Ning Dai, Sheng-Jun Yang, Tian-Ming Zhao, Yu. Jun Rui, Xiao Jiang He, Fan Yang, et al. 2011. Preparation and storage of frequency-uncorrelated entangled photons from cavity-enhanced spontaneous parametric downconversion. *Nature Photonics* 5 (10): 628–632.
50. Zhou, Zong-Quan, Yi-Lin Hua, Xiao Liu, Geng Chen, Xu Jin-Shi, Yong-Jian Han, Chuan-Feng Li, and Guang-Can Guo. 2015. Quantum storage of three-dimensional orbital-angular-momentum entanglement in a crystal. *Physical Review Letters* 115 (7): 070502.

Chapter 6
Raman Quantum Memory of Photonic Polarized Entanglement

Abstract Quantum memories are the key components in quantum technologies with a wide range of applications including long-distance communication, the generation of multi-photon states, linear quantum computation, etc. Constructing quantum memories to store photonic entanglement is essential to overcome the exponential scaling of the error rate with increasing channel lengths [6]. Among the memory protocols reported to date, the Raman scheme has the advantages of a broadband and high-speed [37], resulting in a huge potential in quantum networks. How to demonstrate Raman quantum storing photonic entanglement is a challenging and interesting. In the last Chapter, two storage experiments using the Raman scheme are introduced: (1) storing weak coherent field via Raman scheme in cold atomic ensemble; (2) heralded single-photon entanglement of the path and polarization storage is demonstrated as well as (3) polarization entanglement storage in two cold atomic ensembles. The experimental data clearly show that the quantum entanglement is preserved in this memory platform.

6.1 Research Motivations on Storing Photonic Polarized Entanglement

Long-distance quantum communication requires the distribution of the quantum entanglement among different nodes [8, 27, 31] in which quantum memory is regarded as a dispensable component. A quantum repeater could be established by combining the entanglement swapping operation and quantum memory, with which the problem of the transmission error rates scaling exponentially with the channel length could be overcome [6, 18]. The realization of quantum repeaters requires coherent interactions [8] between the information carrier (usually a photon) and the matter that acts as the storage medium. A photon could be encoded with its intrinsic degrees of freedom, such as polarization, orbital angular momentum, optical path and frequency/time-bins. In these, the photons encoded with polarization degree of freedom are more easily transported in optical fibres and are less affected by decoherence over long-distance transmission channels. Therefore, it is efficient to build a quantum interface that connects different quantum nodes using photonic polarized

D.-S. Ding, *Broad Bandwidth and High Dimensional Quantum Memory Based on Atomic Ensembles*, Springer Theses, https://doi.org/10.1007/978-981-10-7476-9_6

entanglement. It is thus unsurprising that many research groups are actively working on different physical systems for storing polarization entanglement [15, 42].

There are many protocols for photon storage, including EIT [10, 22, 41], far off-resonant two-photon transitions [9, 16, 19, 28, 32, 34, 36, 37], CRIB [1, 3, 29, 33], atomic frequency combs [2], photon echos [7, 24], optomechanical storage [20] and the off-resonant Faraday effect [25, 26]. Of these, the far off-resonant two-photon transition protocol, which will be referred to as Raman quantum memory, uses the off-resonance atomic configuration, in which there is an excited virtual energy level near the two-photon resonance. The band of the excited virtual energy level could be increased by either enlarging the effective optical depth (OD) of the medium or by increasing the intensity of the control laser. Thus, this storage protocol has the ability to store a short time pulse and can operate at high-speed. Theoretically, Raman quantum memory can work over a large range of frequencies because the single photon detuning of the control laser is changeable and is also insensitive to inhomogeneous broadening. All of these properties show that the Raman scheme has huge potential in quantum networks and quantum computation. The Raman protocol was first experimentally realized by Walmsley's group, where the storage of a sub-nanosecond pulse in a hot atomic vapour was reported [36, 37]. This progress was significant in realization of Raman quantum memories, despite the information carrier being weakly attenuated coherent light.

Recently, our group realized a Raman quantum memory with true single photons using an ensemble of trapped rubidium (Rb) atoms [16]. Walmsley's group tried to store single photons generated from the spontaneous parametric downconversion in a nonlinear crystal [32] in a hot atomic vapour. However, as the authors pointed out, the inevitable noise from the accompanying spontaneous four-wave mixing (SFWM) process decrease the quantum properties [32]. A THz-bandwidth tuneable photonic memory for femtosecond pulses has been realized in molecules [9]. A THz optical memory in diamond has also been reported [19]. These results further demonstrate the advantages of the Raman protocol in broadband and high-speed communications. While there has been much progress in photon storage using different storage protocols, only a small fraction of the storage platforms have demonstrated the storage of photonic entanglement using polarization [15, 42], the path [12], time-bins [38] and time-energy [13]. Moreover, as previously mentioned, the storage of photons, or orbital angular momentum entanglement, has been realized with the Raman protocol. However, constructing a quantum memory with Raman scheme for storing photonic polarized entanglement is interesting and difficulty, it contains many problems, for example, how to create short pulse width photonic entangled state; how to match the bandwidth between a Raman quantum memory and a photon.

In this chapter, I will introduce the first experimental realization of a Raman quantum memory for photonic polarization entanglement. Two storage experiments are given: (1) the entanglement of a heralded single photon hybrid entanglement in both path and polarization storage in an ensemble of trapped Rb atoms; (2) polarization entanglement storage using two cold Rb atomic ensembles. In the first experiment, a heralded single photon was generated through SRS process in one atomic ensemble. Then, this heralded photon was sent to and stored by Raman scheme in another cold atomic ensemble, acting as a quantum memory. With the aid of a specific Sagnac interferometer, the single photon that was hybrid-entangled in both path and polarization was stored. The concurrences were measured before and after storage and showed that there was a $20.9 \pm 7.7\%$ transfer efficiency of the quantum entanglement during the storage process. In the second experiment, an actively locked Mach-Zehnder interferometer was used to generate polarization entanglement between an anti-Stokes photon and one atomic ensemble. This photon was then sent to and stored in another cold atomic ensemble with the aid of the Sagnac interferometer using Raman scheme. Polarization entanglement was verified by mapping the excited spin states in the two ensembles to two photons and checking their entanglement. The experimental results show that Bell's inequality was violated by 3.2 standard deviations after storage, without any noise corrections. The fidelity between the reconstructed density matrix before and after storage was calculated to be $85.0 \pm 3.4\%$, showing that the entanglement was preserved. The reported results represent the first demonstration of a bench-marking result for Raman quantum memory, which is promising for the establishment of quantum networks.

6.2 Experimental Setup

There are two beams (typed as pump 1 and pump 2) with respective wavelengths of 795 and 780 nm, from external-cavity diode lasers (DL100, Toptica), were the input pump lasers. The pump 1 laser was 70-MHz blue-detuned to the atomic transition $5S_{1/2}(F = 3)(|1\rangle) \rightarrow 5P_{1/2}(F\prime = 3)(|4\rangle)$, the pump 2 laser was resonant with the atomic transition $5S_{1/2}(F = 2)(|2\rangle) \rightarrow 5P_{3/2}(F\prime = 3)(|4\rangle)$. An anti-Stokes photon was sent to the MOT B and stored with the assistance of the coupling light by the Raman scheme. The experiments were run periodically with a MOT trapping time of 7.5 ms and a photon operation time of 1.5 ms (the another 1 ms was to shut the magnetic field and to prepare the initialize atomic state), which contained 28000 cycles of the single photon generation, storage and retrieval sequence with an operation time of 500 ns. The timing sequence of a single sequence is depicted in Fig. 6.1a.

Two interferometers were constructed in the whole system. One was Sagnac interferometer, which based on a phase-insensitive configuration consisted of two counter-propagated path modes (U and D) in MOT B, this was used to maintain the relative phase of arbitrary polarization superposition. The other was a phase-sensitive Mach-Zehnder interferometer in MOT A, used to prepare the polarization entanglement, in which a mirror attached with a piezoelectric transducer (PZT) was used to stabilize the relative phase difference between the two SRS processes through a fast optoelectronic feedback. Four Bell entangled states could be prepared by turning the PZT and polarization of pump lasers. The method to generate the entangled states was similar to that in Ref. [30]. In the experiment, the locking light propagates at a small angle with respect to pumps 1 and 2 to reduce the scattering noise from the lock light.

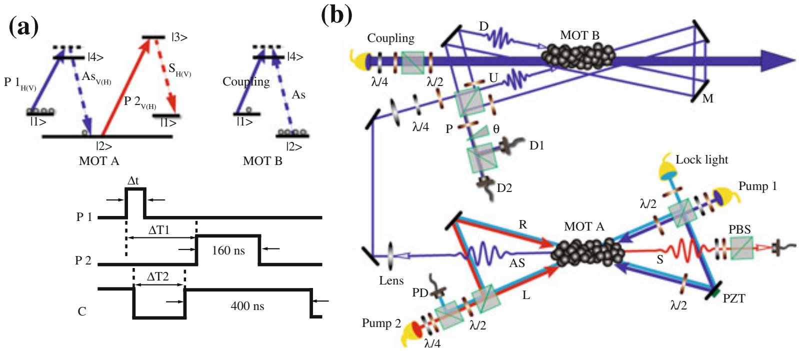

Fig. 6.1 Energy diagram and experimental setup. **a** Simplified energy level diagram used to generate and store the polarization entanglement and the time sequence for the generation, storage and retrieval sequence of a single photon. P1 is pump 1 and P2 is pump 2. **b** Simplified setup depicting the storage of the polarization entanglement. L and R refer to two SRS paths in MOT A. H and V are the horizontal and vertical polarizations, respectively. P 1 and P 2 are the modulated pulses with 25 ns (Δt) and 160 ns from two acoustic optic modulators, respectively. MOT: magneto-optical trap; FC: fibre coupler; PBS: polarization beam splitter; λ/2: half-wave plate. λ/4: quarter-wave plate. S: Stokes photon; As: anti-Stokes photon. D1, D2 and D3 are single photon detectors 1, 2 and 3, respectively (PerkinElmer SPCM-AQR-15-FC). PD: home-made photoelectric detector; PZT: Piezoelectric transducer. U and D are up- and down-optical modes input into MOT B, respectively. P: half-wave plate. θ: the phase of the inserted phase plate

6.2.1 Quantum Memory with Raman Scheme

In order to further illustrate the memory via Raman scheme, we showed the spectrum of transmission of the signal 1 through the atomic ensemble in MOT B by using a weak coherent light. There was a pumping hole in the spectrum of transmission of signal 1 at the detuning of 70 MHz. The power of coupling laser was 12 mW with a beam waist of 2 mm, corresponding to the Rabi frequency of 5.8 Γ (Γ is the decay rate of level $|4\rangle$). The experimental obtained curve was shown in Fig. 6.2a. The main difference between EIT and Raman schemes is that: EIT has a strong transmission peak caused by the coupling beam, while Raman corresponds to a strong absorption valley. The absorption bandwidth in Raman scheme can be increased by the power of the coupling laser and the optical depth of the medium.

Then we stored the weak coherent light via scheme in the atomic ensemble in MOT B. We input a probe light with ∼200 ns pulse width, and record storage efficiency against different storage time, the experimental data were shown by Fig. 6.2b, c. The coherence time of the memory is given by the fitted function in the Fig. 6.2 caption, that is 1434 ns. The fast decoherence is mainly caused by the external magnetic field. One can increase the coherence time by eliminating the residual magnetic field.

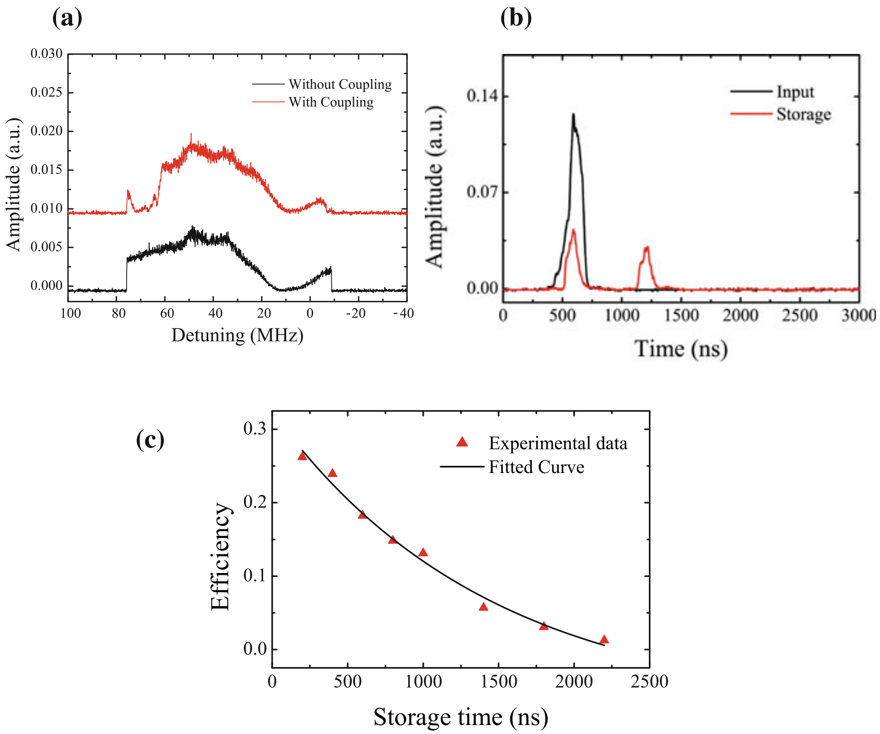

Fig. 6.2 The storage of a weak coherent light via Raman scheme. **a** The transmission spectrum of a weak coherent light through the atomic ensemble in MOT 2. Black line is the transmission spectrum without coupling laser. Red line represents the transmission spectrum with coupling laser. **c** The memory efficiency against the storage time. The solid line is an exponential fit by $g_0 + Ae^{-(\tau-\tau 0)/T}$ ($g_0 = -0.08$; $A = 0.38$; $\tau_0 = 67$; $T = 1434$)

6.2.2 Storing Single Photon with Raman Scheme

The maximum storage bandwidth of our memory was studied. The pulse width of pump 1 laser was changed by using an arbitrary function generator AFG 3252 to change the pulse width of the generated anti-Stokes photons. The pulse widths of the anti-Stokes photons were reduced as much as possible. Because the timing sequence was controlled by the software of card PCI 6602, AOM and AFG 3252, the final width of the anti-Stokes photon at FWHM was about ~7 ns under the limit of our system. The results on storing anti-Stokes photons are given in Fig. 6.3a, where Fig. 6.3c is the input signal without a coupling laser and atoms trapped in MOT B, Fig. 6.3d is the storage data and Fig. 6.3b is the recorded noise, where anti-Stokes photons were blocked, with an opened coupling laser and atoms trapped in MOT B. The storage efficiency was estimated as 10.3%. The measured second-order cross-correlation ($g_{s1,s2}(\tau)$) for the retrieved anti-Stokes and Stokes photons was about 13.6, showing

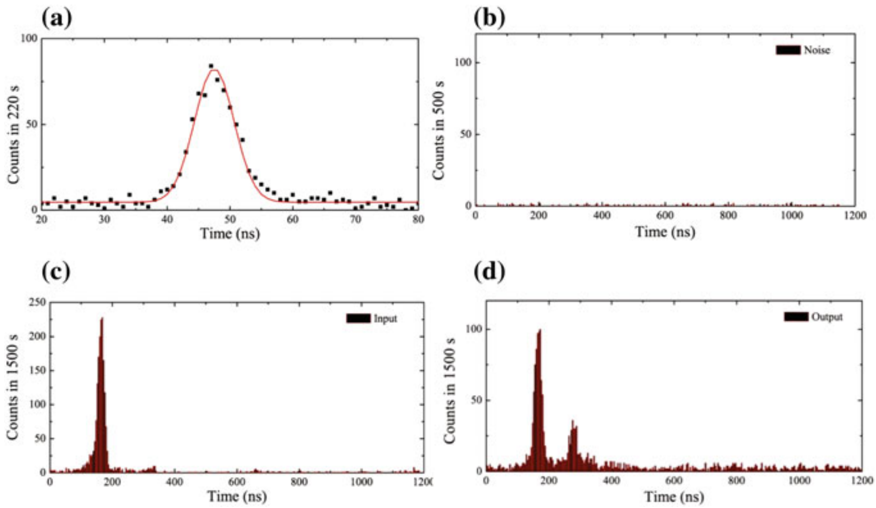

Fig. 6.3 **a** Measurements of the timing pulse width of the anti-Stokes photons excited by pump 1 laser. The coincidence counts between the trigger from AFG 3252 and the detection events of the anti-Stokes photons were recorded. The red line is the fitted curve, found using: $y = y_0 + Aexp^{[-2((t-tc)/w)^2]}$, where $w = 6.3$; $y_0 = 4.6$; $t_c = 47.5$; and $A = 492.9$. **b** Coincidence from noise. **c** Coincidence between the anti-Stokes and Stokes photons without storage. **d** Coincidence between the Stokes and retrieved anti-Stokes photons

the large nonclassical correlation between them. The practical timing pulse width of the measured cross-correlated function was larger than the timing pulse width of the anti-Stokes photons, because of the influence of the life-time of the atomic level, $|4\rangle$. The stronger Rabi frequency of the pump 2 laser could be used to reduce the time pulse width of the cross-correlated function [6, 8, 18]. If the resolution of the timing controller could be improved, then the system could store a pulse with a smaller timing pulse width (<7 ns) in the quantum regime.

In addition, Raman scheme has a advantage of storing signal filed with large frequency range. Then, we studied the memory performance under far-off resonance conditions in cold atomic ensemble. The frequencies of pump 1 and the coupling lasers were changed to be far-detuned, a +200 MHz from the atomic transition of $|1\rangle \rightarrow |4\rangle$. Thus, the generated anti-Stokes photons were also far-detuned by +200 MHz from the atomic transition of $|2\rangle \rightarrow |4\rangle$. The power of the coupling laser was increased as much as possible to perform Raman storage at the single-photon level. With an atomic absorption bandwidth of 5.8 MHz and an almost negligible Doppler linewidth at an atomic temperature of 100 μK, the ratio of detuning and the atomic absorption bandwidth was $200/5.8 = 34.5$. During the storage, the pulse width of pump 1 laser was 50 ns, the power of the coupling laser was 110 mW with a beam waist of 2 mm, corresponding to a Rabi frequency of 17.6 Γ (where Γ is the decay rate of level $|4\rangle$). At the same time, a home-made F-P cavity filter was inserted into the filtering system (3 filters were used in this experiment). The final

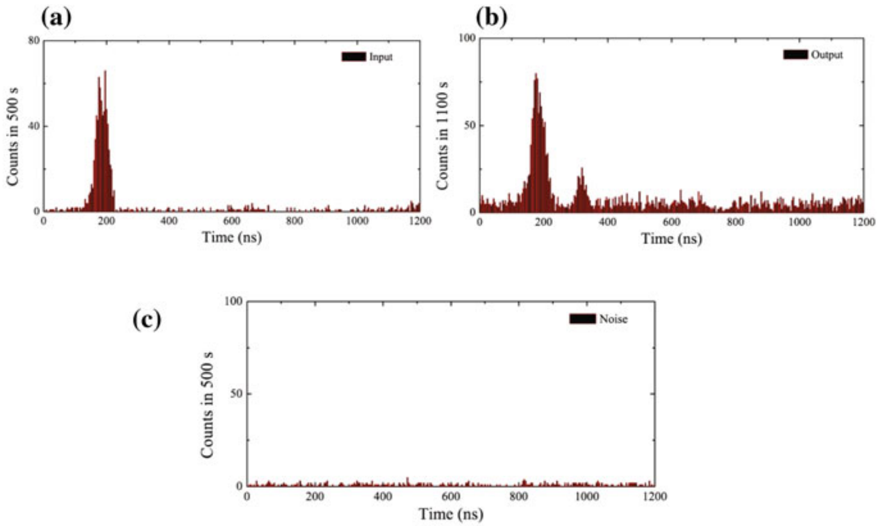

Fig. 6.4 **a/b** Coincidence between the anti-Stokes and the Stokes photons with a single photon detuning of +200 MHz before/after storage. **c** The recorded noise

extinction ratio of about $10^9 : 1$ was enough to reduce the scattering noise from the coupling laser. The results are shown in Fig. 6.4. Figure 6.4a shows the coincidence between the anti-Stokes and Stokes photons without a coupling laser and the trapped atoms in MOT B. Figure 6.4b shows the data of storage and Fig. 6.4c is the recorded coincidence with the anti-Stokes photons blocked, the coupling laser opened and atoms trapped in MOT B. The measured $g_{AS,S}(\tau)$ for the retrieved signal was about 5.6. The signal to noise ratio could be improved if more filters were used to reduce the noise. The noise in Fig. 6.4b is Raman scattering from the few atoms in level $|2\rangle$ that were excited by the anti-Stokes photons.

6.2.3 *Storing Single Photon with Hybrid Entanglement in its Path and Polarization*

Firstly, the storage of a heralded single photon entangled in both path and polarization will be introduced. The heralded single photons used for subsequent storage were directly generated from one SRS process, L in MOT A with the other R blocked. After passing through the polarization beam splitter (PBS), the diagonally polarized heralded anti-Stokes photon was divided into two beams (U and D) and sent to MOT B via the two paths. Paths U and D consisted of a specific Sagnac interferometer with other mirrors and a PBS. These two optical paths completely overlapped in the atomic cloud in MOT B. A coupling laser with a frequency detuning of +70 MHz was input into MOT B at the same angle to the two optical paths, U and D respectively. Since there were Raman interactions between the atoms and the coupling laser, a virtual energy level at a detuning of +70 MHz was excited as explained before, which coupled to the coupling laser and the anti-Stokes photon with two ground states of $|1\rangle$ and $|2\rangle$ via a Λ atomic configuration. The power of the coupling laser was 22 mW with a beam waist of 2 mm, corresponding to a Rabi frequency of 7.8 Γ (Γ is the decay rate of level $|4\rangle$).

The Raman storage works when the bandwidth between the memory in MOT B and the anti-Stokes photons match. Matching the bandwidths between the anti-Stokes photon and the memory can guarantee a high storage efficiency. Whether the bandwidths do or do not match is affected by the frequencies of the coupling and the pump 1 lasers, which could be modulated by the two acoustic optic modulators. The frequency of the anti-Stokes photon was modulated by pump 1 and the Raman excitation absorption spectrum of the memory could be adjusted by the coupling laser. When the spectrum of the anti-Stokes photons were in the middle of the absorption spectrum of the memory, the anti-Stokes photons could be completely absorbed by the atoms in the memory because of the atomic Raman transitions between the excited virtual energy level and the ground state, $|2\rangle$. This method ensured that there was a good match between the anti-Stokes photon and the memory, giving a storage efficiency of 26.8% [16].

The coupling laser was adiabatically turned off and on to store and retrieve the anti-Stokes photon. By using the specific Sagnac interferometer [17], a single photon entangled state was obtained:

$$|\psi_1\rangle = \frac{1}{\sqrt{2}}(|U\rangle\,|H\rangle + e^{i\theta_1}\,|D\rangle\,|V\rangle) \tag{6.1}$$

where $|U\rangle$ and $|D\rangle$ refer to the up and down optical paths in the interferometer, respectively. $|H\rangle$ and $|V\rangle$ represent the horizontal and vertical polarizations, respectively. θ_1 is the phase difference between paths U and D, which was set to zero in these experiments. Equation 6.1 describes the hybrid entanglement state of a single photon entangled in both the optical path and photonic polarization. The reduced density matrix (ρ) was used in the basis $|n_U, m_D\rangle$ with $n, m = 0, 1$, introduced in Ref. [12] to verify the entangled properties of $|\psi_1\rangle$ before and after storage. Here ρ can be written as:

$$\rho = \frac{1}{P}\begin{pmatrix} p_{00} & 0 & 0 & 0 \\ 0 & p_{10} & d & 0 \\ 0 & d^* & p_{01} & 0 \\ 0 & 0 & 0 & p_{11} \end{pmatrix} \tag{6.2}$$

where, p_{ij} is the probability of finding i photons in mode U_k and j photons in mode D_k, k represents the input or output modes, which is shown in Table 6.1, $d \approx V(p_{01} + p_{10})/2$ is the coherence between $|1_U 0_D\rangle$ and $|0_U 1_D\rangle$ and $P = p_{00} + p_{10} + p_{10} + p_{11}$ (see Fig. 6.6). V is the visibility of the interference between modes U and D and could be calculated by recording the coincidence counts between detectors $D3$ and

Table 6.1 Measurements of $\bar{p}_{ij}$ and concurrences $\bar{C}$ before and after storage

	$\bar{\rho}_{\text{input}}$	$\bar{\rho}_{\text{output}}$
$\bar{p}_{00}$	0.990393 ± 0.00006	0.998166 ± 0.000008
$\bar{p}_{10}$	$(4.59 \pm 0.03) \times 10^{-3}$	$(9.64 \pm 0.04) \times 10^{-4}$
$\bar{p}_{01}$	$(5.04 \pm 0.03) \times 10^{-3}$	$(8.71 \pm 0.04) \times 10^{-4}$
$\bar{p}_{11}$	$(1.6 \pm 0.2) \times 10^{-6}$	$(5 \pm 5) \times 10^{-8}$
$\bar{C}$	$(5.8 \pm 0.2) \times 10^{-3}$	$(1.2 \pm 0.4) \times 10^{-3}$

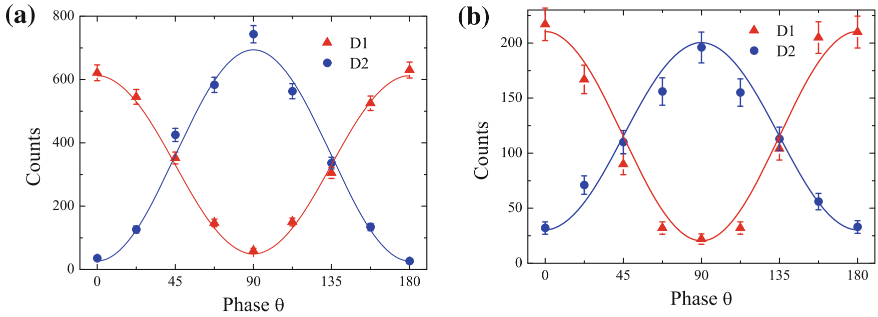

Fig. 6.5 Interference of single photon for input and output. **a** and **b**, The coincidence between the Stokes photon detected by detector D3 and the anti-Stokes photon detected by detector D1 (circular data) and detector D2 (triangular data), respectively, with a different phase before/after storage. The solid lines are the fitted lines. All of the experimental data are raw data without error corrections. The error bars are ±1 standard deviation

$D2$, and detectors $D3$ and $D1$ against the phase (θ) introduced by a phase plate. This is shown in Fig. 6.5, where the half-wave plate was set to 22.5° with respect to its optical axis. The entangled properties of the density matrix (ρ) were characterized by the concurrence

$$C = \frac{1}{P} \max(0, 2\,|d| - 2\sqrt{p_{00}p_{11}}) \tag{6.3}$$

The value of the concurrence between 0–1 represents the state from separable toward the maximally entangled. In these experiments, the calculated concurrences before and after storage were $C_{input} = (5.8 \pm 0.2) \times 10^{-3}$ and $C_{output} = (1.2 \pm 0.4) \times 10^{-3}$, respectively, including a transmission rate of 30% for the three home-made Fabry–Perot cavity filters and a coupling efficiency of 50% for the optical fiber. The factor $\eta = C_{output}/C_{input}$ of $\sim$20.9 ± 7.7% was obtained, which represents the efficiency of the heralded entanglement transfer during the storage process. The Visibilities of $V_{input} = 86.9 \pm 3.1\%$ were obtained for the input before storage and $V_{output} = 82.2 \pm 5.7\%$ for the output states, showing the preservation of the entanglement during the storage process. The high contrast factor of $\beta = V_{output}/V_{input} = 95 \pm 10\%$ represents the high fidelity of the memory system. The average fidelity was calculated

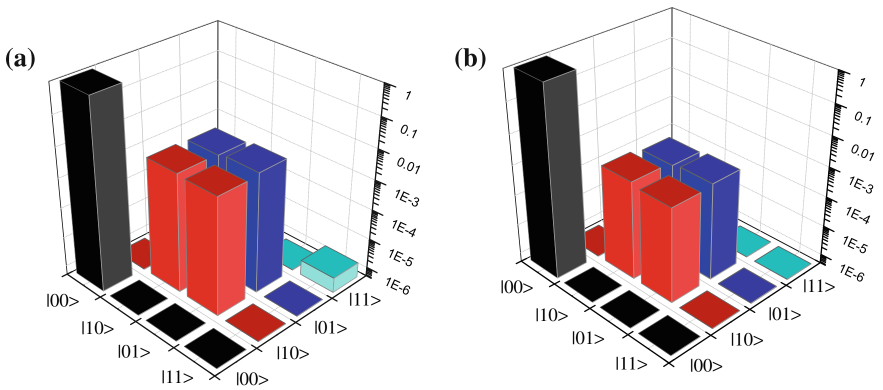

Fig. 6.6 Density matrices for input and output. **a** The density matrices of the input state before storage and **b** the output state after storage. All of the experimental data here are raw data without any error corrections

for all possible input states using and values of 0.994 under the condition of perfect Sagnac interferometer, showing the good performance of the memory.

The visibility obtained was greater than the threshold of 70.7% of the benchmark of Bell's inequality [14] and the experimental proof of the storage of a single-photon entangled in both its photonic path and polarization show the ability of storing a hybrid entangled state, demonstrating the workability of the memory under the quantum regime. The stored anti-Stokes photon was triggered by the Stokes photon. Thus, the quantum memory for the entanglement of a heralded single photon was realized. The heralded Raman memory for a single photon meets the criteria of the DLCZ protocol for long-distance quantum communication [18], where entangled memories should be heralded by the detection of a single photon.

6.2.4 Storing Entanglement of Photonic Polarization

Next, photonic polarized entanglement is stored in two cold atomic ensembles. The polarized entanglement between the anti-Stokes photon and the collective spin excited state of the atomic ensemble was prepared in MOT A, which was created by the coherent superposition of two spatially symmetric SRS processes (L and R paths) driven by two pump beams at 795 nm in a Mach-Zehnder interferometer [11, 30]. The entangled state can be described as:

$$|\psi>=\frac{1}{\sqrt{2}}(|L\rangle\,|H\rangle+e^{i\phi}\,|R\rangle\,|V\rangle) \tag{6.4}$$

The first term refers to the SRS process in L path and the second term refers to R path. Denotes the horizontal (vertical) polarization of the anti-Stokes photon and denotes the collective spin excited state in L(R) path accordingly. Is the phase difference between the two anti-Stokes photons, caused by the phase difference between the two pump paths, which was set to zero in the experiment. The interferometer was stabilized using a locking laser, whose output was detected by a photon detector. The anti-Stokes photon was then sent to MOT B and stored. Thus, entanglement was established between the collective spin excited states of the atoms in MOT A and B, which is

$$|\psi_{aa}\rangle = \frac{1}{\sqrt{2}}(|U\rangle_A|L\rangle_B + |D\rangle_A|R\rangle_B) \tag{6.5}$$

This state shows the entanglement between collective spin excited states with different wave-vectors. After the collective spin excited states of the atoms in MOT B was retrieved to the anti-Stokes photon, the collective spin excited state of the atomic ensemble in MOT A to the Stokes photon was read, resulting in the establishment of polarization entanglement of $|\psi_2\rangle = \frac{1}{\sqrt{2}}(|H\rangle\,|V\rangle + |V\rangle\,|H\rangle)$ between the readout photons.

In this experiment, the generation of the anti-Stokes and Stokes photons were separated with a time sequence. Before the spin wave was read out of the atomic ensemble in MOT A for the Stokes photon, the anti-Stokes photon had already been sent to the atomic ensemble in MOT B for storage. It must be ensured that the storage time of the anti-Stokes photon in MOT B is shorter than the storage time of the spin wave in MOT A to ensure the entanglement was stored. In the experimental time sequence, the storage time of the spin waves in MOT A and B were 160 and 100 ns, respectively, for simplicity. The decay rate of the storage in the system was about 0.7 MHz. Therefore, the storage time of the current memory was limited to $\sim$1.4 μs [16]. The coherence time of the atomic spin wave in MOT A could be enhanced to $\sim$ms using several techniques such as populating atoms into the magnetic-insensitive level [41] or reducing the angle between the coupling laser and the anti-Stokes photon [43], or with the aid of a cavity [4]. It could be increased to $\sim$100 ms by confining the atoms in an optical lattice, suppressing the motional dephasing and the compensation of the lattice light shifts [35, 44]. The above techniques could also be used to increase the storage time of the anti-Stokes photons in MOT B. In addition, the dynamic decoupling method can also improve the storage time [23].

The polarization entanglement was demonstrated in two ensembles by checking the entanglement between the anti-Stokes and Stokes photons. By projecting these two photons into four basis: $|H\rangle$, $|V\rangle$, $(|H\rangle + |V\rangle)/\sqrt{2}$ and $(|H\rangle - i\,|V\rangle)/\sqrt{2}$, the density matrices of the polarized entangled state could be reconstructed.

The ideal retrieved polarized entangled state can be written as:

$$|\psi_2\rangle = \frac{1}{\sqrt{2}}(|H\rangle\,|V\rangle + |V\rangle\,|H\rangle) \tag{6.6}$$

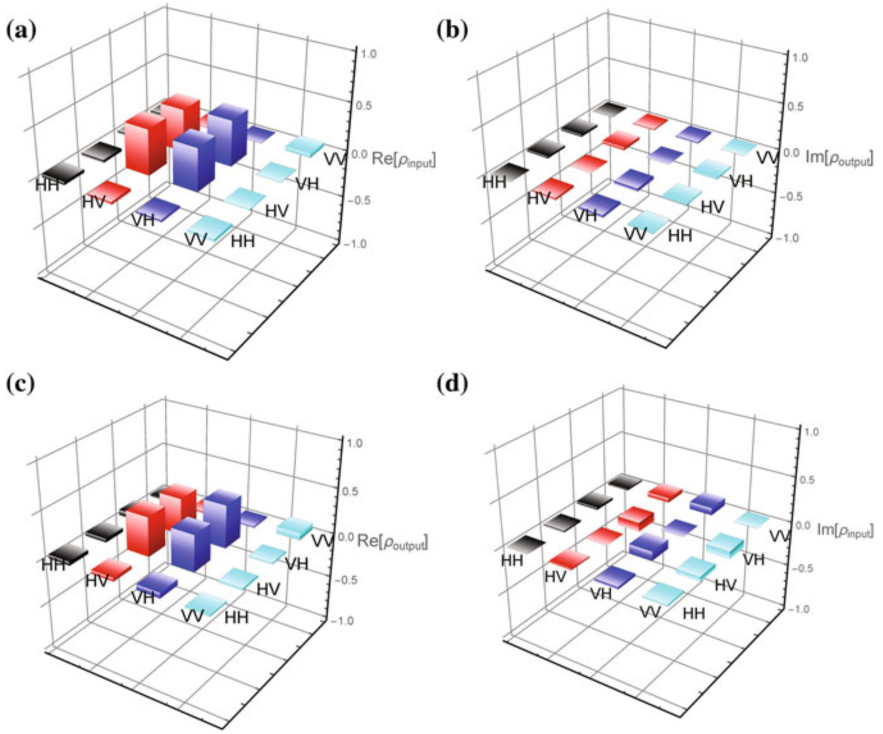

Fig. 6.7 Reconstructed density matrix before and after storage. **a/c** and **b/d**, The reconstructed real and imaginary parts of the input/output density matrix, respectively. The density matrices were reconstructed with losses. All of the experimental data are raw data without error corrections

The real and imaginary parts of the reconstructed density matrices (ρ_{input}) for the input state are given in Fig. 6.7a and b. By using the formula, $F_1 = \mathrm{Tr}(\sqrt{\sqrt{\rho_{input}}\rho_{ideal}\sqrt{\rho_{input}}})^2$, the fidelity (F1) of the reconstructed density matrix was calculated by comparing it with the ideal density matrix (ρ_{ideal}), which was $89.3 \pm 1.7\%$. After the programmed storage time, the retrieved density matrices of the real part and imaginary parts are given in Fig. 6.7c and d. Using the formula: $F_2 = \mathrm{Tr}(\sqrt{\sqrt{\rho_{output}}\rho_{input}\sqrt{\rho_{output}}})^2$, the fidelity (F2) of the output, $85.0 \pm 3.4\%$, was obtained.

The entanglement properties before and after storage were characterized by checking the violation of Bell's inequality using the CHSH inequality [14]. S is defined as:

$$S = \left|E(\theta_A, \theta_S) - E(\theta_A, \theta_S{}') + E(\theta_A{}', \theta_S) + E(\theta_A{}', \theta_S{}')\right| \tag{6.7}$$

where θ_A and θ_S are the angles of the half-wave plates inserted in the paths along which the anti-Stokes and Stokes photons propagate, respectively. $E(\theta_A, \theta_S)$ can be calculated from the coincidence rates at particular orientations:

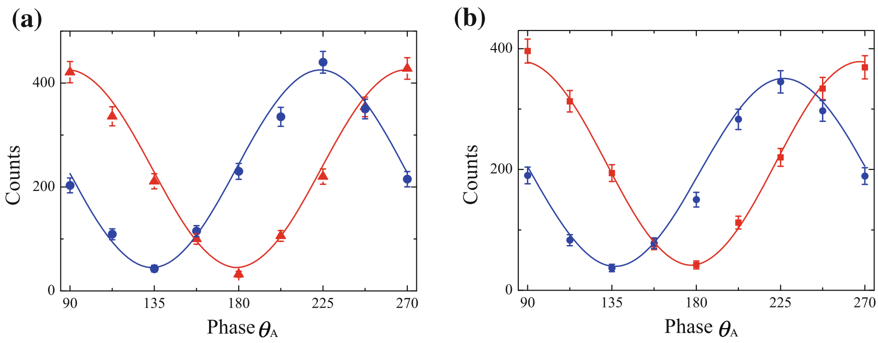

Fig. 6.8 The interference before and after storage. The red (blue) curve represents the coincidence rate for detectors D2 and D3 with the Stokes photons projected in the base: $|H\rangle$ $((|H\rangle - |V\rangle)/\sqrt{2})$. **a** The interference before storage and **b** after storage. The data are all raw data without any corrections. The error bars are ± 1 standard deviation

$$E(\theta_A, \theta_S) = \frac{C(\theta_A, \theta_S) + C(\theta_A + \frac{\pi}{2}, \theta_S + \frac{\pi}{2}) - C(\theta_A + \frac{\pi}{2}, \theta_S) - C(\theta_A, \theta_S + \frac{\pi}{2})}{C(\theta_A, \theta_S) + C(\theta_A + \frac{\pi}{2}, \theta_S + \frac{\pi}{2}) + C(\theta_A + \frac{\pi}{2}, \theta_S) + C(\theta_A, \theta_S + \frac{\pi}{2})} \tag{6.8}$$

Here, $\theta_A = 0$, $\theta_S = \pi/8$, $\theta_{A'} = \pi/4$ and $\theta_{S'} = 3\pi/8$. This equation is not same to the CHSH inequality Eq. 4.7 described in Chap. 4, in which the orientation angles correspond to the different sector states. The calculated S values were 2.40 ± 0.04 before storage and 2.26 ± 0.08 after storage. The two-photon interference curve was also studied. When the Stokes photon was the polarization: $|H\rangle$ $((|H\rangle - |V\rangle)/\sqrt{2})$, we measure the coincidence counts at different θ_A values before and after storage. The results are shown in Fig. 6.8. The calculated visibilities were $85.9 \pm 3.0\%$ before and $80.6 \pm 3.5\%$ after storage. This is much better than the threshold of 70.7% which is the benchmark of Bell's inequality, showing that the polarization entanglement had been preserved during storage.

The two quantum memories realized here are different: the first realized the heralded single photon entanglement storage, the second stored post-selected polarization entanglement. If it is desired to store a heralded two-photon entangled state without any post-selection operation, a heralded Bell's state must be prepared [5, 21, 40]. Preparing such a state itself is difficult and is an active research area. The developed Raman memory takes advantage of broadband storage. In Ref. [32], the storage of a single photon with a GHz bandwidth was attempted (the full width at half maximum (FWHM) of the photon was 1 ns). For our cold atomic quantum memory, the FWHM of the single photon being stored in the current memory was ~7 ns, corresponding to a bandwidth of ~140 MHz.

Upon comparison with other works using the EIT scheme [42], it was found that our memory increased the storage bandwidth by almost one order of magnitude. Therefore, our memory has the ability to store single photons in the quantum regime with a nanosecond pulse width. The storage bandwidth of a Raman memory is limited by the splitting of the ground state and the storage state (here, the states are

$5S_{1/2}(F = 3)$ and $5S_{1/2}(F = 2)$ for ^{85}Rb). An anti-Stokes photon or a coupling laser would address the other state when the bandwidth is larger than half of the splitting size. This will lead to a competition with the other lambda configuration, which will either reduce or disrupt the fidelity and efficiency of the storage. The storage bandwidth is also affected by the power, detuning, bandwidth of the coupling laser and the OD. A larger storage bandwidth requires a large detuning because of the requirement of the adiabatic evolution, which needs the detuning to be much larger than the bandwidth. Additionally, it requires either a strong coupling power or a large OD to compensate for the reduction in the interaction strength between the photon and the media because of the large detuning. Therefore, in practice, the memory performance requires careful assessment of the various parameters in the whole system [37]. References [13, 38] also reported the preservation of the entanglement of broadband photons by quantum storage in a rare-earth doped crystal using the "two-level" atomic frequency comb protocol. The intrinsic large inhomogeneous broadening make rare-earth doped crystals suitable for the storage of broadband photons. The photons were generated by the spontaneous parametric downconversion in a nonlinear crystal, where the time-bin or time-energy entanglement can be stored.

In our experiment, the storage of polarization entanglement was realized. Another important result is that the noise in Raman quantum memory in Ref. [32] mainly came from the accompanying SFWM process, where a hot vapour with a large OD of 1600 was used as the media. However, because of the lower OD and the cold atoms used, the SFWM noise was negligible. The main noise was light scattering from the coupling laser, which was reduced to the dark count level by using three home-made F-P cavity filters with an extinction ratio of $10^7 : 1$. Therefore, the memory could work under the quantum regime. As mentioned earlier, a stronger coupling power was needed to compensate for the large amount of detuning, but it caused more noise, resulting in a reduced fidelity for the storage. The storage efficiency was about 26.7%, achieved by carefully matching the bandwidth of the anti-Stoke photon and the memory. The efficiency was improved by using an appropriately shaped pulse for the anti-Stokes photon to compensate for the distortion caused by the dynamic Stark shift from the strong coupling laser. The efficiency of the Raman quantum memory was mainly limited by the reabsorption of the anti-Stokes photon that was retrieved in the forward direction. Therefore, the maximum efficiency that could be achieved is $\sim$60%. This limitation could be overcome by using a backward direction retrieval, where above 90% efficiency could be achieved [39].

6.3 Summary

The Raman memories of two types of photonic polarization entanglements were implemented experimentally. The experimental data included the concurrences, visibilities and fidelities before and after storage, clearly showed the successful storage of the polarization entanglement. These results should provide a significant step towards quantum communications based on Raman quantum memories. Further more, Raman quantum memory can also be used in Ladder-type atomic configuration, especially for Rydberg atoms where the high lying atoms having long lifetime is suitable for long time storage. More experiments on Raman quantum memories are required to further realize high-speed, long-time and high-fidelity storage in the quantum regime.

However, I think there are many challenges towards this direction:

- Achieving unit storage efficiency for Raman scheme, because many quantum information processes should be based on high efficiency. In EIT scheme, the storage efficiency is dependent on the optical depth of the medium, which can be achieved to unit efficiency in principle.
- Getting long lifetime in Raman storage, in EIT or DLCZ scheme, many techniques, such as magnetically insensitive state, dipole trapping for reducing atomic motion etc., can be used to enhance the coherence time. However, the larger the bandwidth of Raman scheme, the storage decoherence is much stronger. Although, the product of time bandwidth of the Raman scheme can be achieved for large, only having applications for small distant information processing, such as for high-speed quantum computations. But for high-speed quantum communications, the long time storage is needed.
- Avoiding the noise from other channels. As we know that, Raman scheme can be demonstrated by using atomic Λ configuration, but the inevitable noise from FWM process increase the fidelity of the storage process. Maybe, suitable atomic energy diagram can reduce the FWM noise.

References

1. Afzelius, Mikael, Thierry Chaneliere, Rufus L. Cone, Stefan Kröll, Sergey A. Moiseev, Matthew Sellars, et al. 2010. Photon-echo quantum memory in solid state systems. *Laser & Photonics Reviews* 4 (2): 244–267.
2. Afzelius, Mikael, Christoph Simon, Hugues De Riedmatten, and Nicolas Gisin. 2009. Multimode quantum memory based on atomic frequency combs. *Physical Review A* 79 (5): 052329.
3. Alexander, A.L., J.J. Longdell, M.J. Sellars, and N.B. Manson. 2006. Photon echoes produced by switching electric fields. *Physical Review Letters* 96 (4): 043602.
4. Bao, Xiao-Hui, Andreas Reingruber, Peter Dietrich, Jun Rui, Alexander Dück, Thorsten Strassel, Li Li, Nai-Le Liu, Bo Zhao, and Jian-Wei Pan. 2012. Efficient and long-lived quantum memory with cold atoms inside a ring cavity. *Nature Physics* 8 (7): 517–521.
5. Barz, Stefanie, Gunther Cronenberg, Anton Zeilinger, and Philip Walther. 2010. Heralded generation of entangled photon pairs. *Nature Photonics* 4 (8): 553–556.
6. Briegel, H.-J Wolfgang Dür, Juan I Cirac, and Peter Zoller. 1998. Quantum repeaters: the role of imperfect local operations in quantum communication. *Physical Review Letters* 81 (26): 5932.
7. Buchler, B.C. Mahdi Hosseini, Gabriel Hétet, BM Sparkes, and Ping Koy Lam. 2010. Precision spectral manipulation of optical pulses using a coherent photon echo memory. *Optics Letters* 35(7): 1091–1093.
8. Bussières, Félix, Nicolas Sangouard, Mikael Afzelius, Hugues de Riedmatten, Christoph Simon, and Wolfgang Tittel. 2013. Prospective applications of optical quantum memories. *Journal of Modern Optics* 60 (18): 1519–1537.

9. Philip J Bustard, Rune Lausten, Duncan G England, and Benjamin J Sussman. 2013. Toward quantum processing in molecules: A thz-bandwidth coherent memory for light. *Physical Review Letters* 111(8): 083901.
10. Chanelière, T., D.N. Matsukevich, S.D. Jenkins, S.Y. Lan, T.A. Kennedy, and A. Kuzmich. 2005. Storage and retrieval of single photons transmitted between remote quantum memories. *Nature* 438 (7069): 833.
11. Chen, Shuai, Yu-Ao Chen, Bo Zhao, Zhen-Sheng Yuan, Jörg Schmiedmayer, and Jian-Wei Pan. 2007. Demonstration of a stable atom-photon entanglement source for quantum repeaters. *Physical Review Letters* 99 (18): 180505.
12. Choi, K.S., H. Deng, J. Laurat, and H.J. Kimble. 2008. Mapping photonic entanglement into and out of a quantum memory. *Nature* 452 (7183): 67–71.
13. Clausen, C., I. Usmani, F. Bussières, N. Sangouard, M. Afzelius, H. de Riedmatten, and N. Gisin. 2011. Quantum storage of photonic entanglement in a crystal. *Nature* 469 (7331): 508–511.
14. John F Clauser, Michael A Horne, Abner Shimony, and Richard A Holt. 1969. Proposed experiment to test local hidden-variable theories. *Physical Review Letters* 23(15): 880.
15. Dai, Han-Ning, Han Zhang, Sheng-Jun Yang, Tian-Ming Zhao, Jun Rui, You-Jin Deng, Li Li, Nai-Le Liu, Shuai Chen, Xiao-Hui Bao, et al. 2012. Holographic storage of biphoton entanglement. *Physical Review Letters* 108 (21): 210501.
16. Ding, Dong-Sheng, Wei Zhang, Zhi-Yuan Zhou, Shuai Shi, Guo-Yong Xiang, Xi-Shi Wang, Yun-Kun Jiang, Bao-Sen Shi, and Guang-Can Guo. 2015. Quantum storage of orbital angular momentum entanglement in an atomic ensemble. *Physical Review Letters* 114 (5): 050502.
17. Dong-Sheng Ding, Zhi-Yuan Zhou, Bao-Sen Shi, and Guang-Can Guo. 2013. Single-photon-level quantum image memory based on cold atomic ensembles. *Nature Communications*, 4.
18. Duan, L.M., M.D. Lukin, J.I. Cirac, and P. Zoller. 2001. Long-distance quantum communication with atomic ensembles and linear optics. *Nature* 414 (6862): 413.
19. England, D.G., P.J. Bustard, J. Nunn, R. Lausten, and B.J. Sussman. 2013. From photons to phonons and back: a thz optical memory in diamond. *Physical Review Letters* 111 (24): 243601.
20. Fiore, Victor, Yong Yang, Mark C Kuzyk, Russell Barbour, Lin Tian, and Hailin Wang. 2011. Storing optical information as a mechanical excitation in a silica optomechanical resonator. *Physical Review Letters* 107(13): 133601.
21. Deny R Hamel, Lynden K Shalm, Hannes Hübel, Aaron J Miller, Francesco Marsili, Varun B Verma, Richard P Mirin, Sae Woo Nam, Kevin J Resch, and Thomas Jennewein. 2014. Direct generation of three-photon polarization entanglement. *Nature Photonics* 8(10): 801–807.
22. Stephen, E., and J.E. Harris Field, and A Imamoğlu. 1990. Nonlinear optical processes using electromagnetically induced transparency. *Physical Review Letters* 64(10): 1107.
23. Heinze, Georg, Christian Hubrich, and Thomas Halfmann. 2013. Stopped light and image storage by electromagnetically induced transparency up to the regime of one minute. *Physical Review Letters* 111 (3): 033601.
24. Hosseini, Mahdi Ben M Sparkes, Geoff Campbell, Ping K Lam, and Ben C Buchler. 2011. High efficiency coherent optical memory with warm rubidium vapour. *Nature Communications* 2: 174.
25. Julsgaard, B., A. Kozhekin, and E.S. Polzik. 2001. Experimental long-lived entanglement of two macroscopic objects. *Nature* 413 (6854): 400–403.
26. Julsgaard, B., J. Sherson, J.I. Cirac, J. Fiurásek, and E.S. Polzik. 2004. Experimental demonstration of quantum memory for light. *Nature* 432 (7016): 482–486.
27. Kimble, H.J. 2008. The quantum internet. *Nature* 453: 19.
28. AE Kozhekin, Klaus Mølmer, and E Polzik. Quantum memory for light. *Physical Review A*, 62(3):033809.
29. Barbara Kraus, W Tittel, N Gisin, Mattias Nilsson, Stefan Kröll, and JI Cirac. 2006. Quantum memory for nonstationary light fields based on controlled reversible in homogeneous broadening. *Physical Review A* 73(2):020302.
30. Liao, Kaiyu, Hui Yan, Du Junyu He, Zhi-Ming Zhang Shengwang, and Shi-Liang Zhu. 2014. Subnatural-linewidth polarization-entangled photon pairs with controllable temporal length. *Physical Review Letters* 112 (24): 243602.

31. Alexander I Lvovsky, Barry C Sanders, and Wolfgang Tittel. 2009. Optical quantum memory. *Nature Photonics* 3(12): 706–714.
32. Michelberger, P.S., T.F.M. Champion, M.R. Sprague, K.T. Kaczmarek, M. Barbieri, X.M. Jin, D.G. England, W.S. Kolthammer, D.J. Saunders, J. Nunn, et al. 2015. Interfacing ghz-bandwidth heralded single photons with a warm vapour raman memory. *New Journal of Physics* 17 (4): 043006.
33. Moiseev SA, Kroll S. 2001. Complete reconstruction of the quantum state of a single-photon wave packet absorbed by a doppler-broadened transition. *Physical Review Letters* 87 (17): 173601.
34. Nunn, J., I.A. Walmsley, M.G. Raymer, K. Surmacz, F.C. Waldermann, Z. Wang, and D. Jaksch. 2007. Mapping broadband single-photon wave packets into an atomic memory. *Physical Review A* 75 (1): 011401.
35. Radnaev, A.G., Y.O. Dudin, R. Zhao, H.H. Jen, S.D. Jenkins, A. Kuzmich, and T.A.B. Kennedy. 2010. A quantum memory with telecom-wavelength conversion. *Nature Physics* 6 (11): 894.
36. Reim, K.F., P. Michelberger, K.C. Lee, J. Nunn, N.K. Langford, and I.A. Walmsley. 2011. Single-photon-level quantum memory at room temperature. *Physical Review Letters* 107 (5): 053603.
37. Reim, K.F., J. Nunn, V.O. Lorenz, B.J. Sussman, K.C. Lee, N.K. Langford, D. Jaksch, and I.A. Walmsley. 2010. Towards high-speed optical quantum memories. *Nature Photonics* 4 (4): 218–221.
38. Saglamyurek, Erhan, Neil Sinclair, and Jeongwan Jin, Joshua A Slater, Daniel Oblak, Félix Bussières, Mathew George, Raimund Ricken, Wolfgang Sohler, and Wolfgang Tittel. 2011. Broadband waveguide quantum memory for entangled photons. *Nature* 469(7331): 512–515.
39. Surmacz, K., J. Nunn, K. Reim, K.C. Lee, V.O. Lorenz, B. Sussman, I.A. Walmsley, and D. Jaksch. 2008. Efficient spatially resolved multimode quantum memory. *Physical Review A* 78 (3): 033806.
40. Wagenknecht, Claudia, Che-Ming Li, Andreas Reingruber, Xiao-Hui Bao, Alexander Goebel, Yu-Ao Chen, Qiang Zhang, Kai Chen, and Jian-Wei Pan. 2010. Experimental demonstration of a heralded entanglement source. *Nature Photonics* 4 (8): 549–552.
41. Zhongxiao, Xu, Wu Yuelong, Long Tian, Lirong Chen, Zhiying Zhang, Zhihui Yan, Shujing Li, Hai Wang, Changde Xie, and Kunchi Peng. 2013. Long lifetime and high-fidelity quantum memory of photonic polarization qubit by lifting zeeman degeneracy. *Physical Review Letters* 111 (24): 240503.
42. Zhang, Han, Xian-Min Jin, Jian Yang, Han-Ning Dai, Sheng-Jun Yang, Yu. Tian-Ming Zhao, Jun Rui, Xiao Jiang He, Fan Yang, et al. 2011. Preparation and storage of frequency-uncorrelated entangled photons from cavity-enhanced spontaneous parametric downconversion. *Nature Photonics* 5 (10): 628–632.
43. Bo Zhao, Yu-Ao Chen, Xiao-Hui Bao, Thorsten Strassel, Chih-Sung Chuu, Xian-Min Jin, Jörg Schmiedmayer, Zhen-Sheng Yuan, Shuai Chen, and Jian-Wei Pan. 2008. A millisecond quantum memory for scalable quantum networks. *arXiv preprint* arXiv:0807.5064.
44. R Zhao, YO Dudin, SD Jenkins, CJ Campbell, DN Matsukevich, TAB Kennedy, and A Kuzmich. 2009. Long-lived quantum memory. *Nature Physics* 5(2).

Appendix A
Phase Superposition and Tomography Code

```
(*Calculate the intensity/phase of LG5 and LG-1*)
ClearAll["`*"];
ω0 = 4.98*10^-1;
ω1 = 4.98*10^-5;
λ = 780*10^-9;
zr = Pi*ω0^2/λ;
zr1 = Pi*ω1^2/λ;
z = 0.002;
ωz = ω0 Sqrt[1 + (z/zr)^2];
k = 0.01248 Pi/λ;
p = 0; L1 = 5; L2 = -1; r = Sqrt[x*x + y*y]; ϕ = ArcTan[x, y]; ϕ1 = Pi; ϕ2 = 1 Pi/2; h = ϕ2;
U1 = (r^Abs[L1]) LaguerreL[p, Abs[L1], (2 r^2)/(ω0 Sqrt[1 + (z/zr)^2])^2] *
    E^(-r^2/(ω0 Sqrt[1 + (z/zr)^2])^2) Exp[-I (k*z + (k*r^2)/(2 (z + zr^2/z)) + (L1*ϕ) - (2 p + Abs[L1] + 1)*ArcTan[z/zr])];
```


D.-S. Ding, *Broad Bandwidth and High Dimensional Quantum Memory Based on Atomic Ensembles*, Springer Theses, https://doi.org/10.1007/978-981-10-7476-9

$$U2 = \left(r^{Abs[L2]}\right) LaguerreL\left[p, Abs[L2], \frac{2\,r^2}{\left(\omega_0 \sqrt{1 + (z/zr)^2}\right)^2}\right] * E^{\frac{-r^2}{\left(\omega_0\sqrt{1+(z/zr)^2}\right)^2}}$$

$$Exp\left[-I\left(k*z + \frac{k*r^2}{2\left(z + zr^2/z\right)} + (L2*\phi) + 1*\phi 2 - (2\,p + Abs[L2] + 1)*ArcTan\left[\frac{z}{zr}\right]\right)\right];$$

$$U3 = \left(r^{Abs[L2]}\right) LaguerreL\left[p, Abs[L2], \frac{2\,r^2}{\left(\omega_0 \sqrt{1 + (z/zr)^2}\right)^2}\right] * E^{\frac{-r^2}{\left(\omega_0\sqrt{1+(z/zr)^2}\right)^2}}$$

$$Exp\left[-I\left(k*z + \frac{k*r^2}{2\left(z + zr^2/z\right)} + (L2*\phi) - 1*\phi 2 - (2\,p + Abs[L2] + 1)*ArcTan\left[\frac{z}{zr}\right]\right)\right];$$

```
DensityPlot[Arg[U1 + U2], {x, -2.5, 2.5}, {y, -2.5, 2.5}, PlotRange → All, Axes → False,
  PlotPoints → 100, Frame → False, ColorFunction -> "BlueGreenYellow"]
DensityPlot[Arg[U1 + U3], {x, -2.5, 2.5}, {y, -2.5, 2.5}, PlotRange → All, Axes → False,
  PlotPoints → 100, Frame → False, ColorFunction -> "BlueGreenYellow"]
DensityPlot[(Abs[U1 + 0.2 U2])^2, {x, -2.5, 2.5}, {y, -2.5, 2.5}, PlotRange → All,
  Axes → False, PlotPoints → 100, Frame → False, ColorFunction -> "BlueGreenYellow"]
DensityPlot[(Abs[U1 + 0.2 U3])^2, {x, -2.5, 2.5}, {y, -2.5, 2.5}, PlotRange → All,
  Axes → False, PlotPoints → 100, Frame → False, ColorFunction -> "BlueGreenYellow"]
```

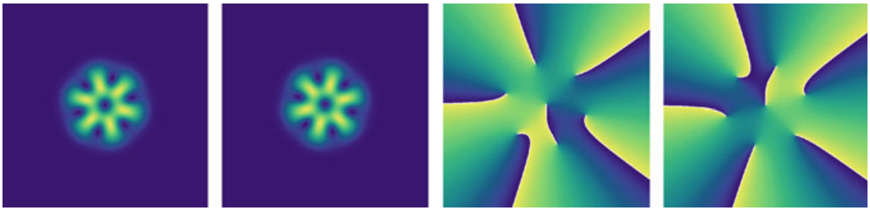

```
(*Qutrit entanglement tomography*)Clear["Global`*"]
```

$$n = \begin{pmatrix} 0 & 0 & 100 & 0 & 50 & 0 & 50 & 50 & 50 \\ 0 & 100 & 0 & 50 & 50 & 50 & 50 & 0 & 0 \\ 100 & 0 & 0 & 50 & 0 & 50 & 0 & 50 & 50 \\ 0 & 50 & 50 & 25 & 100 & 25 & 50 & 25 & 25 \\ 50 & 50 & 0 & 100 & 25 & 50 & 25 & 25 & 25 \\ 0 & 50 & 50 & 25 & 50 & 25 & 100 & 25 & 25 \\ 50 & 50 & 0 & 50 & 25 & 100 & 25 & 25 & 25 \\ 50 & 0 & 50 & 25 & 25 & 25 & 25 & 100 & 50 \\ 50 & 0 & 50 & 25 & 25 & 25 & 25 & 50 & 100 \end{pmatrix};$$

```
data = Flatten[n];
n = Table[data[[i]] * 1.0, {i, 1, 81}];
ϵ = n[[1]] + n[[2]] + n[[3]] + n[[10]] + n[[11]] + n[[12]] + n[[19]] + n[[20]] + n[[21]];
```

```
LL = (1,0,0,0,0,0,0,0,0); LG = (0,1,0,0,0,0,0,0,0); LR = (0,0,1,0,0,0,0,0,0); GL = (0,0,0,1,0,0,0,0,0); GG = (0,0,0,0,1,0,0,0,0); GR = (0,0,0,0,0,1,0,0,0); RL = (0,0,0,0,0,0,1,0,0); RG = (0,0,0,0,0,0,0,1,0); RR = (0,0,0,0,0,0,0,0,1);
```

$$LL = \begin{pmatrix}1\\0\\0\\0\\0\\0\\0\\0\\0\end{pmatrix};\ LG = \begin{pmatrix}0\\1\\0\\0\\0\\0\\0\\0\\0\end{pmatrix};\ LR = \begin{pmatrix}0\\0\\1\\0\\0\\0\\0\\0\\0\end{pmatrix};\ GL = \begin{pmatrix}0\\0\\0\\1\\0\\0\\0\\0\\0\end{pmatrix};\ GG = \begin{pmatrix}0\\0\\0\\0\\1\\0\\0\\0\\0\end{pmatrix};\ GR = \begin{pmatrix}0\\0\\0\\0\\0\\1\\0\\0\\0\end{pmatrix};\ RL = \begin{pmatrix}0\\0\\0\\0\\0\\0\\1\\0\\0\end{pmatrix};\ RG = \begin{pmatrix}0\\0\\0\\0\\0\\0\\0\\1\\0\end{pmatrix};\ RR = \begin{pmatrix}0\\0\\0\\0\\0\\0\\0\\0\\1\end{pmatrix};$$

```
ψ[1] = LL;
ψ[2] = LG;
ψ[3] = LR;
ψ[4] = (LG + LL) / √2 ;
ψ[5] = (LG + LR) / √2 ;
ψ[6] = (LG + i * LL) / √2 ;
ψ[7] = (LG - i * LR) / √2 ;
ψ[8] = (LL + LR) / √2 ;
ψ[9] = (LL + i * LR) / √2 ;
ψ[10] = GL;
ψ[11] = GG;
ψ[12] = GR;
ψ[13] = (GG + GL) / √2 ;
ψ[14] = (GG + GR) / √2 ;
ψ[15] = (GG + i * GL) / √2 ;
ψ[16] = (GG - i * GR) / √2 ;
ψ[17] = (GL + GR) / √2 ;
ψ[18] = (GL + i * GR) / √2 ;
ψ[19] = RL;
ψ[20] = RG;
ψ[21] = RR;
ψ[22] = (RG + RL) / √2 ;
ψ[23] = (RG + RR) / √2 ;
ψ[24] = (RG + i * RL) / √2 ;
ψ[25] = (RG - i * RR) / √2 ;
ψ[26] = (RL + RR) / √2 ;
ψ[27] = (RL + i * RR) / √2 ;
ψ[28] = (GL + LL) / √2 ;
ψ[29] = (GG + LG) / √2 ;
ψ[30] = (GR + LR) / √2 ;
ψ[31] = (GG + GL + LG + LL) / 2;
ψ[32] = (GG + GR + LG + LR) / 2;
```

```
ψ[33] = (GG + ⅈ * GL + LG + ⅈ * LL) / 2;
ψ[34] = (GG - ⅈ * GR + LG - ⅈ * LR) / 2;
ψ[35] = (GL + GR + LL + LR) / 2;
ψ[36] = (GL + ⅈ * GR + LL + ⅈ * LR) / 2;
ψ[37] = (GL + RL) / √2 ;
ψ[38] = (GG + RG) / √2 ;
ψ[39] = (GR + RR) / √2 ;
ψ[40] = (GG + GL + RG + RL) / 2;
ψ[41] = (GG + GR + RG + RR) / 2;
ψ[42] = (GG + ⅈ * GL + RG + ⅈ * RL) / 2;
ψ[43] = (GG - ⅈ * GR + RG - ⅈ * RR) / 2;
ψ[44] = (GL + GR + RL + RR) / 2;
ψ[45] = (GL + ⅈ * GR + RL + ⅈ * RR) / 2;
ψ[46] = (GL + ⅈ * LL) / √2 ;
ψ[47] = (GG + ⅈ * LG) / √2 ;
ψ[48] = (GR + ⅈ * LR) / √2 ;
ψ[49] = (GG + GL + ⅈ * LG + ⅈ * LL) / 2;
ψ[50] = (GG + GR + ⅈ * LG + ⅈ * LR) / 2;
ψ[51] = (GG + ⅈ * GL + ⅈ * LG + ⅈ * ⅈ * LL) / 2;
ψ[52] = (GG - ⅈ * GR + ⅈ * LG - ⅈ * ⅈ * LR) / 2;
ψ[53] = (GL + GR + ⅈ * LL + ⅈ * LR) / 2;
ψ[54] = (GL + ⅈ * GR + ⅈ * LL + ⅈ * ⅈ * LR) / 2;
ψ[55] = (GL - ⅈ * RL) / √2 ;
ψ[56] = (GG - ⅈ * RG) / √2 ;
ψ[57] = (GR - ⅈ * RR) / √2 ;
ψ[58] = (GG + GL - ⅈ * RG - ⅈ * RL) / 2;
ψ[59] = (GG + GR - ⅈ * RG - ⅈ * RR) / 2;
ψ[60] = (GG + ⅈ * GL - ⅈ * RG - ⅈ * ⅈ * RL) / 2;
ψ[61] = (GG - ⅈ * GR - ⅈ * RG + ⅈ * ⅈ * RR) / 2;
ψ[62] = (GL + GR - ⅈ * RL - ⅈ * RR) / 2;
ψ[63] = (GL + ⅈ * GR - ⅈ * RL - ⅈ * ⅈ * RR) / 2;
ψ[64] = (LL + RL) / √2 ;
ψ[65] = (LG + RG) / √2 ;
ψ[66] = (LR + RR) / √2 ;
ψ[67] = (LG + LL + RG + RL) / 2;
ψ[68] = (LG + LR + RG + RR) / 2;
ψ[69] = (LG + ⅈ * LL + RG + ⅈ * RL) / 2;
ψ[70] = (LG - ⅈ * LR + RG - ⅈ * RR) / 2;
ψ[71] = (LL + LR + RL + RR) / 2;
ψ[72] = (LL + ⅈ * LR + RL + ⅈ * RR) / 2;
ψ[73] = (LL + ⅈ * RL) / √2 ;
ψ[74] = (LG + ⅈ * RG) / √2 ;
ψ[75] = (LR + ⅈ * RR) / √2 ;
ψ[76] = (LG + LL + ⅈ * RG + ⅈ * RL) / 2;
ψ[77] = (LG + LR + ⅈ * RG + ⅈ * RR) / 2;
ψ[78] = (LG + ⅈ * LL + ⅈ * RG + ⅈ * ⅈ * RL) / 2;
ψ[79] = (LG - ⅈ * LR + ⅈ * RG - ⅈ * ⅈ * RR) / 2;
ψ[80] = (LL + LR + ⅈ * RL + ⅈ * RR) / 2;
ψ[81] = (LL + ⅈ * LR + ⅈ * RL + ⅈ * ⅈ * RR) / 2;
```

$$\alpha = \begin{pmatrix}
t_1 & 0 & 0 & 0 & 0 & 0 & 0 & 0 & 0 \\
t_{10} + i * t_{11} & t_2 & 0 & 0 & 0 & 0 & 0 & 0 & 0 \\
t_{26} + i * t_{27} & t_{12} + i * t_{13} & t_3 & 0 & 0 & 0 & 0 & 0 & 0 \\
t_{40} + i * t_{41} & t_{28} + i * t_{29} & t_{14} + i * t_{15} & t_4 & 0 & 0 & 0 & 0 & 0 \\
t_{52} + i * t_{53} & t_{42} + i * t_{43} & t_{30} + i * t_{31} & t_{16} + i * t_{17} & t_5 & 0 & 0 & 0 & 0 \\
t_{62} + i * t_{63} & t_{54} + i * t_{55} & t_{44} + i * t_{45} & t_{32} + i * t_{33} & t_{18} + i * t_{19} & t_6 & 0 & 0 & 0 \\
t_{70} + i * t_{71} & t_{64} + i * t_{65} & t_{56} + i * t_{57} & t_{46} + i * t_{47} & t_{34} + i * t_{35} & t_{20} + i * t_{21} & t_7 & 0 & 0 \\
t_{76} + i * t_{77} & t_{72} + i * t_{73} & t_{66} + i * t_{67} & t_{58} + i * t_{59} & t_{48} + i * t_{49} & t_{36} + i * t_{37} & t_{22} + i * t_{23} & t_8 & 0 \\
t_{80} + i * t_{81} & t_{78} + i * t_{79} & t_{74} + i * t_{75} & t_{68} + i * t_{69} & t_{60} + i * t_{61} & t_{50} + i * t_{51} & t_{38} + i * t_{39} & t_{24} + i * t_{25} & t_9
\end{pmatrix};$$

$$\beta = \begin{pmatrix} t_1 & t_{10} - i * t_{11} & t_{26} - i * t_{27} & t_{40} - i * t_{41} & t_{52} - i * t_{53} & t_{62} - i * t_{63} & t_{70} - i * t_{71} & t_{76} - i * t_{77} & t_{80} - i * t_{81} \\ 0 & t_2 & t_{12} - i * t_{13} & t_{28} - i * t_{29} & t_{42} - i * t_{43} & t_{54} - i * t_{55} & t_{64} - i * t_{65} & t_{72} - i * t_{73} & t_{78} - i * t_{79} \\ 0 & 0 & t_3 & t_{14} - i * t_{15} & t_{30} - i * t_{31} & t_{44} - i * t_{45} & t_{56} - i * t_{57} & t_{66} - i * t_{67} & t_{74} - i * t_{75} \\ 0 & 0 & 0 & t_4 & t_{16} - i * t_{17} & t_{32} - i * t_{33} & t_{46} - i * t_{47} & t_{58} - i * t_{59} & t_{68} - i * t_{69} \\ 0 & 0 & 0 & 0 & t_5 & t_{18} - i * t_{19} & t_{34} - i * t_{35} & t_{48} - i * t_{49} & t_{60} - i * t_{61} \\ 0 & 0 & 0 & 0 & 0 & t_6 & t_{20} - i * t_{21} & t_{36} - i * t_{37} & t_{50} - i * t_{51} \\ 0 & 0 & 0 & 0 & 0 & 0 & t_7 & t_{22} - i * t_{23} & t_{38} - i * t_{39} \\ 0 & 0 & 0 & 0 & 0 & 0 & 0 & t_8 & t_{24} - i * t_{25} \\ 0 & 0 & 0 & 0 & 0 & 0 & 0 & 0 & t_9 \end{pmatrix};$$

$$\rho P = \frac{\beta.\alpha}{\mathrm{Tr}[\beta.\alpha]};$$

```
k1 = Simplify[Conjugate[Transpose[ψ[1]]].ρP.ψ[1]];
k2 = Simplify[Conjugate[Transpose[ψ[2]]].ρP.ψ[2]];
k3 = Simplify[Conjugate[Transpose[ψ[3]]].ρP.ψ[3]];
k4 = Simplify[Conjugate[Transpose[ψ[4]]].ρP.ψ[4]];
k5 = Simplify[Conjugate[Transpose[ψ[5]]].ρP.ψ[5]];
k6 = Simplify[Conjugate[Transpose[ψ[6]]].ρP.ψ[6]];
k7 = Simplify[Conjugate[Transpose[ψ[7]]].ρP.ψ[7]];
k8 = Simplify[Conjugate[Transpose[ψ[8]]].ρP.ψ[8]];
k9 = Simplify[Conjugate[Transpose[ψ[9]]].ρP.ψ[9]];
k10 = Simplify[Conjugate[Transpose[ψ[10]]].ρP.ψ[10]];
k11 = Simplify[Conjugate[Transpose[ψ[11]]].ρP.ψ[11]];
k12 = Simplify[Conjugate[Transpose[ψ[12]]].ρP.ψ[12]];
k13 = Simplify[Conjugate[Transpose[ψ[13]]].ρP.ψ[13]];
k14 = Simplify[Conjugate[Transpose[ψ[14]]].ρP.ψ[14]];
k15 = Simplify[Conjugate[Transpose[ψ[15]]].ρP.ψ[15]];
k16 = Simplify[Conjugate[Transpose[ψ[16]]].ρP.ψ[16]];
k17 = Simplify[Conjugate[Transpose[ψ[17]]].ρP.ψ[17]];
k18 = Simplify[Conjugate[Transpose[ψ[18]]].ρP.ψ[18]];
k19 = Simplify[Conjugate[Transpose[ψ[19]]].ρP.ψ[19]];
k20 = Simplify[Conjugate[Transpose[ψ[20]]].ρP.ψ[20]];
k21 = Simplify[Conjugate[Transpose[ψ[21]]].ρP.ψ[21]];
k22 = Simplify[Conjugate[Transpose[ψ[22]]].ρP.ψ[22]];
k23 = Simplify[Conjugate[Transpose[ψ[23]]].ρP.ψ[23]];
k24 = Simplify[Conjugate[Transpose[ψ[24]]].ρP.ψ[24]];
k25 = Simplify[Conjugate[Transpose[ψ[25]]].ρP.ψ[25]];
k26 = Simplify[Conjugate[Transpose[ψ[26]]].ρP.ψ[26]];
k27 = Simplify[Conjugate[Transpose[ψ[27]]].ρP.ψ[27]];
k28 = Simplify[Conjugate[Transpose[ψ[28]]].ρP.ψ[28]];
k29 = Simplify[Conjugate[Transpose[ψ[29]]].ρP.ψ[29]];
k30 = Simplify[Conjugate[Transpose[ψ[30]]].ρP.ψ[30]];
k31 = Simplify[Conjugate[Transpose[ψ[31]]].ρP.ψ[31]];
k32 = Simplify[Conjugate[Transpose[ψ[32]]].ρP.ψ[32]];
k33 = Simplify[Conjugate[Transpose[ψ[33]]].ρP.ψ[33]];
k34 = Simplify[Conjugate[Transpose[ψ[34]]].ρP.ψ[34]];
k35 = Simplify[Conjugate[Transpose[ψ[35]]].ρP.ψ[35]];
k36 = Simplify[Conjugate[Transpose[ψ[36]]].ρP.ψ[36]];
k37 = Simplify[Conjugate[Transpose[ψ[37]]].ρP.ψ[37]];
k38 = Simplify[Conjugate[Transpose[ψ[38]]].ρP.ψ[38]];
k39 = Simplify[Conjugate[Transpose[ψ[39]]].ρP.ψ[39]];
k40 = Simplify[Conjugate[Transpose[ψ[40]]].ρP.ψ[40]];
k41 = Simplify[Conjugate[Transpose[ψ[41]]].ρP.ψ[41]];
k42 = Simplify[Conjugate[Transpose[ψ[42]]].ρP.ψ[42]];
k43 = Simplify[Conjugate[Transpose[ψ[43]]].ρP.ψ[43]];
k44 = Simplify[Conjugate[Transpose[ψ[44]]].ρP.ψ[44]];
k45 = Simplify[Conjugate[Transpose[ψ[45]]].ρP.ψ[45]];
k46 = Simplify[Conjugate[Transpose[ψ[46]]].ρP.ψ[46]];
k47 = Simplify[Conjugate[Transpose[ψ[47]]].ρP.ψ[47]];
k48 = Simplify[Conjugate[Transpose[ψ[48]]].ρP.ψ[48]];
k49 = Simplify[Conjugate[Transpose[ψ[49]]].ρP.ψ[49]];
k50 = Simplify[Conjugate[Transpose[ψ[50]]].ρP.ψ[50]];
k51 = Simplify[Conjugate[Transpose[ψ[51]]].ρP.ψ[51]];
k52 = Simplify[Conjugate[Transpose[ψ[52]]].ρP.ψ[52]];
k53 = Simplify[Conjugate[Transpose[ψ[53]]].ρP.ψ[53]];
k54 = Simplify[Conjugate[Transpose[ψ[54]]].ρP.ψ[54]];
k55 = Simplify[Conjugate[Transpose[ψ[55]]].ρP.ψ[55]];
k56 = Simplify[Conjugate[Transpose[ψ[56]]].ρP.ψ[56]];
```

```
k57 = Simplify[Conjugate[Transpose[ψ[57]]].ρP.ψ[57]];
k58 = Simplify[Conjugate[Transpose[ψ[58]]].ρP.ψ[58]];
k59 = Simplify[Conjugate[Transpose[ψ[59]]].ρP.ψ[59]];
k60 = Simplify[Conjugate[Transpose[ψ[60]]].ρP.ψ[60]];
k61 = Simplify[Conjugate[Transpose[ψ[61]]].ρP.ψ[61]];
k62 = Simplify[Conjugate[Transpose[ψ[62]]].ρP.ψ[62]];
k63 = Simplify[Conjugate[Transpose[ψ[63]]].ρP.ψ[63]];
k64 = Simplify[Conjugate[Transpose[ψ[64]]].ρP.ψ[64]];
k65 = Simplify[Conjugate[Transpose[ψ[65]]].ρP.ψ[65]];
k66 = Simplify[Conjugate[Transpose[ψ[66]]].ρP.ψ[66]];
k67 = Simplify[Conjugate[Transpose[ψ[67]]].ρP.ψ[67]];
k68 = Simplify[Conjugate[Transpose[ψ[68]]].ρP.ψ[68]];
k69 = Simplify[Conjugate[Transpose[ψ[69]]].ρP.ψ[69]];
k70 = Simplify[Conjugate[Transpose[ψ[70]]].ρP.ψ[70]];
k71 = Simplify[Conjugate[Transpose[ψ[71]]].ρP.ψ[71]];
k72 = Simplify[Conjugate[Transpose[ψ[72]]].ρP.ψ[72]];
k73 = Simplify[Conjugate[Transpose[ψ[73]]].ρP.ψ[73]];
k74 = Simplify[Conjugate[Transpose[ψ[74]]].ρP.ψ[74]];
k75 = Simplify[Conjugate[Transpose[ψ[75]]].ρP.ψ[75]];
k76 = Simplify[Conjugate[Transpose[ψ[76]]].ρP.ψ[76]];
k77 = Simplify[Conjugate[Transpose[ψ[77]]].ρP.ψ[77]];
k78 = Simplify[Conjugate[Transpose[ψ[78]]].ρP.ψ[78]];
k79 = Simplify[Conjugate[Transpose[ψ[79]]].ρP.ψ[79]];
k80 = Simplify[Conjugate[Transpose[ψ[80]]].ρP.ψ[80]];
k81 = Simplify[Conjugate[Transpose[ψ[81]]].ρP.ψ[81]];
```

$$L = \sum_{i=1}^{81} \frac{(\epsilon * k_i - n[[i]])\,\hat{}\,2}{2 * \epsilon * k_i};$$

```
NMinimize[L[[1, 1]], {t1, t2, t3, t4, t5, t6, t7, t8, t9, t10, t11, t12, t13, t14, t15, t16, t17, t18, t19,
    t20, t21, t22, t23, t24, t25, t26, t27, t28, t29, t30, t31, t32, t33, t34, t35, t36, t37, t38, t39, t40,
    t41, t42, t43, t44, t45, t46, t47, t48, t49, t50, t51, t52, t53, t54, t55, t56, t57, t58, t59, t60, t61,
    t62, t63, t64, t65, t66, t67, t68, t69, t70, t71, t72, t73, t74, t75, t76, t77, t78, t79, t80, t81}];
%[[2]];
ρP /. %;
ρ = %;
g1 = BarChart3D[Re[ρ], Axes → True, AxesLabel → " Re[χ] ",
  PlotRange → {-0.5, 0.5}, FaceGrids → {{0, 1, 0}, {0, 0, -1}, {-1, 0, 0}},
  FaceGridsStyle → Directive[{Gray, Thickness[0.003]}], ChartLayout → "Grid",
  ChartLabels → {{"LL", "LG", "LR", "GL", "GG", "GR", "RL", "RG", "RR"},
    {"LL", "LG", "LR", "GL", "GG", "GR", "RL", "RG", "RR"}},
  AxesStyle → Thickness[0.005], BarSpacing -> {1, 1}, BoxRatios → {1, 1, 1}, ViewPoint → {2, -3, 2},
  ChartStyle → "DarkRainbow", Method → {"Canvas" → None}, AxesStyle → Directive[FontSize → 15]]
g2 = BarChart3D[Im[ρ], Axes → True, AxesLabel → " Im[χ] ",
  PlotRange → {-0.5, 0.5}, FaceGrids → {{0, 1, 0}, {0, 0, -1}, {-1, 0, 0}},
  FaceGridsStyle → Directive[{Gray, Thickness[0.003]}], ChartLayout → "Grid",
  ChartLabels → {{"LL", "LG", "LR", "GL", "GG", "GR", "RL", "RG", "RR"},
    {"LL", "LG", "LR", "GL", "GG", "GR", "RL", "RG", "RR"}},
  AxesStyle → Thickness[0.005], BarSpacing -> {1, 1}, BoxRatios → {1, 1, 1}, ViewPoint → {2, -3, 2},
  ChartStyle → "DarkRainbow", Method → {"Canvas" → None}, AxesStyle → Directive[FontSize → 15]]
```

Out[105]=

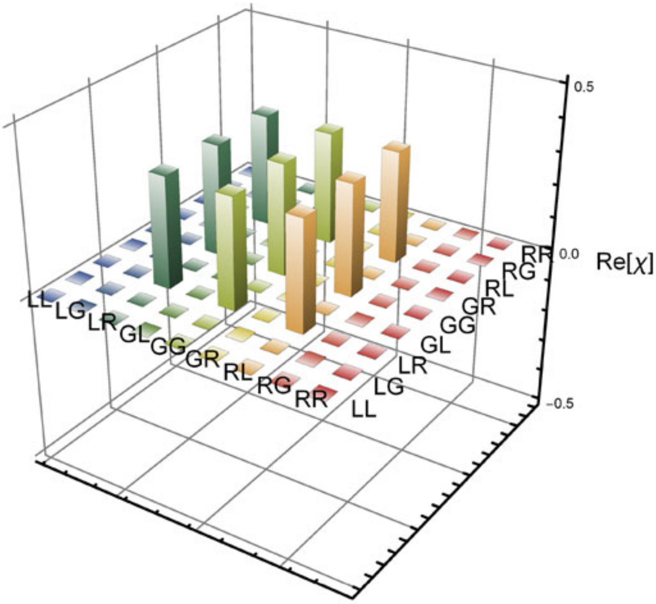

Out[106]=

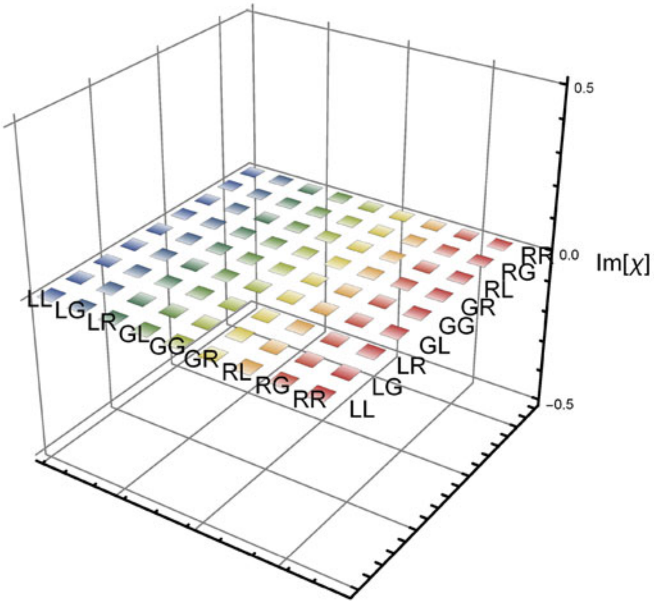

Prospective and Challenge in Future

- **Storage time** Building up a high-dimensional quantum network needs quantum storing high-dimensional state with long lifetime. The storage time of photons carried by image information is reported up to the regime of one minute in a rare-earth-ion-doped solid [9], and in atomic ensemble the storage time is achieved to be one minute [6] by using Gaussian beam. The optical beams in these two works are constructed with equal phase wave fronts. More complex scenarios with structured wave fronts, for example OAM light, have not been studied for long storage time. There are many intriguing questions for this project, one of examples is how to eliminate decoherence from the inhomogeneous wave front. If the transverse azimuthal phase difference between the control and probe beams is mapped onto the spin wave, and the atomic motion during the storage results in dephasing of the atomic spin wave with transverse azimuthal phase [14]. The storage of light with higher OAM has a faster decoherence rate. In order to increase the storage time of light with high OAM, introducing the same quanta of OAM to the control beam to suppress the transverse azimuthal dephasing.
- **Balanced efficiency** The different storage efficiency for different OAM modes can affect the memory fidelity, which is also critical to the quantum information processing in OAM space. The previous reported results show that the quantum efficiency of OAM would decrease with increasing the quanta of OAM [3, 4]. Thus, how to achieve a balanced unit efficiency for each OAM mode is challenging and interesting. The possible solution is that imaging the phase structure OAM beam into the center of atomic ensemble, thus the stored information is always a phase structured information, thus there is no inhomogeneous coupling efficiency between probe and coupling beams. In practical experimental demonstration, the diameter of coupling needs to be larger so that it can cover the probe completely. The final method would be how to avoid the inhomogeneous memory efficiency.
- **High quanta** Because the merit of OAM DOF is the infinite Hilbert space, storing high quanta of OAM entangled state shows an ability of implementing high-dimensional quantum networks. However, the OAM entangled state generated from nonlinear crystal or atomic ensemble is limited by the beam waist of the pump laser. In addition, the photon pair from nonlinear crystal has a large

D.-S. Ding, *Broad Bandwidth and High Dimensional Quantum Memory Based on Atomic Ensembles*, Springer Theses, https://doi.org/10.1007/978-981-10-7476-9

bandwidth of GHz, which is hard to match the work bandwidth of a memory, in general, the bandwidth of atomic memory is limited by the nature linewidth of the excited level of atoms, about ~MHz. Thus, as described before, the photon pair is generated from an atomic ensemble where the bandwidth is the same order to the memory [5]. However, the spiral bandwidth of photon pair reported in Chap. 5 is limited to $w = 4.57$ from quanta of OAM -7 to 7 [3]. Constructing a photon pair with large spiral bandwidth is helpful to demonstrate quantum memory of high quanta OAM entanglement. Maybe, it is promising to modulate the ratio of quanta of OAM modes of pump lasers, for example decreasing the amplitude of Gaussian mode of pump lasers and increase the amplitude of high quanta, thus we can achieve a high spiral bandwidth of OAM entangled state.

- **Embedded with different DOFs** Entanglement in multiple DOFs has many benefits over entanglement in a single one. The former enables quantum communication with higher channel capacity and more efficient quantum information processing and is compatible with diverse quantum networks. Establishing multi-DOFs entangled memories is not only vital for high capacity quantum communication and computing, but also promising for enhanced violations of nonlocality in quantum systems. For example, multi-DOF hyperentanglement enables more efficient Bell measurements [2, 13, 15] and makes superdense coding that breaks the conventional linear-optics threshold achievable [1, 8]. Meanwhile, entanglement in multiple DOFs can be utilized in asymmetrical optical quantum networks [10] and to generate multi-qubit entangled states [7]. Thus, it is promising to construct a quantum memory with multi-DOFs, such as OAM, optical path, polarization, frequency, time bin and so on.
- **GHz-bandwidth single photon storage** The bandwidth of Raman memory in hot vapor cell is ~GHz, as reported in Ref. [11, 12]. The frequency bandwidth of Raman quantum memory in cold atoms as stated in Chap. 6 is about 200 MHz, the main limitation on this is clock frequency of system, for example, the pump pulse generated from AOM is limited by the rising edge of ~10 ns, and the switching speed of the arbitrary wavefunction generation of ~4 ns (250 MHz for AFG 3252). In order to get GHz single photon, there are two methods for our system, one is using a fast EOM switch to modulate a pump pulse with ~ns width; another is using a fast EOM to switch signal pulse. If someone want to build up a Raman quantum memory in cold atoms in GHz scenario, they need to increase the OD of the atoms and the power of the coupling laser.

Papers During PHD

(* contributed equally, † corresponding author)

1. **Dong-Sheng Ding**, Zhi-Yuan Zhou, Bao-Sen Shi & Guang-Can Guo. "Single-photon-level quantum image memory based on cold atomic ensembles". Nat. Commun. 4. 2527 (2013).
2. **Dong-Sheng Ding**, Wei Zhang, Zhi-Yuan Zhou, Shuai Shi, Xi-Shi Wang,Yun-Kun Jiang, Bao-Sen Shi. and Guang-Can Guo. "Quantum Storage of Orbital Angular Momentum Entanglement in an Atomic Ensemble". Physical Review Letters. 114, 050502 (2015).
3. **Dong-Sheng Ding***, Wei Zhang*, Zhi-Yuan Zhou, Shuai Shi, Bao-Sen Shi, Guang-Can Guo. "Raman Quantum Memory of Photonic Polarized Entanglement." Nature Photonics. 9, 332–338 (2015)
4. **Dong-Sheng Ding***, Yun Kun Jiang*, Wei Zhang, Zhi-Yuan Zhou, Bao-Sen Shi, Guang-Can Guo. "Observation of optical filtering effects with four-wave mixing in a cold atomic ensemble". Physical Review Letters. 114, 093601 (2015).
5. **Dong-Sheng Ding†**, Wei Zhang, Shuai Shi, Zhi-Yuan Zhou, Yan Li, Bao-Sen Shi, and Guang-Can Guo, High-dimensional entanglement between distant atomic-ensemble memories, Light science & applications 5, e16157 (2016).
6. **D. -S. Ding***, W. Zhang*, S. Shi*, Z.-Y. Zhou, Y. Li, B.-S. Shi, G.-C. Guo, Hybrid-cascaded generation of tripartite telecom photons using an atomic ensemble and a nonlinear waveguide, Optica 2, 642–645(2015).
7. **Dong-Sheng Ding**, Zhi-Yuan Zhou, Wen Huang, Bao-Sen Shi, Xu-Bo Zou, and Guang-Can Guo. "Experimental up-conversion of images". Phys. Rev. A 86, 033803 (2012).
8. **Dong-Sheng Ding**, Zhi-Yuan Zhou, Bao-Sen Shi, Xu-Bo Zou, and Guang-Can Guo. "Image transfer through two sequential four-wave-mixing processes in hot atomic vapor". Phys. Rev. A 85, 053815 (2012).
9. **Dong-Sheng Ding**, Zhi-Yuan Zhou, Bao-Sen Shi, Xu-Bo Zou, and Guang-Can Guo. "Generation of non-classical correlated photon pairs via a ladder-type atomic configuration: theory and experiment". OPTICS EXPRESS 20, 11433 (2012).

D.-S. Ding, *Broad Bandwidth and High Dimensional Quantum Memory Based on Atomic Ensembles*, Springer Theses, https://doi.org/10.1007/978-981-10-7476-9

10. **Dong-Sheng Ding**, Jing-Hui Wu, Zhi-Yuan Zhou, Yang Liu, Bao-Sen Shi, Xu-Bo Zou, and Guang-Can Guo “Multimode image memory based on a cold atomic ensemble” Phys. Rev. A 87, 013835 (2013)
11. **D.-S. Ding**, Z.-Y. Zhou, B.-S. Shi, X.-B. Zou, and G.-C. Guo. “Linear up-conversion of orbital angular momentum”. OPTICS LETTERS 37, 3270 (2012).
12. **Dong-Sheng Ding**, Jing-Hui Wu, Zhi-Yuan Zhou, Bao-Sen Shi, Xu-Bo Zou, and Guang-Can Guo “Multiple images storage and frequency conversion in a cold atomic ensemble” Phys. Rev. A 87, 053830 (2013).
13. **D.-S. Ding**, Z.-Y. Zhou, B.-S. Shi. “Image cloning beyond diffraction based on coherent population trapping in a hot Rubidium vapor”. OPTICS LETTERS. 39, 240–242 (2014).
14. **Dong-Sheng Ding**, Wei Zhang, Zhi-Yuan Zhou, Jian-Song Pan, Guo-Yong Xiang, Xi-Shi Wang, Bao-Sen Shi, and Guang-Can Guo. “Toward high dimensional state quantum memory in a cold atomic ensemble”. Phys. Rev. A 90, 042301 (2014).
15. Jinghui Wu*, Yang Liu*, **Dong-Sheng Ding***, Zhi-Yuan Zhou, Bao-Sen Shi, and Guang-Can Guo “Light storage based on four-wave mixing and electromagnetically induced transparency in cold atoms” Phys. Rev. A 87, 013845 (2013).
16. **Dong-Sheng Ding**, Zhi-Yuan Zhou, Bao-Sen Shi, Xu-Bo Zou, Guang-Can Guo. “Modulating an image through a non-material lens in a vapor cell”. Optics Communications 285, 1954–1958 (2012).
17. **Dong-Sheng Ding**, Zhi-Yuan Zhou, Bao-Sen Shi, Xu-Bo Zou, and Guang-Can Guo. “Two-color ghost interference with photon pairs generated in hot atoms”. AIP Advances 2, 032177 (2012).
18. **DING Dong-Sheng**, ZHOU Zhi-Yuan, SHI Bao-Sen, ZOU Xu-Bo, GUO Guang-Can. “Two-Photon Atomic Coherence Effect of Transition 5S1/2–5P3/2–4D5/2 (4D3/2) of 85Rb atoms”. CHIN. PHYS. LETT. 29, 024202 (2012).
19. **Dong-Sheng Ding**, Zhi-Yuan Zhou, Bao-Sen Shi and Xu-Bo Zou. “Efficient infrared upconversion via a ladder-type atomic configuration”. Journal of Modern Optics 59, 1768–1771 (2012).
20. **Ding Dong-Sheng**, Zhou Zhi-Yuan, Shi Bao-Sen Slow “Light via Four-Wave Mixing in a Hot Rubidium Vapor”. Chin. Phys. B 22, 114203 (2013).
21. S. Shi, **D.-S. Ding**†, Z.-Y. Zhou, Y. Li, W. Zhang, and B.-S. Shi, Magnetic-field-induced rotation of light with orbital angular momentum, App. Phys. Lett. 106, 261110 (2015)
22. Zhi-Yuan Zhou, **Dong-Sheng Ding**, Bao-Sen Shi, Xu-Bo Zou, and Guang-Can Guo. “Characterizing dispersion and absorption parameters of metamaterial using entangled photons”. Phys. Rev. A 85, 023841 (2012).
23. Zhou Zhi-Yuan, **Ding Dong-Sheng**, Shi Bao-Sen, Zou Xu-Bo, and Guo Guang-Can. “Properties of a dielectric plate using entangled two-photon states”. Chin. Phys. B 21, 094204 (2012).
24. Yang Liu, Jinghui Wu, **Dongsheng Ding**, Baosen Shi and Guangcan Guo. “Bichromatic field generation from double-four-wave mixing in a double-electromagnetically induced transparency system”. New Journal of Physics 14, 073047 (2012).

25. Zhi-Yuan Zhou, Yun-Kun Jiang, **Dong-Sheng Ding**, Bao-Sen Shi, and Guang-Can Guo “Actively switchable nondegenerate polarization-entangled photon-pair distribution in dense wave-division multiplexing” Phys. Rev. A 87, 045806 (2013).
26. Zhi-Yuan Zhou, Yun-Kun Jiang, **Dong-Sheng Ding** & Bao-Sen Shi. “An ultra-broadband continuously-tunable polarization entangled photon-pair source covering the C+L telecom bands based on a single type-II PPKTP crystal”. Journal of Modern Optics. 60, 807363 (2013).
27. Zhi-Yuan Zhou, **Dong-Sheng Ding**, Yan Li, Fu-Yuan Wang, Bao-Seng Shi, Guang-Can Guo. “Cavity-enhanced narrow bandwidth photon pairs generation at the telecom wavelength with a triple resonance configuration”. JOSAB, 31, 128–134 (2014).
28. J.-S. Pan, X.-B. Zou, Z.-Y. Zhou, **D.-S. Ding**, B.-S. Shi, G.-C. Guo. “Nonlocal linear compression of two-photon time interval distribution”. Phys. Rev. A 88, 061802(R) (2013).
29. Wei Zhang, **Dong-Sheng Ding**, Yun-Kun Jiang, Bao-Sen Shi, and Guang-Can Guo. “Indirect precise angular control using four-wave mixing”. Applied Physics Letters 104, 171103 (2014)
30. ZHANG Wei. **DING Dong-Sheng**, PAN Jian-Song. SHI Bao-Sen. “Non-Classical Correlated Photon Pairs Generation via Cascade Transition of5S1/2–5P3/2–5D5/2 in a Hot 85Rb Atomic Vapor”. CHIN. PHYS. LETT. 31, 064208 (2014)
31. Zhi-Yuan Zhou, Yan Li, **Dong-Sheng Ding**, Yun-Kun Jiang, Wei Zhang, Shuai Shi, Bao-Sen Shi & Guang-Can Guo. “Generation of light with controllable spatial patterns via the sum frequency in quasi-phase matching crystals”. SCIENTIFIC REPORTS. 4, 5650 (2014)
32. Zhi-Yuan Zhou, **Dong-Sheng Ding**, Yun-Kun Jiang, Yan Li, Shuai Shi, Xi-Shi Wang, and Bao-Sen Shi. “Orbital angular momentum light frequency conversion and interference with quasi-phase matching crystals”. OPTICS EXPRESS 22, 20298 (2014).
33. Zhi-Yuan Zhou, Yan Li, **Dong-Sheng Ding**, Wei Zhang, Shuai Shi, and Bao-Sen Shi. “Optical vortex beam based optical fan for high-precision optical measurements and optical switching”. OPTICS LETTERS. 39, 5098 (2014).
34. Zhi-Yuan Zhou, Yan Li, **Dong-Sheng Ding**, Wei Zhang, Shuai Shi, Bao-Sen Shi, and Guang-Can Guo. “Highly efficient second harmonic generation of a light carrying orbital angular momentum in an external cavity”. Optics Express 22, 23673–23678 (2014).
35. Yan Li, Zhi-Yuan Zhou, **Dong-Sheng Ding**, and Bao-Sen Shi. “Low-power-pumped high-efficiency frequency doubling at 397.5 nm in a ring cavity”. COL 12(11), 111901 (2014)
36 Li, Yan; Zhou, Zhi-Yuan; **Ding, Dong-Sheng**; Shi, Bao-Sen. Sum frequency generation with two orbital angular momentum carrying laser beams. JOSA B, 32 407–411 (2015)

References

1. Barreiro, Julio T., Tzu-Chieh Wei, and Paul G. Kwiat. 2008. Beating the channel capacity limit for linear photonic superdense coding. *Nature Physics* 4 (4): 282–286.
2. Calsamiglia, John, and Norbert Lütkenhaus. 2001. Maximum efficiency of a linear-optical bell-state analyzer. *Applied Physics B: Lasers and Optics* 72 (1): 67–71.
3. Dong-sheng Ding, Wei Zhang, Shuai Shi, Zhi-yuan Zhou, Yan Li, Bao-sen Shi, and Guang-can Guo. 2016. High-dimensional entanglement between distant atomic-ensemble memories. *Light: Science and Applications* 5(10):e16157.
4. Ding, Dong-Sheng, Wei Zhang, Zhi-Yuan Zhou, Shuai Shi, Jian-song Pan, Guo-Yong Xiang, Xi-Shi Wang, Yun-Kun Jiang, Bao-Sen Shi, and Guang-Can Guo. 2014. Toward high-dimensional-state quantum memory in a cold atomic ensemble. *Physical Review A* 90 (4): 042301.
5. Dong-Sheng Ding, Zhi-Yuan Zhou, Bao-Sen Shi, and Guang-Can Guo. 2013. Single-photon-level quantum image memory based on cold atomic ensembles. *Nature Communications*, 4.
6. Dudin, Y.O., L. Li, and A. Kuzmich. 2013. Light storage on the time scale of a minute. *Physical Review A* 87 (3): 031801.
7. Gao, Wei-bo, Lu Chao-yang, Xu Xing-can Yao, Otfried Gühne Ping, Alexander Goebel, Yu-ao Chen, Cheng-zhi Peng, Zeng-bing Chen, and Jian-wei Pan. 2010. Experimental demonstration of a hyper-entangled ten-qubit schrödinger cat state. *Nature Physics* 6 (5): 331.
8. Trent M Graham, Herbert J Bernstein, Tzu-Chieh Wei, Marius Junge, and Paul G Kwiat. 2015. Superdense teleportation using hyperentangled photons. *Nature communications*, 6.
9. Heinze, Georg, Christian Hubrich, and Thomas Halfmann. 2013. Stopped light and image storage by electromagnetically induced transparency up to the regime of one minute. *Physical Review Letters* 111 (3): 033601.
10. Nagali, Eleonora, and Fabio Sciarrino. 2010. Generation of hybrid polarization-orbital angular momentum entangled states. *Optics Express* 18 (17): 18243–18248.
11. Reim, K.F., P. Michelberger, K.C. Lee, J. Nunn, N.K. Langford, and I.A. Walmsley. 2011. Single-photon-level quantum memory at room temperature. *Physical Review Letters* 107 (5): 053603.
12. Reim, K.F., J. Nunn, V.O. Lorenz, B.J. Sussman, K.C. Lee, N.K. Langford, D. Jaksch, and I.A. Walmsley. 2010. Towards high-speed optical quantum memories. *Nature Photonics* 4 (4): 218–221.
13. Schuck, Carsten, Gerhard Huber, Christian Kurtsiefer, and Harald Weinfurter. 2006. Complete deterministic linear optics bell state analysis. *Physical Review Letters* 96 (19): 190501.
14. Shi, Shuai, Dong-Sheng Ding, Wei Zhang, Zhi-Yuan Zhou, Ming-Xin Dong, Shi-Long Liu, Kai Wang, Bao-Sen Shi, and Guang-Can Guo. 2017. Transverse azimuthal dephasing of a vortex spin wave in a hot atomic gas. *Physical Review A* 95 (3): 033823.
15. Walborn, S.P., S. Pádua, and C.H. Monken. 2003. *Hyperentanglement-assisted bell-state analysis. Physical Review A* 68 (4): 042313.